AN ABSTRACT OF THE DISSERTATION OF

David R. Conklin for the degree of Doctor of Philosophy in Biological and Ecological Engineering presented on October 29, 2009.

Title: Simulating Vegetation Shifts and Carbon Cycling in Yosemite National Park

Abstract approved:

_____

Dominique Bachelet John Bolte

The vegetation in Yosemite National Park changed during the 20th century and may change in the 21st century in response to climate change. Vegetation surveys made during the 1930s and the 1990s provide benchmark records separated by 60 years. This study uses the MC1 dynamic global vegetation model to forecast and hindcast spatially explicit potential vegetation patterns in Yosemite National Park for the 20th and 21st centuries, and uses the vegetation surveys to calibrate the model and assess model performance. The model hindcast for the 20th century was for minor vegetation changes, the most significant being a shift from montane conifer forest to mixed forest in 5% of the Park area. However the vegetation surveys record an *increase* of montane conifer forest amounting to 15% of the Park area, most coming from subalpine forest. The fact that the 1997 survey is more closely matched by simulation results from earlier in the 20th century than by the simulation results for the late 20th century leads to an interpretation of the "hindcast" as being temporally ahead of the observed vegetation, and of the observed vegetation change as reflecting a transition from earlier climates. In contrast to the minimal change simulated for the 20th century, the simulations for the future show large changes in potential vegetation in the mid and late 21st century, brought about by rising temperatures and by a large increase in wildfire, especially near the end of the century. Results of these simulations at 800 m resolution are compared with results from earlier studies at coarser spatial resolution. The biogeography algorithm used in this study is described in detail. A metric for comparing two time series of annual vegetation maps is developed.

Simulating Vegetation Shifts and Carbon Cycling in Yosemite National Park

by

David R. Conklin

A DISSERTATION

submitted to

Oregon State University

in partial fulfillment of
the requirements for the
degree of

Doctor of Philosophy

Presented October 29, 2009
Commencement June 2010

Doctor of Philosophy dissertation of David R. Conklin presented on October 29, 2009.

APPROVED:

_____

Co-Major Professor, representing Biological and Ecological Engineering

_____

Co-Major Professor, representing Biological and Ecological Engineering

_____

Head of the Department of Biological and Ecological Engineering

_____

Dean of the Graduate School

I understand that my dissertation will become part of the permanent collection of Oregon State University libraries. My signature below authorizes release of my dissertation to any reader upon request.

_____

David R. Conklin, Author

ACKNOWLEDGMENTS

"I have tried to make this book as good as I could. But some things I wrote are wrong or confused. If I knew which these were, I would not have written them..." (Gomberg 2007, p. vii). That line from my brother-in-law the philosophy professor goes for me too. But since this is a dissertation, I have an advantage that he lacked when he wrote his book. The members of my committee - Professors Bachelet, Nolin, Garcia, Bolte, and Turner - have undertaken to point out to me the things on which I am wrong or confused, and for this I am deeply grateful, especially to Dominique Bachelet, who has been burdened with reading every draft, beginning with the roughest, most error-laden ones. Although my PhD work did not begin until 2006, Dominique Bachelet has been an inspirational colleague for me since 2001. Similarly, Dave Turner has been discussing vegetation modeling with me as if I were a scientist since 2002. John Bolte has been teaching me things that I didn't know about my own field, computer science, for several years now, and has given me the opportunity to learn and contribute to his Envision model this past year. Anne Nolin graciously agreed to go on my committee during my second year, and each time we hold a meeting I feel increasingly how fortunate I am to have her help. Tiffany Garcia, my grad rep, has given me encouragement and counsel when I've needed it. Thank you, thank you, one and all.

I have also benefitted from the help and friendship of many who are not on my committee. Chris Daly and his staff provided the climate data for the historical period. Chris himself helped me understand the PRISM climate mapping model, gave me a summer job working on it, and included me as a co-author on a recent paper. Rebecca Shaw at the Nature Conservancy provided a job for a subsequent summer on the California Scenarios 2008 project. Jim Thorne at UC-Davis provided the Wieslander VTM data and helped me make sense of it. Similarly, Bill Kuhn and Jan van Wagtendonk at Yosemite provided the 1997 Yosemite Vegetation Survey data, and other Yosemite data, and helped me understand it. Jeanne Panek, now at UC-Berkeley, made sense out of the Yosemite simulation data that I provided to her, and turned it into a report to the National Park Service on which I am proud and grateful to be a co-author. Gordon Godshalk of Alfred University volunteered time on his sabbatical to create a trustworthy soil depth data layer for my simulations. Jeff Kern in Eugene has been helping me come to grips with a new set of soil data. Lisa Graumlich at the University of Arizona dug into her archives to provide me with the digital form of the data from a paper she published in 1993. John Van Sickle at the Environmental Protection Agency reviewed my map comparison methods and called my attention to other methods. My

neighbor Tim Righetti, a professor in the OSU Horticulture Department, got me started using GIS software. Another neighbor, Gordon Grant of the USFS, has been advising me informally about federal science and academia since 2001, and was on my PhD committee for my first year. My fellow students Maureen McGlinchy and Brendan Rogers provided climate data, sympathy, and inspiration. I got hooked on vegetation modeling while working for Ron Neilson of the USFS. Jim Lenihan, my colleague in Neilson's group, has continued to work with me on the MC1 model ever since. Barbara Bond in the OSU College of Forestry convinced me that returning to graduate school was feasible, and facilitated it by taking me on as her own PhD student during my first year. Mike Unsworth and John Selker allowed me to use office space in their respective labs, even though I was not actually their student.

A substantial portion of this research was funded by the Great Basin Cooperative Ecosystem Studies Unit of the National Park Service through task agreement #J8R07070021 and cooperative agreement #H8R07060001. Funds for my summer jobs in 2007 and 2008 were provided by the Nature Conservancy.

TABLE OF CONTENTS

LIST OF FIGURES

LIST OF FIGURES (Continued)

Figure Page

LIST OF FIGURES (Continued)

Figure Page

LIST OF FIGURES (Continued)

Figure Page

LIST OF FIGURES (Continued)

Figure Page

LIST OF TABLES

LIST OF ACRONYMS AND ABBREVIATIONS

ArcGIS	ESRI's brand name for its geographical information system software
BNF	biological nitrogen fixation
DGVM	dynamic global vegetation model
EQ	initial "equilibrium" part of MC1 simulation protocol
ESRI	ESRI Corporation, manufacturer of ArcGIS software
ET	evapotranspiration
FACE	free air CO_2 enrichment
GCM	general circulation model
gdd	growing degree-day
GDD	annual growing degree-day sum
IPCC	Intergovernmental Panel on Climate Change
LAI	leaf area index
LPJ	Lund-Pottsdam-Jena dynamic global vegetation model
MAPSS	Mapped Atmosphere-Plant-Soil System biogeography model; also refers to the USFS research group associated with the MAPSS model
MC1	MAPSS-Century hybrid model, version 1
minT	lowest monthly mean temperature of the year
MSDI	map series difference index
MSSI	map series similarity index
NBP	net biome production
NPP	net primary production
NPS	National Park Service
OSU	Oregon State University
PNW	Pacific northwest
RCM	regional climate model
SRES	Special Report on Emissions Scenarios
tdmean	monthly mean dewpoint temperature
tmax	monthly mean of daily maximum temperatures
TMAX	annual average of monthly means of daily maximum temperatures
tmin	monthly mean of daily minimum temperatures
TMIN	annual average of monthly means of daily minimum temperatures
UC	University of California
USFS	United States Forest Service
USGS	United States Geological Survey

VEMAP	Vegetation/Ecosystem Modeling and Analysis Project
VPD	annual mean vapor pressure deficit
VTM	Wieslander Vegetation Type Maps
WHR	California Wildlife Habitat Relationships classification scheme
YNP	Yosemite National Park

DEDICATION

To my wife Carol Sweeney, who has endured my return to graduate school cheerfully, patiently, and gracefully, and who provided me much-needed encouragement all along the way.

Simulating Vegetation Shifts and Carbon Cycling in Yosemite National Park

CHAPTER ONE: INTRODUCTION

Yosemite National Park is one of the crown jewels of the U.S. National Park system. The question of how Yosemite has been and will be impacted by climate change is important, not only to the natural resource managers in the National Park Service (NPS), but also to members of the public for whom Yosemite is an icon of the natural world. MC1 (MAPSS-Century hybrid model, version 1) (Daly et al. 2000), a dynamic global vegetation model (DGVM), was used in this research to simulate future vegetation, carbon density patterns, and fire regimes in Yosemite.

Yosemite National Park (YNP) covers 302,688 ha of the western slope of the central Sierra Nevada mountain range in California (fig. 1.1). Elevations within the Park range from 657 m on the western side to 3997 m along the crest of the Sierra Nevada. The crest runs roughly SE to NW, and forms the eastern edge of the Park. References to vegetation shifting "upslope" generally mean a shift towards the east.

The Park has two major valleys which run east-west: Yosemite Valley in the south, drained by the Merced River, and the Tuolumne River canyon in the north, now partially occupied by Hetch Hetchy Reservoir. Tuolomne Meadows, at the center of the Park, lies at an elevation of 2700 m. A substantial part of the high elevation area is bare rock.

Yosemite's modern vegetation is the result of a complex interaction of geology, climate trends, and human impacts. Yosemite owes its famous rugged topography and extensive exposed rock areas to glaciation. During the Tioga glacial maximum 18-20 ka B.P., ice covered all but the highest ridges and extended westward down as low as 600-1200 m (Woolfenden 1996). For reference, the present town of El Portal, just outside the western entrance to the Park, is at elevation 591 m. Glacial conditions began to abate about 11,000 years ago. Temperatures increased until the Holocene maximum, 4,000 to 8,000 years ago, when they were about 2°C warmer than the present (Millar & Woolfenden 1999).

Globally, since the Holocene maximum, there has been a millenial-scale trend of slowly decreasing temperatures. Superimposed on the millenial trend, there are two notable centennial-scale periods: the Medieval Warm Period (MWP, 900-1350 A.D.), and the Little Ice Age (LIA, 1400-1900 A.D.). Relative to the long term trend, conditions were both warmer and drier during the MWP than during the late 20th century, and as much as 2°C cooler during the LIA (Millar & Woolfenden 1999). In the Sierra Nevada, the MWP period manifested itself as persistent positive temperature anomalies from 1100 to 1375 A.D relative to 1928-88, and the

LIA produced temperatures about 0.5°C below modern levels from ca. 1450 to 1850 A.D. (Graumlich 1993).

Archeological research shows evidence of native American human presence in Yosemite starting about 1000 A.D. In Yosemite Valley itself, native Americans used fire to maintain desired landscapes (Woolfenden 1996). European settlers and descendants began to have an impact starting in about 1860, through logging, livestock grazing (Muir 1911), and

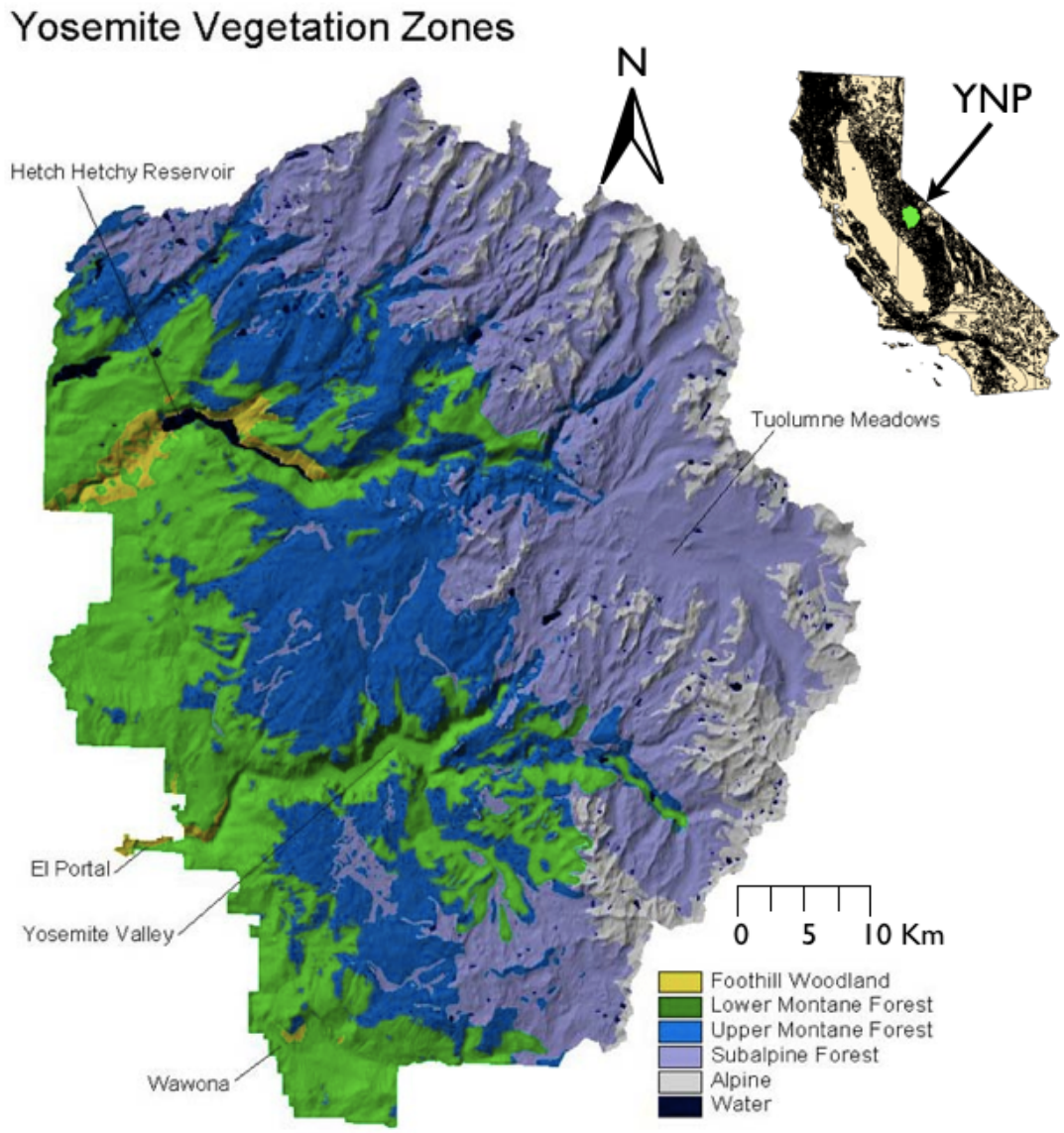

Fig. 1.1 Map of vegetation zones in Yosemite National Park from National Park Service. Inset shows location of Yosemite in California. (http://www.nps.gov/archive/yose/nature)

tourism. Tourism increased dramatically with first rail access and later, starting in 1913, access by private automobiles (Beesley 1996).

When questions are asked about the impact of future climate change on a protected natural area like Yosemite, it is often assumed that an optimum equilibrium state existed before anthropogenic climate change began. The MC1 DGVM incorporates such an assumption in its "spinup" process of establishing equilibrium carbon pools prior to "transient" simulation of historical and future periods. The assumption is that whatever actual disequilibrium exists in the real world in the year used for the beginning of the transient simulation will eventually be reproduced by the simulation as it goes forward in time and the "memory" diminishes of the artificial equilibrium used for the initial conditions.

Yosemite's vegetation was significantly different from its potential condition in 1895, the year when the transient runs begin. At present, the mid-elevation in YNP is heavily forested, and much of this forest has never been logged. Old growth stands contain many individual trees which have been living for several centuries (*Abies magnifica*, red fir) up to a few millenia (*Sequoiadendron giganteum*, giant sequoia) (Fites-Kaufman et al. 2007). During the lifetimes of the mature red firs, the climate emerged from the LIA. During the lifetimes of the largest sequoias, the climate passed through both the MWP and the LIA. Native Americans began intentional burning in some areas during the last millennium, but the native American fire regime ended with the arrival of steel saws and domesticated livestock 35 years before 1895. In Yosemite's forests, both climate and disturbance patterns had been changing prior to 1895 over time periods which were short, compared to the lifespans of the trees themselves.

The ultimate goal of this study is to shed light on how Yosemite's vegetation may be expected to change in response to projected climate changes, of a magnitude larger than any since the last glaciation, and at an unprecedented rate. In order to test the credibility of MC1's projections of future vegetation, MC1 was also used to hindcast the "known" changes during the period of historical record. Although getting the right answer in the hindcast would not necessarily assure the correctness of the projections for the future, getting the wrong answer, on the other hand, could raise doubts about the validity of the projections. Establishing what is known about Yosemite's vegetation shifts during the 20th century turned out to be a research project in its own right.

Specific research questions for the work at Yosemite National Park were formulated as follows:

- How much did the vegetation change in the 20th century?

- Where in YNP did the vegetation change in the 20th century?
- Why did it change?
- How accurately can MC1 simulate the vegetation patterns, carbon density, and fire history of the 20th century?
- How is the climate projected to change under our future scenarios and how much different is the magnitude of change in comparison to historical or paleological change in the area?
- What changes in vegetation patterns, carbon density, and fire history are projected as a consequence of changing climate?

Yosemite has been much studied (table 1.1). We particularly benefitted from and made extensive use of two observational surveys of Yosemite's vegetation: one in the 1930s led by Albert Wieslander at the U.S. Forest Service (Wieslander 1935) and made accessible by the California Energy Commission (Thorne et al. 2006), and the second based on aerial photographs taken in 1997 and made available by the NPS (Aerial Information Systems 1997). Wieslander's project will be referred to from this point on as the Vegetation Type Map survey (VTM[1]). An enabling element for our simulation work is the existence of the PRISM (Parameter-elevation Relationships on Independent Slopes Model) monthly climate time series at 30 arc-second resolution for 1895 through 2006 (Daly et al. 2008). The PRISM data set covers the entire conterminous United States; we used only the portion for Yosemite and environs. The 30 arc-second resolution is commonly referred to as "800 meter" resolution, since 800 meters is a typical distance for 30 seconds of latitude or longitude in the conterminous U.S.

To answer the first research question, "*How much did the vegetation change in the 20th century?*", the VTM survey was compared with the 1997 survey. Others have used different methods to draw conclusions about how and why Yosemite's vegetation has changed in the past (table 1.1).

Although there have been many studies using MC1 and other DGVMs to simulate vegetation patterns, there are no others that quantitatively assess the simulation's accuracy to

[1] Wieslander called his project "the Forest Survey in California" (Wieslander 1935). Thorne calls Wieslander's project "the Wieslander Vegetation Type Map survey" (Thorne et al. 2006) and "the Wieslander Vegetation Type Map Project" (Thorne et al. 2008), and uses the acronym "VTM" as an adjective to refer to it, e.g. "VTM Maps". Kelly describes Wieslander's work product, preserved at the University of California-Berkeley, as "the Vegetation Type Mapping Collection", and uses the VTM acronym the same way Thorne does, e.g. "VTM plot maps" (Kelly et al. 2005). Keeley uses the acronym VTM in the title of his 2004 paper, "VTM Plots as Evidence of Historical Change: Goldmine or Landmine?" (Keeley 2004).

hindcast historical shifts in vegetation. Prior studies that compare biogeographical simulation results from MC1 with observations are listed in table 1.2.

Table 1.1 Other research pertaining to historical vegetation and vegetation change in Yosemite. FIA: Forest Inventory and Analysis.

reference	method	notable conclusions
Muir 1911	personal experience hiking through the area which later became the Park	description of old growth forest conditions ca. 1869, & of the effects of sheep grazing
Wieslander 1935	field survey	vegetation map
Graumlich 1993	tree ring studies	mid-20th century anomalously wet relative to the last 1000 years
Woolfenden 1996	pollen & charcoal studies, archaeological research	native American fire regime beginning about 1300 A.D. in Yosemite Valley
Millar & Woolfenden 1999	synthesis from multiple methods	increased tree growth at treeline, increases in *Abies* abundance at mid-elevations
Klett et al. 2005	repeat photography	forests have become denser
Aerial Information Systems 1997, NatureServe 2007	1997 aerial photography & field survey by Aerial Information Systems and NatureServe	vegetation map
Moritz et al. 2007	resurvey of the Grinnell vertebrate survey transect	upward shifts in elevational limits averaging 500 m for half the species surveyed
van Mantgem & Stephenson 2007 van Mantgem et al. 2009	longitudinal analysis of FIA & other vegetation plots which have been inventoried at least 3 times between 1983 and 2004	increased tree mortality, inconclusive about seedling recruitment
Lutz 2008	repeated vegetation plot surveys	decline of large diameter trees

Table 1.2 Prior studies which compare biogeographical simulation results from MC1 with observations.

reference	method	notable conclusions
Bachelet et al. 2000	comparison of spatially averaged, temporally explicit grassland/savanna/forest dynamics with historical record in Wind Cave N.P.	MC1 can reproduce the major features of the historical record of grassland/savanna/forest temporal dynamics
Bachelet et al. 2003	comparison of MC1 and LPJ vegetation maps for 1900 and 1990 with Küchler's map of potential vegetation	MC1agrees with Küchler on 47-51% of cells LPJ agrees with Küchler on 36-38% of cells
Lenihan et al. 2003	comparison of modal 1961-90 simulated, aggregated vegetation maps and vegetation type % cover with a map of aggregated Küchler types	MC1 simulates areas of mixed forest which are not in Küchler, but are in Terrestrial Vegetation of California, 1995 (Barbour & Major, eds.)

Between 1995 and 2009, ten modeling studies projected future vegetation patterns at continental and smaller scales for areas which included Yosemite (table 1.3). A number of other studies were conducted using equilibrium and dynamic vegetation models for past, present, and future time periods, at the global scale and at smaller scales for areas which did not include Yosemite (table 1.4). The focus of many of these studies has been on carbon flux rather than vegetation patterns; not all of the publications include maps of vegetation. Prentice et al. (1992) report a kappa statistic value of 0.49 for the comparison of a simulated vegetation map to a reference map for the twentieth century, using their equilibrium vegetation model. In Prentice et al. (1993), their model is referred to as the "biome model" and is used to simulate vegetation at the last glacial maximum. In the 1993 paper, the earlier paper is referenced and we learn that the 0.49 κ value represented a 55% match between the simulated vegetation types and the reference map. The Haxeltine & Prentice study in 1996 uses a later version of the biome model, and names it "BIOME3". In the 1996 report, the kappa statistic is again used to measure the agreement between the simulated vegetation map and a reference map for the twentieth century. They give values of kappa for each of 6 aggregated vegetation types which range from 0.42 to 0.84 at 0.5° resolution, and which range from 0.50 to 0.83 at 2.5° resolution. Friend & White published a study in 2000 using a

dynamic model, Hybrid v4.1, which included simulated and reference maps of pre-industrial global vegetation. They omitted any quantitative measure of similarity between the simulated and reference maps, saying only that "the comparison is clearly reasonable". Cramer et al. (2001) included global maps of aggregated vegetation types for the present as simulated by 6 different DGVMs, the corresponding modal map, and a reference map based on satellite imagery. They used the kappa statistic to measure the overall agreement between the modal map and the reference map; $\kappa = 0.42$. Brovkin et al. (2002) simulated the changes in global vegetation from the Holocene maximum to the present using the VECODE (VEgetation COntinuous DEscription) vegetation model and the CLIMBER-2 (CLIMate BiosphERe) climate model, running at very coarse spatial resolution, and using only 3 vegetation cover types. Cox et al. (2004) use the TRIFFID (Top-down Representation of Interactive Foliage and Flora Including Dynamics) model in a study focused on Amazonia; they include simulated and observed vegetation maps of South America for the present. They discuss the differences between the maps at some length, but they do not use a quantitative measure. In the Cramer et al. (2004) study of tropical forests and deforestation using the LPJ (Lund-Pottsdam-Jena) model, the global map of simulated potential tropical forests is taken to be the reference map; the extent of deforestation is assessed by comparison to a database of historical land use change. Bachelet et al. (2005) present maps of potential vegetation in Alaska for the 20th century, from the United States Geological Survey (USGS) and from their MC1 simulations. Like Cox et al. (2004), they discuss the differences, but do not use a quantitative measure. Krinner et al. (2005) describe the ORCHIDEE (ORganizing Carbon and Hydrology In Dynamic EcosystEms) model, including an innovative global map of simulated vegetation which uses combinations of hue (red for broadleaf, blue for needleleaf, green for herbaceous) and saturation (proportional to annual maximum foliage projective cover). For a quantitative measure of the agreement of simulation results with observations, they use a figure of merit calculated from simulated and observed values of leaf area index, where the observations are derived from satellite imagery. Lucht et al. (2006), like Cramer et al. (2004), take the simulated vegetation map produced by LPJ to be the reference map.

With the exception of the very first MC1 study (Bachelet et al. 2000), work before 2009 with MC1 has been done at regional, continental, and global scales, all having spatial pixels with areas at least 100 times larger than those in our study. This seems to be also true for other DGVMs. The PRISM group's creation of the 30 arc-second historical climate data set in 2008 has facilitated several new studies at high spatial resolution, all (so far) at Oregon State University: ours on Yosemite, Maureen McGlinchy's (M.S. student, OSU, Dept. of Forest

Ecology and Society) study of central and northern California, Brendan Rogers' study of the Pacific Northwest (Rogers 2009), Guy Pinjuv's (OSU post doctoral fellow, Dept. of Forest Ecology and Society) work on the Rocky Mountains region, and Bear Pitts' (MAPSS Team, USFS PNW Research Station, Corvallis) project for the southwestern U.S. Those studies, some of which are still in progress, are of regional extent (which results in hundreds of thousands of cells). Our study is the first to use the 800m resolution and data for a smaller area like Yosemite, where we simulate only 4400 cells. The smaller scale of our study gives us the opportunity to use the very high resolution VTM and 1997 Survey observational data sets for fine-scale comparisons, which would be impractical for the regional studies.

The modal value of the simulated potential vegetation type for 1905—1935 matched the VTM vegetation class for 60% of the gridcells covering YNP. The modal simulated value matched the 1997 NPS Survey for 54% of the gridcells. These percentages are somewhat higher than those reported (36 – 51%) for the match between the Küchler vegetation map and simulations using the MC1 and LPJ DGVMs in the VEMAP II study (table 3 in Bachelet et al. 2003). VEMAP was conducted at the continental scale with a half-degree grain (~50 km). Differences between MC1 results and the VTM and 1997 survey data are described in detail in **chapter 2**.

We used the available data from published results for larger areas which include YNP (table 1.3) to compare with model results for this project. Comparisons of projected future vegetation in Yosemite from the present study and older studies are presented in **chapter 3**. The biogeography algorithm and a quantitative technique for comparing two sets of annual vegetation maps from different periods are presented in **chapter 4.**

My simulations, driven by historical climate with little long term trend, were moderately successful at reproducing the observed patterns of vegetation in the early and late 20th century, but produced different and smaller vegetation shifts than those inferred from comparing the observations from the two time periods. In response to the strong climate change signal in the future climate scenarios, the simulations project a widespread shift from dense forests and infrequent fires toward more open vegetation classes, lower carbon densities, and larger, more frequent fires by the late 21st century. The results of all phases of the study are summarized, and some suggestions offered for ways to improve simulation studies of Yosemite in the future, in the final **chapter 5.**

Table 1.3 Publications containing projections of future climate and vegetation change at continental and smaller scales for areas that include Yosemite.

Abbreviations and sources for table 1.3

A1B, A2, B1, B2: IPCC emissions scenarios (IPCC 2000)
BIOME2: biogeography model (Haxeltine et al. 1996)
CCSM3: National Center for Atmospheric Research Community Climate System Model, version 3 (Collins et al. 2006)
CGCM1, CGCM2: first and second generation Coupled Global Climate Models from the Canadian Centre for Climate Modeling and Analysis (Boer et al. 2000, Flato et al. 2000)
CSIRO Mk2, Mk3: Commonwealth Scientific and Industrial Research Organisation GCM versions Mk2, Mk3 (H. Gordon et al. 2002)
CSIRO B1: CSIRO Mk3 GCM using emission scenario B1
DOLY: Dynamic Global Phytogeography Model (Woodward et al. 1995)
GFDL: Geophysical Fluid Dynamics Laboratory general circulation model (Manabe et al. 1990, Wetherald et al. 1990)
GFDL-A2: Geophysical Fluid Dynamics Laboratory general circulation model using IPCC emission scenario SRES-A2
GFDL-CM2.1: version 2.1 of the GFDL general circulation model (Delworth et al. 2006)
GFDL-R30: GFDL model using rhomboidal 30 truncation (Delworth et al. 2002).
GISS: Goddard Institute for Space Studies three-dimensional model (Hansen et al. 1988)
HADCM2: the second Hadley Centre coupled ocean-atmosphere GCM (Hakkarinen & Smith 2006, Johns et al. 1997).
HADCM2GHG: HADCM2 using a 1% per year compounded increase in greenhouse gases from 1900 to 2100 (Johns et al. 1997)
HADCM2SUL: HADCM2GHG plus the direct radiative effect of sulphate aerosols (Mitchell & Johns 1997)
HADCM3: the third Hadley Centre coupled ocean-atmosphere GCM, which does not use flux adjustments (C. Gordon et al. 2000, Johns et al. 2003)
Hadley A1B: HADCM3 GCM using emission scenario A1B
MAPSS: Mapped Plant-Atmosphere-Soil System (Neilson 1995)
MIROC 3.2 medres: Model for Interdisciplinary Research on Climate, version 3.2, medium resolution (Hasumi & Emori 2004)
MIROC A2: MIROC 3.2 medres GCM using emission scenario A2
OSU: Oregon State University atmospheric GCM – mixed layer ocean model (Schlesinger & Zhou 1989)
PCM and PCM1: National Center for Atmospheric Research Parallel Climate Model scenario (Hakkarinen & Smith 2006, Dai et al. 2001, Washington et al. 2000).
PCM-A2: Parallel Climate Model using IPCC emission scenario SRES-A2.
PCM B06.06: Parallel Climate Model B06.06 simulation (Dai et al. 2001).
UKMO: United Kingdom Meteorology Office GCM (Wilson & Mitchell 1987)
VEMAP: Vegetation/Ecosystem Modeling and Analysis Project (VEMAP members 1995)

Table 1.3

study, year	area, grain	reference	scenario, GCM	projection for YNP
VEMAP I 1995	U.S. 0.5 deg (~50 km)	VEMAP members, 1995	2X CO_2; GFDL, OSU, UKMO	MAPSS: conifer forest & woodland BIOME2: forest, woodland, shrubland DOLY: boreal, tundra, forest, woodland
MAPSS+ MC1 1999	U.S. 10km and 0.5 deg (~50km)	Bachelet et al. 2001a	UKMO, CGCM1, GISS, GFDL-R30, HADCM2GHG, OSU, HADCM2SUL	conifer forest or woodland
California 2000	California 10 km	Lenihan et al. 2006a	HADCM2, PCM	mixed forest and conifer forest move upslope; decrease in subalpine and alpine areas
VEMAP II 2000	U.S. 0.5 deg (~50 km)	Bachelet et al. 2003	HADCM2SUL, CGCM1	conifer and mixed forests, woodland, and shrubland
California 2003	California 10 km	Lenihan et al. 2003	HADCM2SUL, PCM B06.06	conifer and mixed forests, shrubland, alpine and subalpine
California Scenarios 2006	California 10 km	Lenihan et al. 2008a	GFDL-A2, PCM-A2	GFDL-A2: conifer and mixed forests, mixed woodland, shrubland, grassland PCM-A2: conifer and mixed forests, shrubland, alpine and subalpine
VINCERA 2006	U.S. 0.5 deg (~50 km)	Lenihan et al. 2008b	{CGCM2, HADCM3, CSIRO Mk2} x {A2, B2}	warm temperate mixed forest, woodland/savanna, temperate conifer forest
LYNX 2007	North America 5 arc-minutes (~8 km)	Gonzalez et al. 2007	{CSIRO Mk3, HADCM3, MIROC 3.2 medres} x {B1, A1B, A2}	temperate evergreen needleleaf forest temperate deciduous broadleaf forest subtropical mixed forest temperate grassland

Table 1.3 (Continued)

study, year	area, grain	reference	scenario, GCM	projection for YNP
California Scenarios 2008	California 7' 30" (~12 km)	Shaw et al. 2008	{PCM, GFDL, CCSM3} x {A2, B1}	GFDL-A2: conifer and mixed forests & woodlands, hardwood woodland, chaparral, grassland CCSM3-A2: subalpine, conifer & mixed forests, conifer woodland, sagebrush PCM1-A2: subalpine, conifer and mixed forests
TOPS 2009	YNP ~12 km	Nemani et al. 2009	GFDL, medium high emissions	30% decrease in photosynthesis for YNP as a whole; no projection of vegetation types
NPS Yosemite Study	YNP 30 arc-seconds ~800m	Panek et al. 2009	CSIRO B1, HADCM3 A1B, MIROC A2	alpine zone disappears subalpine forest zone diminishes montane conifer forest shifts upward mixed forest increases

Table 1.4 Studies using equilibrium and dynamic global vegetation models at the global scale and at smaller scales for areas that do not include Yosemite. Grain in degrees is stated as latitude x longitude.

Abbreviations and sources for table 1.4

A1B, A1F1, A2, B1, B2: IPCC emissions scenarios (IPCC 2000)
BIOME3: biogeography model (Haxeltine & Prentice 1996)
Bern CC: Bern carbon cycle-climate model (Joos et al. 2001)
CLIMBER-2: climate system model (Petoukhov et al. 2000)
CLM: regional climate model (Steppeler et al. 2003)
CSIRO, CSIRO Mk3: Commonwealth Scientific and Industrial Research Organisation GCM (H. Gordon et al. 2002), Mk3 is version 3
ECHAM4: ECMWF/HAMBURG general circulation model v. 4 (http://www.ipcc-data.org/is92/echam4_info.html)
ECHAM5: ECMWF/HAMBURG general circulation model v. 5 (Roeckner et al. 2003)
ECHAM4/OPYC3: coupled general circulation model (Roeckner et al. 1999)
ESCM: UVic Earth System Climate Model (Meissner et al. 2003)
HadAM3H: general circulation model (Hudson & Jones 2002)
HadCM2-SUL: the second Hadley Centre coupled ocean-atmosphere GCM, using a 1% per year compounded increase in greenhouse gases from 1900 to 2100, plus the direct radiative effect of sulphate aerosols (Mitchell & Johns 1997)
HadCM3, HadCM3LC: the third Hadley Centre coupled ocean-atmosphere general circulation model (C. Gordon et al. 2000, Johns et al. 2003)
HadRM3H: regional climate model (Buonomo et al. 2007)
HIRHAM: regional climate model (Christensen et al. 1996)
HRBM: High Resolution Biosphere Model (Esser et al. 1994)
Hybrid v4.1: dynamic global vegetation model Hybrid version 4.1 (Friend & White 2000)
HyLand: the Hybrid DGVM with modifications (Levy et al. 2004)
IBIS: Integrated Biosphere Simulator (Foley et al. 1996, Kucharik et al. 2000)
IS92a: “business as usual” emissions scenario (IPCC 1994)
LPJ: Lund-Potsdam-Jena Dynamic Global Vegetation Model (Sitch 2000, Prentice et al. 2000)
LPJ-GUESS: dynamic global vegetation model (Smith et al. 2001, Sitch et al. 2003)
MC1: dynamic global vegetation model (Daly et al. 2000)
MIROC 3.2 medres: Model for Interdisciplinary Research on Climate, version 3.2, medium resolution (Hasumi & Emori 2004)
PCTM: ocean-atmosphere climate model (Thompson et al. 2004)
ORCHIDEE: dynamic global vegetation model (Krinner et al. 2005)
QTCM: atmospheric model (Zeng et al. 2004)
RCAO: Rossby Centre regional Atmosphere-Ocean model (Döscher et al. 2002)
REMO: regional climate model of the Max-Planck Institute for Meteorology (Jacob 2001)
SDGVM: dynamic global vegetation model (Woodward et al. 1998, Woodward et al. 2001)
TEM: Terrestrial Ecosystem Model (Tian et al 1999)
TRIFFID: dynamic global vegetation model (Cox 2001)
VECODE: dynamic global vegetation model (Brovkin et al. 1997)
VEGAS: VEgetation-Global-Atmosphere-Soil terrestrial carbon model (Zeng et al. 2004)

Table 1.4

reference, area, grain, time period	veg maps	vegetation model(s) (DGVM unless noted)	GCM(s) and RCM(s)	Emissions scenario(s)
Prentice et al. 1992, global, 0.5˚ x 0.5˚, 20th century	yes	biome equilibrium model	n. a.	n. a.
Prentice et al. 1993, global, 0.5˚ x 0.5˚, last glacial maximum	yes	biome equilibrium model	n. a.	n. a.
Haxeltine & Prentice 1996, global, 0.5˚ x 0.5˚, 20th century	yes	BIOME3 (equilibrium model)	n. a.	n. a.
Bachelet et al. 2000, Wind Cave National Park, 50 m, 1895—2094	no	MC1	HadCM2-SUL	1% yr^{-1} increase in greenhouse gases
Friend & White 2000, global, 2.5˚ x 3.75˚, pre-industrial	yes	Hybrid v4.1	n. a.	n. a.
Cramer et al. 2001, global, 2.5˚ x 3.75˚, 1861—2100	yes	Hybrid, IBIS, LPJ, SDGVM, TRIFFID, VECODE	HadCM2-SUL	IS92a
McGuire et al. 2001, global, 0.5˚ x 0.5˚, 1860—1992	no	HRBM, IBIS, LPJ, TEM	n. a.	n. a.
Cox et al. 2000, global, 2.5˚ x 3.75˚	no	TRIFFID	HadCM3LC	IS92a
Brovkin et al. 2002, global, 10˚ x 51˚, the Holocene	yes	VECODE	CLIMBER-2	n. a.
Cox et al. 2004, South America, 2.5˚ x 3.75˚, 1860—2100	yes	TRIFFID	HadCM3LC	IS92a
Cramer et al. 2004, the tropics, 0.5˚ x 0.5˚, 1901—2100	yes	LPJ	HadCM3, ECHAM4, CSIRO, CGCM	IS92a
Bachelet et al. 2005, Alaska, 0.5˚ x 0.5˚, 1922—2100	yes	MC1	CGCM1, HadCM2-SUL	IS92a
Krinner et al. 2005, global, 4˚ x 2.5˚, 1961—1990	yes	ORCHIDEE	n. a.	n. a.
Friedlingstein et al. 2006, global, typically 2.5˚ x 3.75˚,	no	MOSES/TRIFFID IBIS VEGAS LPJ	HADCM3, EMBM PCTM QTCM CLIMBER-2, Bern CC	A2

Table 1.4 (Continued)

reference, area, grain, time period	veg maps	vegetation model(s) (DGVM unless noted)	GCM(s) and RCM(s)	Emissions scenario(s)
Lucht et al. 2006, global, 0.5˚ x 0.5˚, 1860—2100	yes	LPJ	ECHAM5, HadCM3	B1, A2
Morales et al. 2007, Europe, ~50km, 1961—2100	no	LPJ-GUESS	GCMs: HadAM3H, ECHAM4/OPYC3 RCMs: RCAO, HIRHAM, HadRM3H, CLM, REMO	A2, B2
Sitch et al. 2008, global	no	HyLand, LPJ, ORCHIDEE, SDGVM, TRIFFID	HadCM3LC	A1F1, A2, B1, B2
Rogers 2009, Pacific Northwest, 30” x 30”, 1895—2099	yes	MC1	CSIRO Mk3, HadCM3, MIROC 3.2 medres	B1, A1B, A2

CHAPTER TWO: THE HISTORICAL PERIOD

It is important to know how the Park's climate and vegetation have changed in the recent past, to provide a context for projections of future change. We address 4 questions in this chapter: *How much* did Yosemite's vegetation change in the 20th century? *What* were the changes? *Where* did they occur? *Why*?

The MC1 model (Daly et al. 2000) was used to simulate Yosemite National Park's vegetation and carbon dynamics for the 20th century, using PRISM's reconstruction of local historical climate (Daly et al. 2008). Observation-based vegetation maps from the 1930s and the 1990s were compared with each other to detect actual 20th century change, and compared with simulation results to assess the model's skill. Based on the performance of the MC1 model in other studies, we expected it to produce a pattern of potential vegetation similar to the pattern of actual vegetation. We hoped that any significant observed changes in the vegetation pattern would also be present in the simulation output.

Many factors influence how skillful a model is at hindcasting and forecasting. Among these factors are the type of model, the level of detail represented in the model, the accuracy of the data used to drive the model, the degree to which model calculations are constrained by known boundary conditions, and the specificity of the model calibration to the study area. MC1 is a process model, actually a coordinated suite of process models, which enables us to use it for future conditions for which there are no historical analogues. It operates at a monthly timestep. It accommodates two canopy layers, but parameterizes their net primary productivity rather than including submodels for photosynthesis and autotrophic respiration. Maximum potential productivity is set separately for each canopy layer with a parameter, and then modulated with dimensionless environmental scalars. MC1 is intermediate in complexity between highly parameterized models with an annual timestep like VECODE (Brovkin et al. 1997) and more detailed process models with a daily timestep like Biome BGC (Thornton 1998). The fine spatial resolution used in this study strains our knowledge of the historical input data, and complicates our use of future climate data from general circulation models. When we analyze vegetation trends using simulations driven by the historical PRISM climate data, we are effectively ignoring the caveat from the PRISM group that their data should not be used for detecting climate trends (Chris Daly, pers. comm.). General circulation models (GCMs) work at far coarser spatial resolution than we use, and the downscaling technique used to adapt the GCM output to our needs relies on the spatial variation in the historical PRISM climate data to become a proxy for the spatial pattern in future climates, a known

oversimplification (Daly et al. 2009). While MC1 makes use of site information about soil depth and texture, elevation, and latitude, and is driven by time series of monthly climate data, it is not constrained by known existing vegetation types or disturbance histories. The calibration used for MC1 in this study is a refinement of that used in an earlier statewide California study (Shaw et al. 2008). The calibration, which had been used in the statewide study, was adjusted for our Yosemite study to improve the match between the simulated potential vegetation distribution for 1905—1935 and the VTM vegetation distribution.

Methods

Climate data

Gridded monthly climate data from 1895 through 2006 were obtained from the PRISM group at Oregon State University. The grid has a grain of 30 arc-seconds in both latitude and longitude, resulting in grid cells which are ~730 m east-west and ~920 m north-south. The PRISM climate mapping method has been described extensively elsewhere (e.g. Daly et al. 1994, Daly et al. 2008). PRISM uses available meteorological station data within a reasonable radius of the target point when estimating climate for that point. The number of stations providing data used by PRISM for the Yosemite region varied from 21 in 1900 to as many as 85 later in the century (Joseph Smith, Oregon State University, pers. comm.).

The PRISM climate input data for temperature consists of three monthly series: the monthly means of the daily extrema (*tmin*, *tmax*) and the monthly mean dewpoint temperature (*tdmean*). Monthly mean temperature is estimated as the average of the *tmin* and *tmax* values. From these monthly series, five annual series were derived and analyzed:

- annual average minimum temperature (*TMIN*), the average for a given year of the monthly *tmin* values
- annual average maximum temperature (*TMAX*), the average for a given year of the monthly *tmax* values
- for each year, the average temperature in the coldest month (*minT*), the lowest of the 12 monthly averages of *tmin* and *tmax*
- growing degree-days above 0°C (*GDD*), made by summing daily values constructed by linear interpolation between monthly mean temperatures
- annual average vapor pressure deficit (*VPD*)

Climate averages for two different 31-year periods were examined: 1905—1935 and 1967—1997. Averages for 1905—1935 were taken as representative of the climate

associated with the VTM vegetation map, and the climate averages for 1967—1997 as representative of the climate associated with the 1997 survey map.[2]

We examined the gridded monthly PRISM climate data for the area within the YNP boundaries for trends. We wished to determine the amount of climate change in the Park as a whole during the twentieth century, and also to gauge the degree to which the changes varied spatially across the Park. Two types of analysis were performed: trend lines were fitted to time series of Park-wide spatial averages, and differences in temporal averages were mapped for the periods 1905—1935 and 1967—1997.

Description of soils

Some areas in the Park are dominated by rock outcrop, but include small pockets of soil which support isolated patches of trees or shrubs. Depending on the relative amounts of rock outcrop and vegetation, such areas may be classified as barren, or as one of the vegetation types. In the 1997 NPS survey (U.S. Department of Agriculture Natural Resources Conservation Service CA790 soil survey, http://soils.usda.gov), the patches of vegetation can occupy as little as 10% of the polygon area, and still result in the polygon being classified as vegetated rather than barren (Bill Kuhn, NPS, pers. comm.).

Observed vegetation distribution

Two detailed maps of vegetation distribution are available for YNP: the Wieslander Vegetation Type Map (VTM) dating from the 1930s (Wieslander 1935, Thorne et al. 2006), and the 1997 NPS Yosemite Vegetation Survey map (Aerial Information Systems 1997). As explained in greater detail below, the original VTM observations were made visually from terrain high points and then drawn in by hand on topographic maps. A group at the University of California-Davis under the direction of Dr. James Thorne has recently converted the original hand drawn VTM maps into a digital dataset (Thorne et al. 2006). The 1997 survey is based on aerial photography combined with ground observations. The existence of these datasets of vegetation separated by 6 decades presented the opportunity to look for nearly-centennial-

[2] A 31-year averaging period was used in order to be consistent with the division of the future climate study into three 31-year periods: 2007—2037, 2038—2068, and 2069—2099.

scale changes, and to relate them to historical climate records. Another vegetation map, CALVEG (Schwind & Gordon 2001), was considered as an additional source. Although based on satellite imagery outside the Park, within the Park the CALVEG map is derived from the 1997 NPS Vegetation Survey (Hazel Gordon, pers. comm.), and so does not represent an independent data set for the purposes of the current study.

Wieslander VTM map

The VTM survey began in 1928 and continued until the early 1940s. The VTM maps for the central Sierra Nevada were made in 1935 and 1936 (Walker 2000). The survey field work was performed before aerial photographs were available; crews sketched vegetation patches from terrain high points that afforded views of the landscape (Keeler-Wolf 2007). Observations were recorded directly on photographic enlargements of US Geological Survey (USGS) topographic maps, mostly 30' quadrangles. "First edition" maps were used, based on topographic surveys in the late 1800s (Walker 2000).

The high quality of the fieldwork on which the VTM map is based has been noted. Thorne cites Wieslander's unpublished "Instructions for the preparation of the vegetative type map of California" (on file in the library at YNP) to show Wieslander's determination to obtain the best possible data, and Wieslander's appreciation of the value of the VTM maps to future researchers (Thorne et al. 2008). The detailed protocol prescribed by Wieslander is summarized by Keeler-Wolf (Keeler-Wolf 2007). The consensus of these modern experts is that the VTM maps were produced in a consistent way using a well-defined, detailed protocol, which is available to current researchers. However, Keeley (2004) noted that it is difficult to relocate and resurvey VTM plots.

Seven decades after they were first made by Wieslander's U.S. Forest Service crews, the hand-drawn VTM maps for the central Sierra Nevada, including YNP, were digitized by Thorne and colleagues at the University of California-Davis. Benefiting from Walker's earlier experience in attempting to convert the first edition topographical maps to current editions (Walker 2000), Thorne's group chose instead to retain the projection used in the original USGS topo maps (Jim Thorne, pers. comm.). The final project report (Thorne et al. 2006) summarizes their painstaking, labor-intensive effort:

> "...the project team developed new methods, which included the following steps: the historical VTM maps were scanned; the scans were georectified;

> the vegetation polygons on the maps were traced; the species codes on the maps were transcribed into a standardized digital table; and the species combinations were assigned to vegetation types according to the *Manual of California Vegetation* (Sawyer and Keeler-Wolf 1995) and the Wildlife Habitat Relationships (WHR) model developed by the California Department of Fish and Game (2004)."

In keeping with the example set by Wieslander, the procedures used are described in a methods manual, that although unpublished is referenced in Thorne et al. (2006) as "available from the author upon request".

1997 NPS Vegetation Survey

Color infrared aerial photography (1:15,860) taken in August of 1997 was used as the starting point for the 1997 NPS Vegetation Survey. The final vegetation map was derived through a coordinated process of photo-interpretation, field reconnaissance, plot sampling, verification, and accuracy assessment (Aerial Information Systems 2007). The minimum mapping unit area was 0.5 hectare. A correspondence of the original vegetation classes used in the survey to California Wildlife Habitat Relationship (WHR) classes was developed by Bill Kuhn (NPS), in consultation with Dr. Jan van Wagtendonk (USGS) and Dr. James Thorne (U.C. Davis).

Conversion to the 800 m grid

The digital VTM and 1997 NPS Survey vegetation maps are tilings of the Park area by thousands of irregularly shaped polygons (table 2.1). The more recent survey was done at finer spatial resolution, resulting in 7 times as many polygons as in the older map (fig. 2.1). To each polygon is associated a cover type. We aggregated these multiple cover types into a coarser common set of vegetation types and resampled the polygons to the 800 m spatial grid in two steps.

First, one of 30 WHR classes was assigned to each of the cover types used on the original maps (table 2.2 and Aerial Information Systems 1997). Then the WHR classes were further aggregated into 12 vegetation/land cover types used in the biogeography classification scheme of the MC1 dynamic global vegetation model (table 2.3).

Table 2.1 Characteristics of Wieslander Vegetation Type Map (Thorne et al. 2006) and 1997 National Park Service Vegetation Survey map (Aerial Information Systems 1997) of Yosemite National Park.

	VTM	1997 Survey
number of polygons in YNP boundaries	6,760	46,528
mean polygon area (ha)	45	6.5
number of vegetation classes	6,476 statewide	129

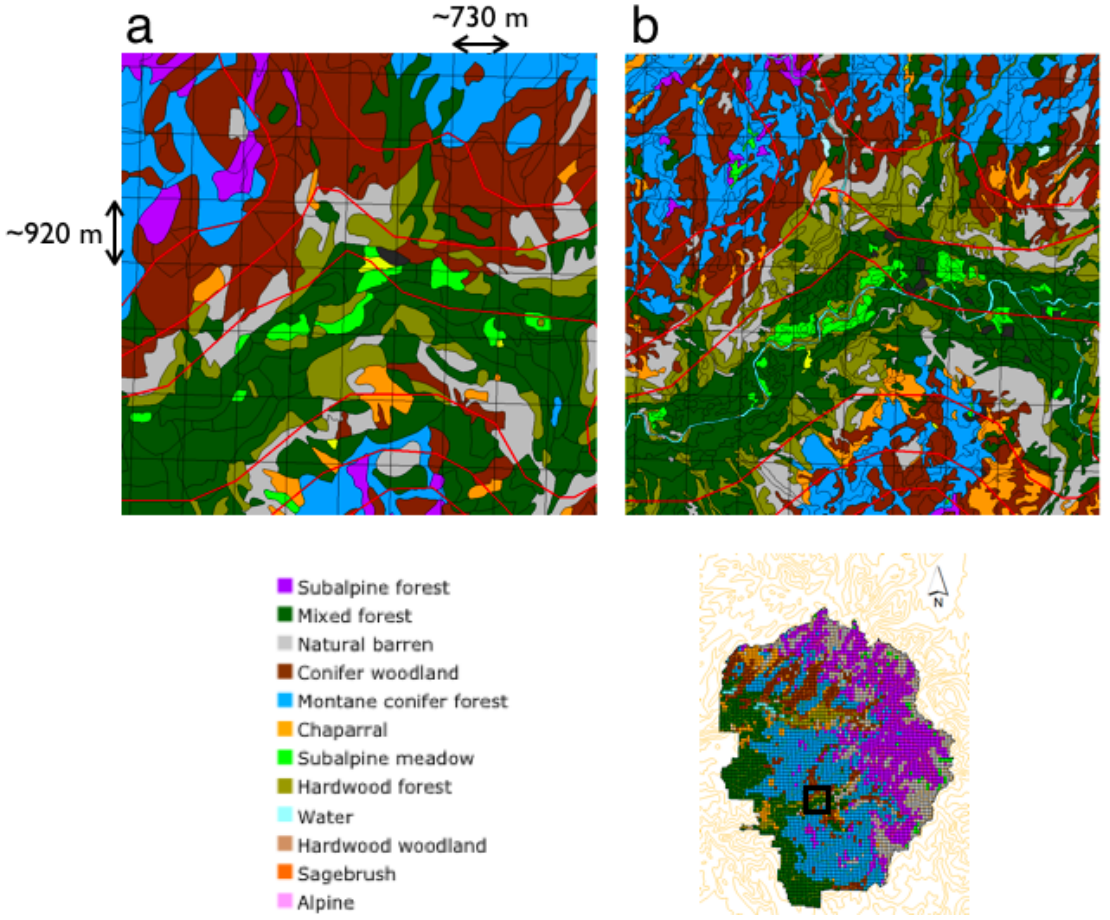

Fig. 2.1 Illustration of the two datasets: (a) Wieslander VTM (Thorne et al. 2006), (b) 1997 NPS Yosemite Vegetation Survey (Aerial Information Systems 1997). Maps in their original polygon form, with topographic lines and 30 arc-second grid lines. The area shown is part of Yosemite Valley including Yosemite Falls. Topographic contours are at 1000 ft intervals.

Table 2.2 1997 NPS Vegetation Survey types and corresponding MC1 vegetation types and California Wildlife Habitat Relationship (WHR) types. See table 2.3 for the key to the WHR type abbreviations.

1997 Vegetation Survey type number and name		MC1 vegetation type	WHR
100	Alpine talus slope	natural barren	BAR
200	Alpine scree slope	natural barren	BAR
300	Alpine Snow Patch Communities	alpine	BAR
500	Mesic rock outcrop	natural barren	BAR
700	Boulder field	natural barren	BAR
910	Conifer reproduction	missing data	UKW
920	Conifer plantation	montane conifer forest	SMC
940	Sparsely vegetated undifferentiated	natural barren	BAR
941	Sparsely vegetated riverine flat	natural barren	BAR
950	Non-alpine talus	natural barren	BAR
961	Sparsely vegetated to non-vegetated exposed rock	natural barren	BAR
963	Dome	natural barren	BAR
964	Fissured rock outcrop	natural barren	BAR
965	Sparsely vegetated rocky streambed	natural barren	BAR
970	Snowfield/Glacier	water	GLA
980	Water	water	LAC
981	Permanently flooded, emergent, or floating vegetation	water	FEW
990	Urban/Developed	developed	URB
1020	Canyon live oak forest	hardwood forest	MHW
1022	Canyon live oak/manzanita forest	hardwood forest	MHW
1023	Canyon live oak/ponderosa pine/incense cedar forest	mixed evergreen forest	MHC
1024	Canyon live oak/California laurel forest	hardwood forest	MHW
1026	Canyon live oak/foothil pine forest	mixed evergreen forest	MHC
1029	Canyon live oak/manzanita forest	hardwood forest	MHW
1043	Interior live oak/canyon live oak woodland	hardwood woodland	MHW
1510	Canyon live oak/buckeye woodland	hardwood woodland	MHW
1520	Blue oak woodland	hardwood woodland	BOW
1530	Interior live oak woodland	hardwood woodland	MHW
2010	Quaking aspen forest	hardwood forest	ASP
2011	Quaking aspen/false hellbore forest	hardwood forest	ASP
2013	Quaking aspen/willow forest	hardwood forest	ASP
2014	Quaking aspen/willow talus slope	hardwood woodland	ASP
2015	Quaking aspen/jeffrey pine forest	mixed evergreen forest	ASP
2016	Quaking aspen/big sagebrush forest	hardwood forest	ASP
2020	California black oak forest	hardwood forest	MHW
2021	California black oak/manzanita forest	hardwood forest	MHW
2022	California black oak/incense cedar forest	mixed evergreen forest	MHC
2025	California black oak/bracken fern forest	hardwood forest	MHW
2040	Valley oak woodland	hardwood woodland	VOW
2050	Black cottonwood forest	hardwood forest	MRI

Table 2.2 (Continued)

	1997 Vegetation Survey type number and name	MC1 vegetation type	WHR
2052	Black cottonwood/quaking aspen/jeffrey pine forest	hardwood forest	MRI
2070	Mountain alder forest	hardwood forest	MRI
2510	Willow forest	hardwood forest	MRI
2520	White alder/bigleaf maple forest	hardwood forest	MRI
3010	Lodgepole pine/quaking aspen/jeffrey pine forest	subalpine forest	LPN
3012	Lodgepole pine/quaking aspen forest	subalpine forest	LPN
3020	Lodgepole pine forest	subalpine forest	LPN
3022	Lodgepole pine/bog blueberry forest	subalpine forest	LPN
3026	Lodgepole pine woodland	subalpine forest	LPN
3027	Lodgepole pine/big sagebrush forest	subalpine forest	LPN
3028	Lodgepole pine/whitebark pine forest	subalpine forest	LPN
3047	Lodgepole pine/big sagebrush/kentucky bluegrass forest	subalpine forest	LPN
3048	Lodgepole pine mesic forest	subalpine forest	LPN
3049	Lodgepole pine xeric forest	subalpine forest	LPN
3050	Ponderosa pine woodland	conifer woodland	PPN
3053	Ponderosa pine/black oak/manzanita woodland	mixed evergreen woodland	PPN
3060	Ponderosa pine/incense cedar forest	montane conifer forest	PPN
3066	Ponderosa pine/incense cedar/black oak/canyon live oak forest	mixed evergreen forest	MHC
3070	Jeffrey pine woodland	conifer woodland	JPN
3072	Jeffrey pine/manzanita woodland	conifer woodland	JPN
3073	Jeffrey pine/ceanothus woodland	conifer woodland	JPN
3075	Jeffrey pine/huckleberry oak woodland	conifer woodland	JPN
3076	Jeffrey pine/antelopoe bitterbrush woodland	conifer woodland	JPN
3081	Jeffrey pine/pinyon pine woodland	conifer woodland	JPN
3082	Jeffrey pine/mountain mahogany woodland	conifer woodland	JPN
3083	Jeffrey pine/white fir woodland	conifer woodland	JPN
3084	Jeffrey pine/canyon live oak/manzanita woodland	mixed evergreen woodland	JPN
3085	Jeffrey pine/red fir woodland	conifer woodland	JPN
3090	Foothill pine woodland	mixed evergreen woodland	BOP
3097	Foothill pine/interior live oak/manzanita woodland	mixed evergreen woodland	MHC
3101	Knobcone pine/manzanita woodland	conifer woodland	CPC
3102	Knobcone pine/canyon live oak woodland	mixed evergreen woodland	CPC
3105	Knobcone pine/chamise woodland	conifer woodland	CPC
3110	Pinon pine woodland	conifer woodland	EPN
3112	Pinon pine/mountain mahogany/sagebrush woodland	conifer woodland	EPN
3113	Pinon pine/goosberry/sagebrush woodland	conifer woodland	EPN
3131	Western white pine/needlegrass woodland	conifer woodland	SCN

Table 2.2 (Continued)

	1997 Vegetation Survey type number and name	MC1 vegetation type	WHR
3140	Whitebark pine woodland	subalpine forest	SCN
3143	Whitebark pine/sedge woodland	subalpine forest	SCN
3147	Whitebark pine/mountain hemlock woodland	subalpine forest	SCN
3149	Whitebark pine/lodgepole pine/mountain hemlock krummholz forest	alpine	ADS
3150	Limber pine woodland	subalpine forest	SCN
4012	Douglas fir/canyon live oak forest	mixed evergreen forest	DFR
4014	Douglas fir/white alder forest	mixed evergreen forest	DFR
4020	Giant sequoia forest	montane conifer forest	SMC
4021	Giant sequoia/sugar pine/dogwood forest	montane conifer forest	SMC
4035	Mountain hemlock/western white pine/lodgepole pine forest	subalpine forest	SCN
4056	Ref fir/lodgepole pine forest	montane conifer forest	RFR
4069	Red fir/western white pine forest	montane conifer forest	RFR
4070	Red fir/white fir forest	montane conifer forest	RFR
4085	White fir forest	montane conifer forest	WFR
4100	Sierra juniper woodland	conifer woodland	JUN
4101	Sierra juniper/oceansprary woodland	conifer woodland	JUN
4107	Sierra juniper/mountain mahogany/sagebrush woodland	conifer woodland	JUN
4111	Incense cedar/white alder forest	mixed evergreen forest	MHC
4510	Western white pine/red fir/lodgepole pine forest	montane conifer forest	RFR
4520	White fir/red fir/sugar pine/jeffrey pine forest	montane conifer forest	WFR
4530	White fir/sugar pine/incense cedar/jeffrey pine forest	montane conifer forest	WFR
4550	Douglas fir/white fir/incense cedar/ponderosa pine forest	montane conifer forest	DFR
5021	Chamise	montane chaparral	CRC
5041	Interior live oak/buckeye	hardwood woodland	MHW
5060	Whitethorn chaparral	montane chaparral	MCP
5110	Whitethorn ceanothus	montane chaparral	MCP
5120	Tobacco brush	montane chaparral	MCP
5130	Mountain misery	montane chaparral	MCP
5160	Big sagebrush	sagebrush	SGB
5210	Low sagebrush	sagebrush	LSG
5230	Mountain mahogany woodland	montane chaparral	MCP
5240	Antelope bitterbrush	sagebrush	SGB
5250	Silver lupine/brome	montane chaparral	MCP
5260	Big sagebrush/silver sagebrush	sagebrush	SGB
5510	Mountain big sagebrush/timberline sagebrush/oceanspray	sagebrush	SGB
5560	Chamise/buckbrush/manzanita	montane chaparral	CRC
5570	Manzanita/chinquapin/huckleberry oak	montane chaparral	MCP
5580	Mountain mahogany/buckbrush/manzanita	montane chaparral	MCP
6010	Deerbrush	montane chaparral	MCP
6012	Deerbrush/manzanita	montane chaparral	MCP
6020	Oregon white oak	montane chaparral	MCP
6110	Sierra willow/swamp onion	montane chaparral	MCH

Table 2.2 (Continued)

1997 Vegetation Survey type number and name		MC1 vegetation type	WHR
6500	Willow/meadow shrubland	montane chaparral	MRI
6600	Willow riparian shrubland	montane chaparral	MRI
6700	Willow talus shrubland	montane chaparral	MCH
6900	Mesic montane shrubland	montane chaparral	MCP
7120	Shorthair sedge herbaceous	grassland	PGS
7260	California annual grassland	grassland	AGS
7550	Upland herbaceous	grassland	PGS
7701	Post-clearcut shrub/herbaceous	montane chaparral	MCH
7702	Mesic post-fire herbaceous	grassland	AGS
8000	Intermittantly to seasonally flooded meadow	meadow	WTM
9000	Semi-permanently to permanently flooded meadow	meadow	WTM

Secondly, the maps were resampled to the 800 m grid (table 2.4). Each grid cell was assigned the cover type from the polygon covering the largest amount of the grid cell. When two or more polygons with the same cover type overlapped the grid cell, the portions of their areas which overlapped the grid cell were added together and the sum treated as if it were from a single polygon. ESRI ArcGIS 9.3 software was used to do the resampling. Both original maps have ranges of polygon sizes (fig. 2.2). The 68 ha area of the 800-m gridcells was larger than most polygon areas in either of the historical surveys.

Details of the vegetation classification methods

Vegetation classification protocols and technology used for the 1997 survey are different from the protocols and technology used for the VTM survey. These differences are minimized here by reducing the different classes to a common smaller set of classes (WHR). Dr. James Thorne (U.C. Davis) provided a VTM polygon map for the Yosemite area with WHR classes already assigned. Bill Kuhn (NPS) provided the corresponding map from the 1997 survey.

The further aggregation of WHR classes into vegetation classes used by MC1 was performed by Bill Kuhn for the 1997 Survey map. I did the same for the VTM map. Both of us used the same basic aggregation scheme, but Kuhn's method also distinguished grassland polygons from subalpine meadows on the basis of a 5500 ft elevation threshold, and used the

Table 2.3 MC1 vegetation/land cover classes and corresponding classes from the California Wildlife Habitat Relationship (WHR) classification system (California Department of Fish and Game 2004).

MC1 vegetation type	California Wildlife Habitat Relationship type (WHR)
alpine vegetation	ADS Alpine Dwarf Shrub
subalpine forest	LPN Lodgepole Pine SCN Subalpine Conifer
montane conifer forest	ASP Aspen RFR Red Fir
conifer woodland	EPN Eastside Pine JPN Jeffrey Pine JUN Juniper
mixed forest	DFR Douglas Fir MHC Montane Hardwood - Conifer PPN Ponderosa Pine SMC Sierran Mixed Conifer WFR White Fir
hardwood forest	MHW Montane Hardwood MRI Montane Riparian
hardwood woodland	BOP Blue Oak - Foothill Pine BOW Black Oak Woodland VOW Valley Oak Woodland VRI Valley Foothill Riparian
sagebrush	LSG Low Sage SGB Sagebrush
chaparral	CRC Chamise - Redshank Chaparral MCH Mixed Chaparral MCP Montane Chaparral
subalpine meadow	PGS Perennial Grassland WTM Wet Meadow
natural barren	BAR Barren
water	FEW Fresh Emergent Wetland GLA Glacier LAC Lacustrine

vegetation type of neighboring polygons to infer the appropriate type for recently disturbed areas. I did not incorporate Kuhn's criteria when developing the VTM/MC1 crosswalk table. Grasslands and subalpine meadows are two of the smallest vegetation classes by area, so the absence of the elevation threshold for the VTM map did not affect the comparison.

Table 2.4 Characteristics of study grid over Yosemite National Park.

cell size	30” latitude x 30” longitude, ~920m x ~730m
northern edge, southern edge	38° 10’ 45” N, 37° 29’ 45” N
western edge, eastern edge	119° 53’ 15” W, 119° 12’ 15” W
area of cells in top row, bottom row (ha)	67, 68
number of rows, columns	82, 82
number of cells in grid	6,724
number of grid cells used in study	4,463
total area of cells used in study (ha)	303,105

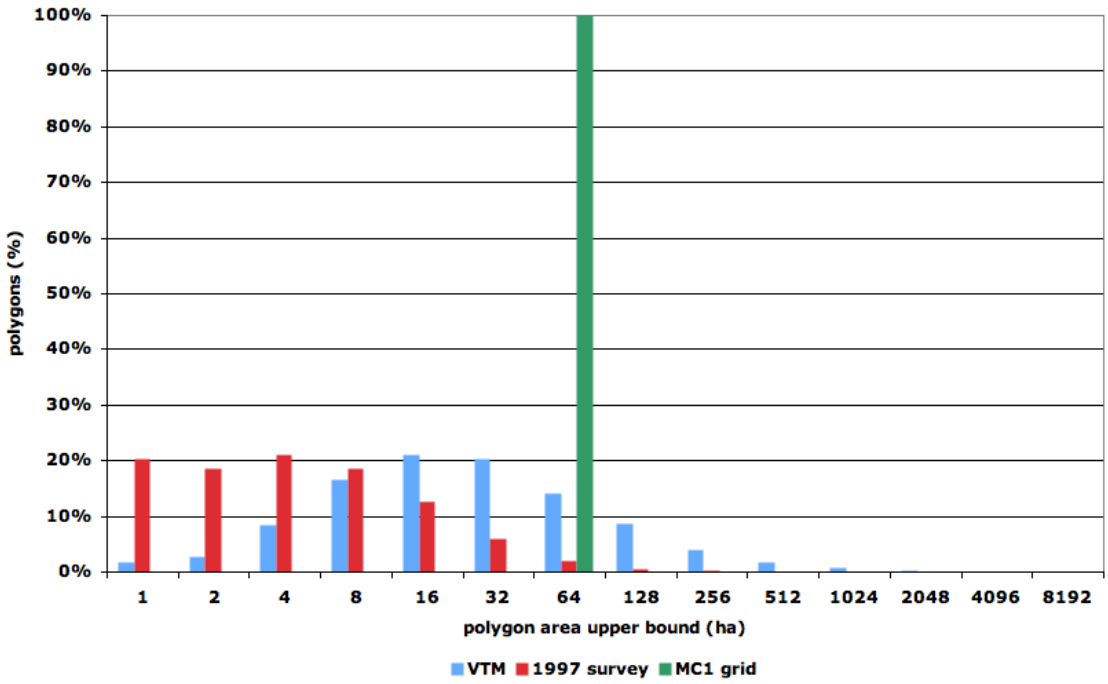

Fig. 2.2 Size distribution of polygons in the VTM and 1997 Survey vegetation maps and the MC1 800 m grid.

Allowing for georeferencing error and resampling distortion

The spatial accuracy of the VTM map (263 m) is lower than that of the 1997 survey map (Thorne et al. 2008). As a result, some differences between the final, gridded maps are due to misregistration of the original polygon maps. Resampling to the 800 m grid resulted in changes, by up to a few percent, in the area associated with different vegetation classes. Vegetation classes representing small fractions of the total area in the original polygon maps were affected the most (fig. 2.3). Note that the resampling error is independent of the georeferencing error. Conclusions about how much area is occupied by each vegetation type in the different time periods do not make use of information about where the area is located, so are unaffected by the location errors.

Both georeferencing errors and resampling distortions contribute to differences between gridded simulated vegetation types and gridded observed vegetation types. The intrinsic georeferencing error of the VTM data (263 m, Thorne et al. 2008) is a substantial fraction of the 800 m grain used for the comparison. Grid cells on the boundary between two vegetation polygons in the VTM data might be classified into either of the vegetation types as a result of georeferencing imprecision in the location of the boundary between the polygons.

To allow for the combined georeferencing error and resampling distortion when estimating the change in cover from any type A to any other type B, I took the smaller of the number of cells switching from A to B and the number switching from B to A. For example, 2.1% of the total area, which shows as barren land in the gridded VTM map, appears instead as subalpine forest in the gridded 1997 survey map. But another 2.5% of the total area in subalpine forest on the VTM map corresponds to barren land on the 1997 survey map. To be conservative, I took the trend of vegetation shift between subalpine forest and barren to be just 0.4% from subalpine forest in the 1930s to barren land in 1997, with the remaining 2.1% attributed to spatial misregistration. It is possible that this remaining small fraction reflects different standards used for classifying areas as barren in the two surveys, but I did not investigate this conjecture.

Fig. 2.3 Comparison between land fraction occupied by different vegetation classes on original and resampled vegetation maps: (a) VTM map, (b) 1997 survey map, (c) change in area occupied by each vegetation type, between the original polygon maps and the resampled maps.

Model description

The MC1 DGVM has been used in a number of studies at regional, continental, and global scales (e.g. Daly et al. 2000, Bachelet et al. 2003, Gonzalez et al. 2007). The original version of MC1 was described in detail in a lengthy USFS document (Bachelet et al. 2001b). Biogeochemical processes are simulated using a modified version of the CENTURY model (Parton et al. 1987, 1993). MC1 is currently being used by several researchers, and there is no canonical version of MC1 source code. The source code used for this study is recorded in the author's Subversion archive as version 136.

Model requirements

MC1 requires monthly values of precipitation, vapor pressure or dewpoint temperature, and temperature extrema. MC1 also requires non-temporal site data for each gridcell: elevation, latitude, soil depth, soil bulk density, and soil texture information for each of three soil layers. The non-temporal data for the 800m gridcells in YNP were obtained principally from an 800 m data set for most of California provided by the MAPSS (Mapped Atmosphere-Plant-Soil System) group of the USFS PNW Research Station.

Soil data

Using the initial soil data set (MAPSS team, pers. comm., Kern 1995 and 2000), MC1 simulated forests all across the Sierra Nevada crest, a result clearly inconsistent with the appearance of the high Sierra. Inspection of the soil data revealed deep soils in the data for many areas which are, in reality, mostly bare rock. The original soil depth layer appeared to have systematic errors. To fix the forests-on-bare-rock problem, unvegetated areas in the VTM and 1997 survey maps were used as masks to determine which gridcells to classify as barren. The simulations for 1905—1935 used the barren cells from the VTM survey, while the simulations for 1967—1997 use the barren cells from the 1997 survey, To correct the soil depth errors in vegetated areas, Dr. Gordon Godshalk (Alfred University, NY) developed an improved soil depth data layer for our study site, derived from the soil data available on

Pennsylvania State University's website[3] (Miller & White 1998). An attempt to improve the soil depth and texture by making use of the CA790 soil data from the US Dept. of Agriculture website for the Natural Resources Conservation Service was not successful. Jeff Kern (Eugene, OR) converted the CA790 data into the format needed by MC1. Whereas the original soil data did not have enough rocky areas, the CA790 soil data classified the majority of the Park as rocky outcrops (fig. 2.4).

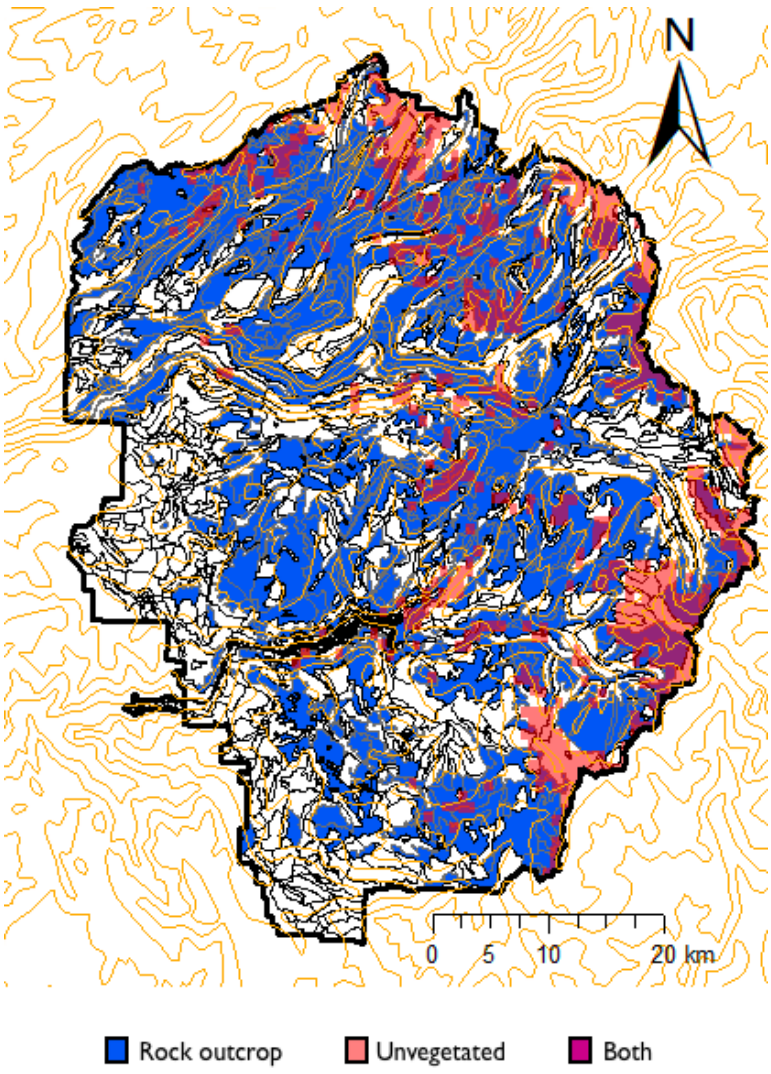

Fig. 2.4 Rock outcrops in Yosemite National Park as described by the CA790 soil survey (http://www.soilinfo.psu.edu) compared to the unvegetated areas in the 1997 NPS Survey.

[3] http://www.soilinfo.psu.edu/index.cgi?-soil_data&conus

Nitrogen availability

MC1 constrains the C:N ratio of live plant parts to prescribed ranges. When live biomass is increasing, MC1 transfers N from soil pools to biomass. When soil N is insufficient, MC1 has two options. In its "limited nitrogen" mode, MC1 curtails the increase in biomass to an amount for which nitrogen from the soil pool and atmospheric deposition is sufficient to keep the C:N ratio within the prescribed range; in other words, N limits growth. In its "unlimited nitrogen" mode, MC1 assumes there is sufficient additional N available from biological fixation to maintain the C:N ratio within its prescribed range in the new growth. All the simulations for this study have been run in unlimited nitrogen mode.

Biogeography rules

A set of biogeography rules in the MC1 model take climate and leaf area into account to determine vegetation type. Three important variables which are used by the biogeography rules are growing degree-days above 0°C, a temperature index, and the projected leaf area index of any woody vegetation. The temperature index ranges from -100 to +100, and is used to characterize the type of woody vegetation across a spectrum from pure needleleaf (-100) to pure broadleaf (+100). Intermediate values represent mixtures of types. The calculation of the index is based on where the minimum mean monthly temperature falls in the range -15°C to +18°C. A more detailed account of the biogeography rules is given in chapter 4.

Fire model

The fire model calculates rate of spread, Buildup Index[4] (BUI), and Fine Fuel Moisture Code[5] (FFMC) on a daily timestep. A fire is simulated when FFMC is greater than or equal to

[4] The Buildup Index (BUI) was part of the 1964 National Fire Danger Rating System (NFDRS). It is defined as "a number that reflects the combined cumulative effects of daily drying and precipitation in fuels with a 10 day time lag constant".

[5] The Fine Fuel Moisture Code (FFMC) is a numerical rating of the moisture content of litter and other cured fine fuels. This is made up mostly of dead and down needles and leaves, as

87 and BUI is greater than or equal to 290 for needleleaf woody vegetation, 310 for mixed woody vegetation, or 270 for broadleaf woody vegetation. The threshold values for BUI and FFMC were calibrated in a recent statewide California study (Panek et al. 2008). Only one fire per simulation year per cell is simulated. The operation of the fire model has been summarized in a number of papers (e.g. Lenihan et al. 2008a, 2008b). A complete description of an earlier but similar version of the fire model exists as a lengthy, unpublished document (Lenihan et al. 2006b).

Other MC1 versions

To compare results from calibration at coarse scale with calibration using fine scale observations, the latest available version of MC1 calibrated for North America, obtained from Dr. James Lenihan (USFS MAPSS group) on June 5, 2009, was run on the 800 m gridcells within the Yosemite Park boundary. In addition, the source code for my version 136 of MC1 was compared to the source code for the North America version (Lenihan, pers. comm.) and to a variant of the North America version developed for simulations of the Pacific Northwest (Rogers 2009). While investigating discrepancies between simulated fire and actual fire in Yosemite, I also did a spot check comparison of the threshold values for the BUI and the FFMC in the fire occurrence algorithm, between my MC1 version and a third variant of the North America version being used by Maureen McGlinchy (M.S. student, OSU, Dept. of Forest Ecology and Society) for simulations of northern and central California. My version 136, together with the unnamed versions of Lenihan, Rogers, and McGlinchy, account for most of the known MC1 versions in active use at this time.

Results

Climate

The climate data used to drive the MC1 model for Yosemite is the result of work by the PRISM group, not a result of this study. This study makes use of only a very small fraction of the PRISM group's 800 m climate data set for the conterminous United States (fig. 2.5).

---

well as lichens, mosses and other small, loose debris. The FFMC is an indicator of the relative ease of ignition and flammability of fine fuel.

Fig. 2.5 Climatic averages across Yosemite National Park for the period 1895-2006: (a) climograph, (b) average daily minimum temperature for the entire year, (c) average daily maximum temperature for the entire year, (d) growing degree-days (above 0°C), (e) annual precipitation, (f) annual average vapor pressure deficit, and (g) average daily mean temperature in the coldest month of the year. (PRISM climate data, Daly et al. 2008)

Figure 2.5

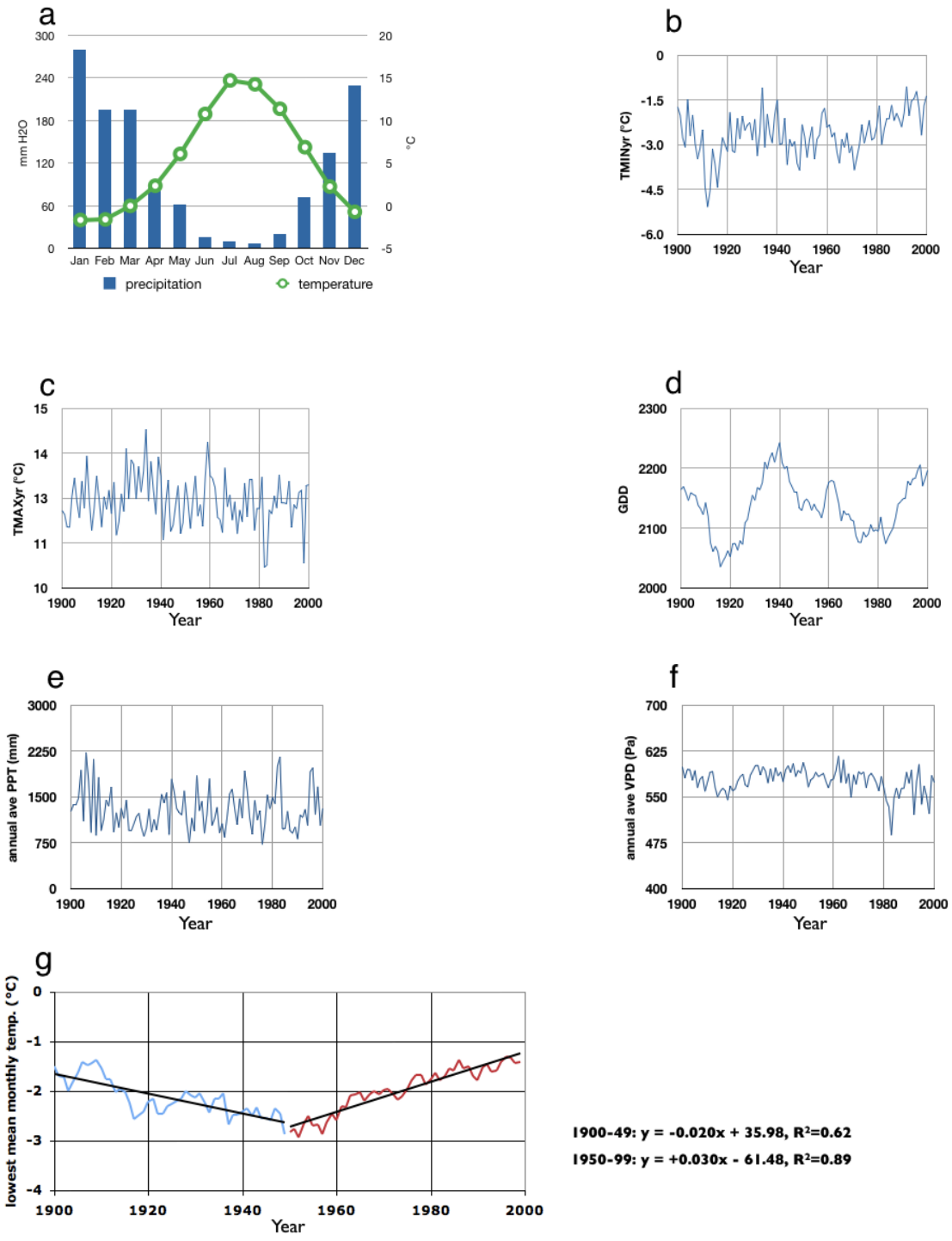
a
mm H2O
°C
Jan Feb Mar Apr May Jun Jul Aug Sep Oct Nov Dec
precipitation
temperature
b
TMINyr (°C)
Year
c
TMAXyr (°C)
Year
d
GDD
Year
e
annual ave PPT (mm)
Year
f
annual ave VPD (Pa)
Year
g
lowest mean monthly temp. (°C)
Year
1900-49: y = -0.020x + 35.98, R²=0.62
1950-99: y = +0.030x - 61.48, R²=0.89

The narrow geographic focus of this study makes possible a more detailed analysis of the PRISM climate data than has been done previously. The analysis itself, limited as it is in geographic scope to Yosemite National Park, is appropriately regarded as a result of this study.

For the 20th century as a whole, there is no meaningful linear trend in the average temperature of the coldest month (a.k.a. lowest mean monthly temperature, minT, fig. 2.5g). Instead, there is a downward trend in the first half of the century (slope = -0.02°C yr^{-1}, r^2 = 0.62) followed by an upward trend in the second half (slope = +0.03°C yr^{-1}, r^2 = 0.89). The annual average monthly minimum temperature (TMIN) also shows an upward trend in the late 20^{th} century, but shows a different pattern than the lowest mean monthly temperature in the first part of the century and instead of the downward trend there are only a few years of colder weather in 1911-16 (fig. 2.5b). The linear fit to 20th century monthly minimum temperatures is poor (r^2 = 0.13). The annual average of monthly maximum temperature shows no linear trend (TMAX , fig. 2.5c). There is no linear trend in growing degree-days, but the two periods 1905—1935 and 1967—1997 have lower values relative to the rest of the century (GDD, fig. 2.5d). Neither precipitation nor vapor pressure deficit shows any trend during the 20th century (figs. 2.5e and 2.5f).

Despite the lack of statistically significant centennial-scale trends, there were some small differences in climate between the 1905—1935 period and the 1967—1997 period. For YNP as a whole, the 1967—1997 period had slightly warmer minimum temperatures (TMIN changed by +0.6°C) and slightly cooler maximum temperatures (TMAX changed by -0.4°C). The maximum temperatures decreased everywhere in the Park (TMAX, fig. 2.6a). The minimum temperatures increased by small amounts nearly everywhere, with larger increases of ≥1°C in Yosemite Valley, along the Hetch Hetchy reservoir, and near the Badger Pass ski area. A few small areas in the southeast and at the southern tip of the Park had minor decreases in minimum temperatures (TMIN , fig. 2.6b). Precipitation in the Park increased by 6%, from 1230 to 1301 mm yr^{-1}, but the spatial variation was considerable, ranging from increases of up to 181 mm in the central part, west of the Sierra crest, to decreases of 297 mm in the eastern tip of the Park along the crest itself (fig. 2.7a). Average annual vapor pressure deficit decreased by 2%, from 577 to 566 Pa, but, as for precipitation, the spatial variation was large relative to the average change, ranging from increases up to 25 Pa in the central area to decreases of 60 Pa in the southern tip and the northwestern part of the Park (fig. 2.7b). Growing-degree-days increased on average by less than 1%, from 2110 to 2121 degree-days. Increases in local areas, especially Yosemite Valley, ranged as high as 187

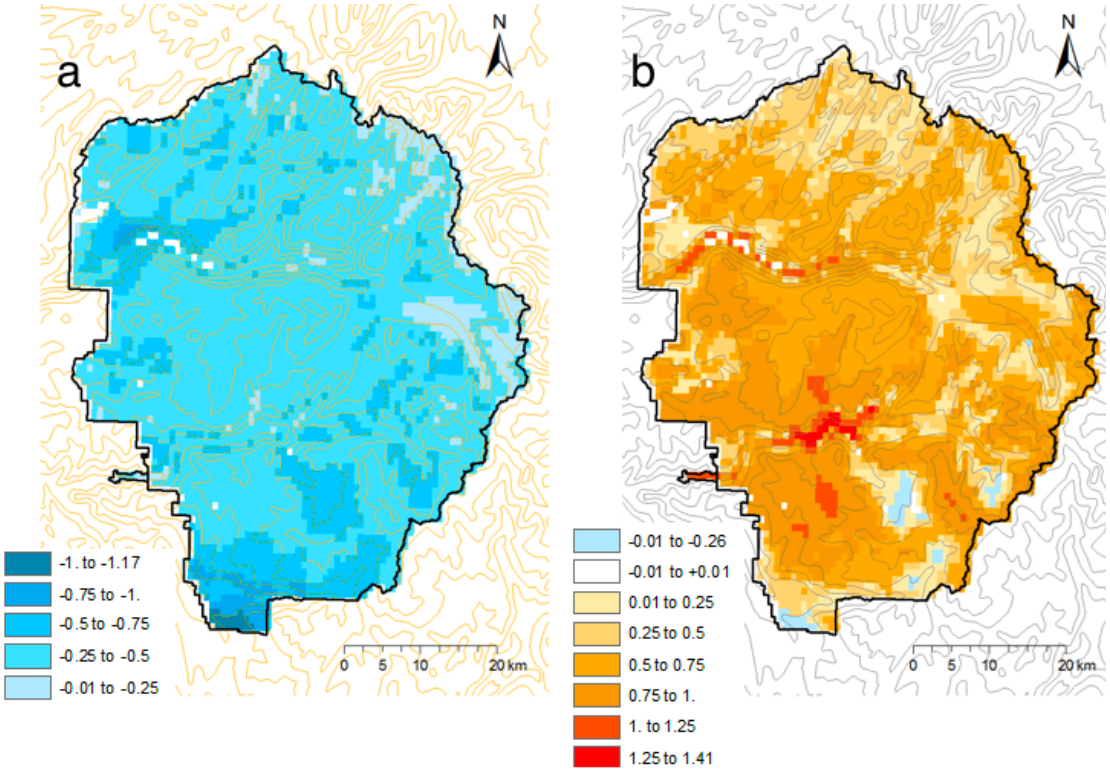

Fig. 2.6 (a) Decreases in maximum and (b) increases and decreases in minimum monthly temperatures (°C) between 1905—1935 and 1967—1997. (PRISM climate data, Daly et al. 2008)

degree-days; there were also extensive areas where the growing degree sum dropped by up to 144 degree-days (fig 2.7c). There is no significant temporal trend in the spatially averaged value of the first snowfree month ($y = -0.0044*(x-1895) + 7.21$, $R^2 = 0.02$).

In the PRISM climate data for YNP in the 20th century as a whole, the climate change signal, if any, is small relative to interannual and interdecadal variation, and relative to the natural range of variation experienced by long-lived forest trees. Similarly, although the climate averages for the 1967—1997 period were slightly different from the averages for the 1905—1935 period, the differences are small compared to the spatial variation in the differences, especially for precipitation, vapor pressure deficit, and growing degree days.

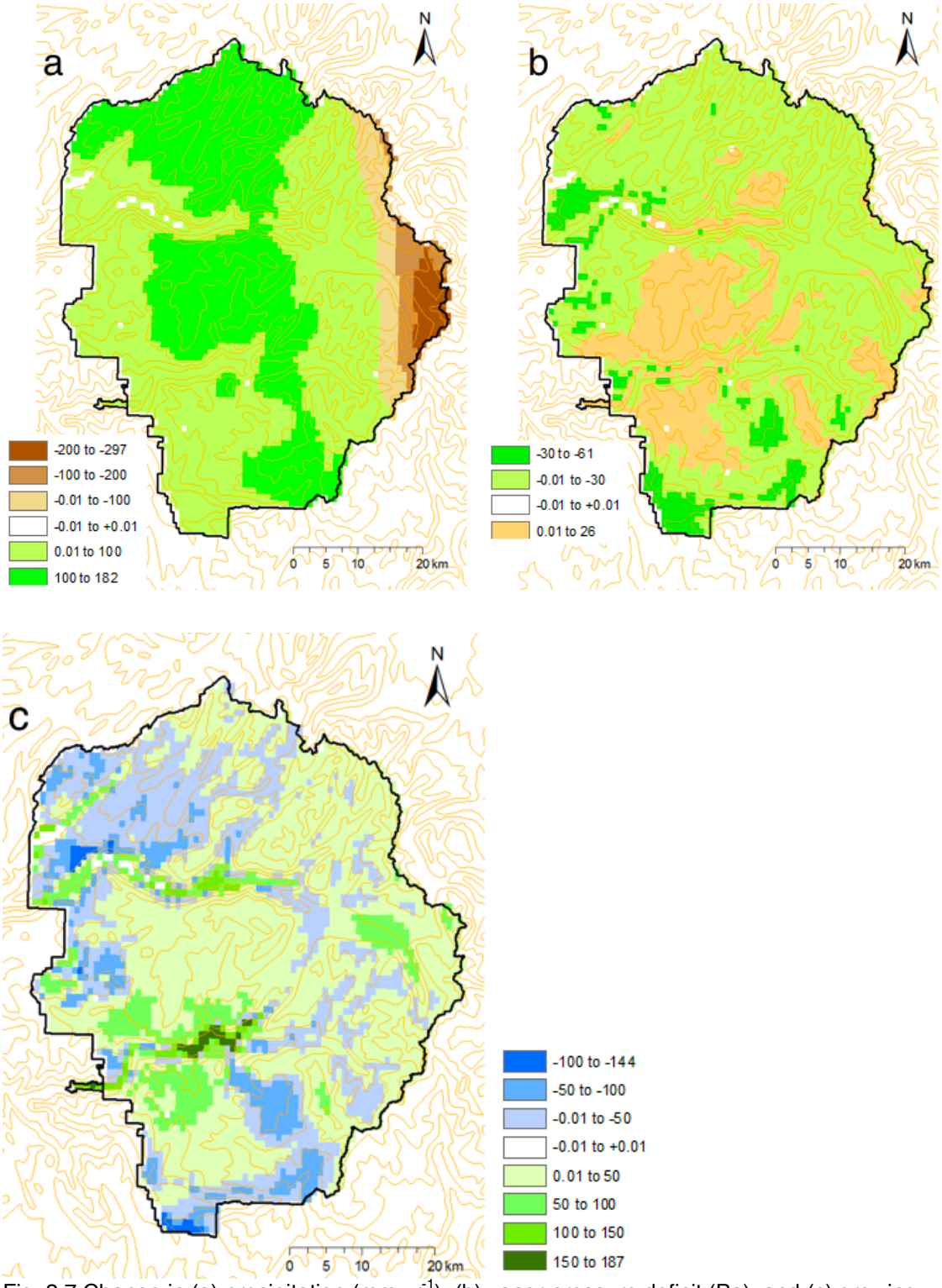

Fig. 2.7 Change in (a) precipitation (mm yr^{-1}), (b) vapor pressure deficit (Pa), and (c) growing degree-days (above 0°C), between 1905—1935 and 1967—1997. (PRISM climate data, Daly et al. 2008)

Observed and simulated vegetation shifts

When translated into MC1's land cover types and resampled to the 800 m grid, the VTM and 1997 Survey vegetation types were different on 38% of the Park area (fig. 2.8). Resampling the survey polygons to the 800 m grid changed the land fractions associated with vegetation types (figs. 2.3a and 2.3b). The areas associated with the three most common vegetation types (subalpine forest, montane conifer forest, and mixed forest) increased, and the areas associated with the least common types (chaparral, subalpine meadow, hardwood forest, and sagebrush) decreased. The resampling process resulted in a distortion of the differences between the VTM and 1997 surveys since sampling at coarser spatial resolution fails to distinguish the finer details. It serves as a caution that the gridded observations cannot be relied on for quantitative conclusions about the less common vegetation types.

In the 1930s, 37% of the Park was covered by subalpine forest, and only 12% by montane conifer forest. By 1997, the relative fractions had reversed: 28% of the Park was montane conifer forest, and only 25% remained in subalpine forest (fig. 2.9). Of the 16% of total area classified as montane conifer forest in the 1997 Survey but not in VTM, the majority (10% of total area) was classified as subalpine forest on the VTM map; other vegetation type switches were smaller in terms of total area (fig. 2.10).

Applying the allowance for georeferencing imprecision to the switch between subalpine forest and montane conifer forest has only a minor effect: while 13.5% of the cells switched from subalpine forest in the VTM map to montane conifer forest in the 1997 survey map, only 0.1% of all the cells switched the other way. When all the switches are thus adjusted, the total change is reduced from 38% of the Park area to 27%, with only four switches involving more than 1% of the Park area: from subalpine forest to montane conifer forest (10.3%), from conifer woodland to montane conifer forest (2.9%), from mixed forest to montane conifer forest (2.3%), and from subalpine forest to conifer woodland (1.2%).

The switch from subalpine forest to montane conifer forest

To understand the mechanism of the 10% switch from subalpine forest to montane conifer forest, gridded maps at the WHR level of cover type aggregation were compared. After applying the allowance for georeferencing imprecision, 10% of the Park area had switched from the WHR lodgepole pine (LPN) class to the WHR red fir (RFR) class. The two species are in multiple classes in the original classification schemes used in the 1930s data and

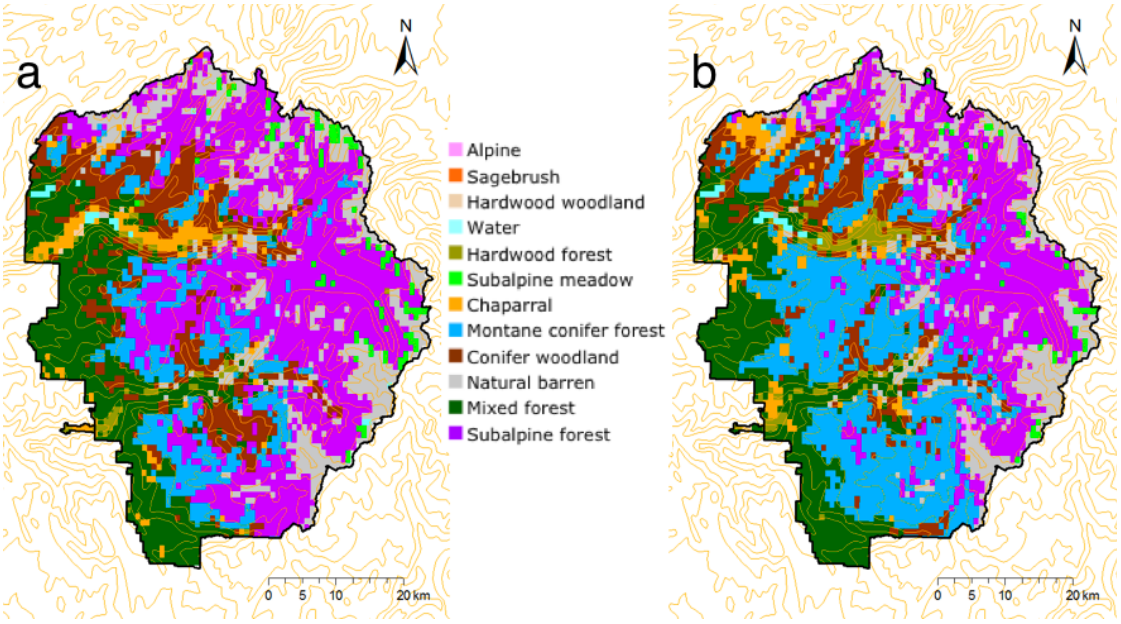

Fig. 2.8 Observed vegetation types, as resampled to the 30 arc-second grid: (a) Wieslander VTM for 1935, (b) 1997 NPS Survey.

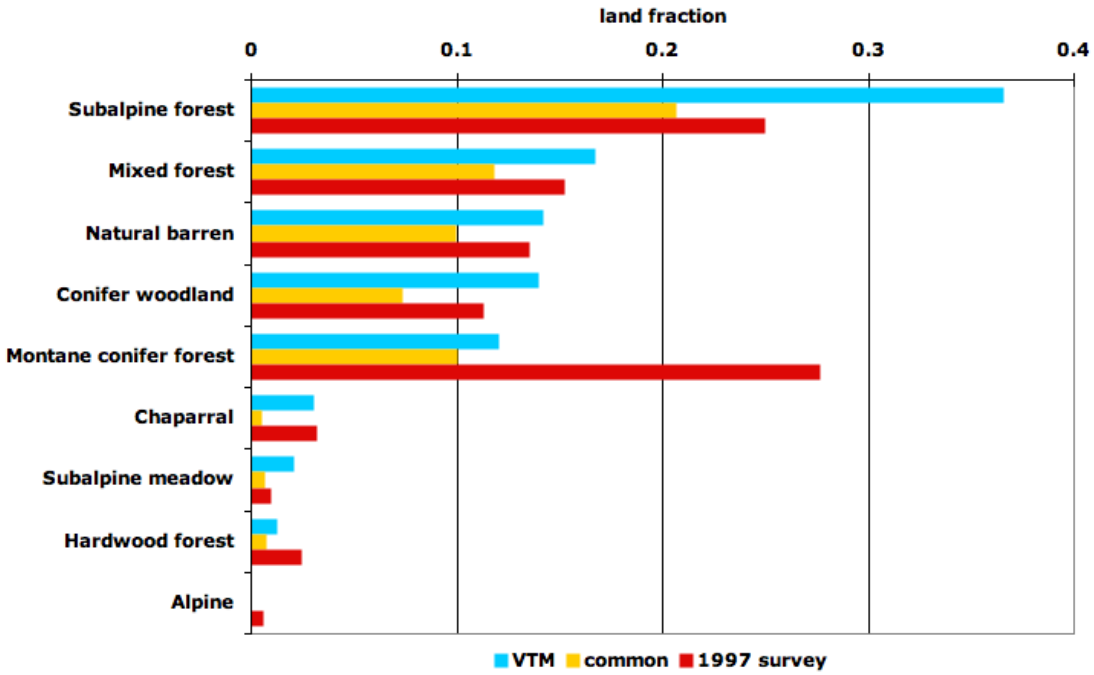

Fig. 2.9 Vegetation land cover fractions within the boundaries of Yosemite National Park included in VTM (Thorne et al. 2006), the 1997 NPS Survey map (Aerial Information Systems 1997), and that are common to both maps.

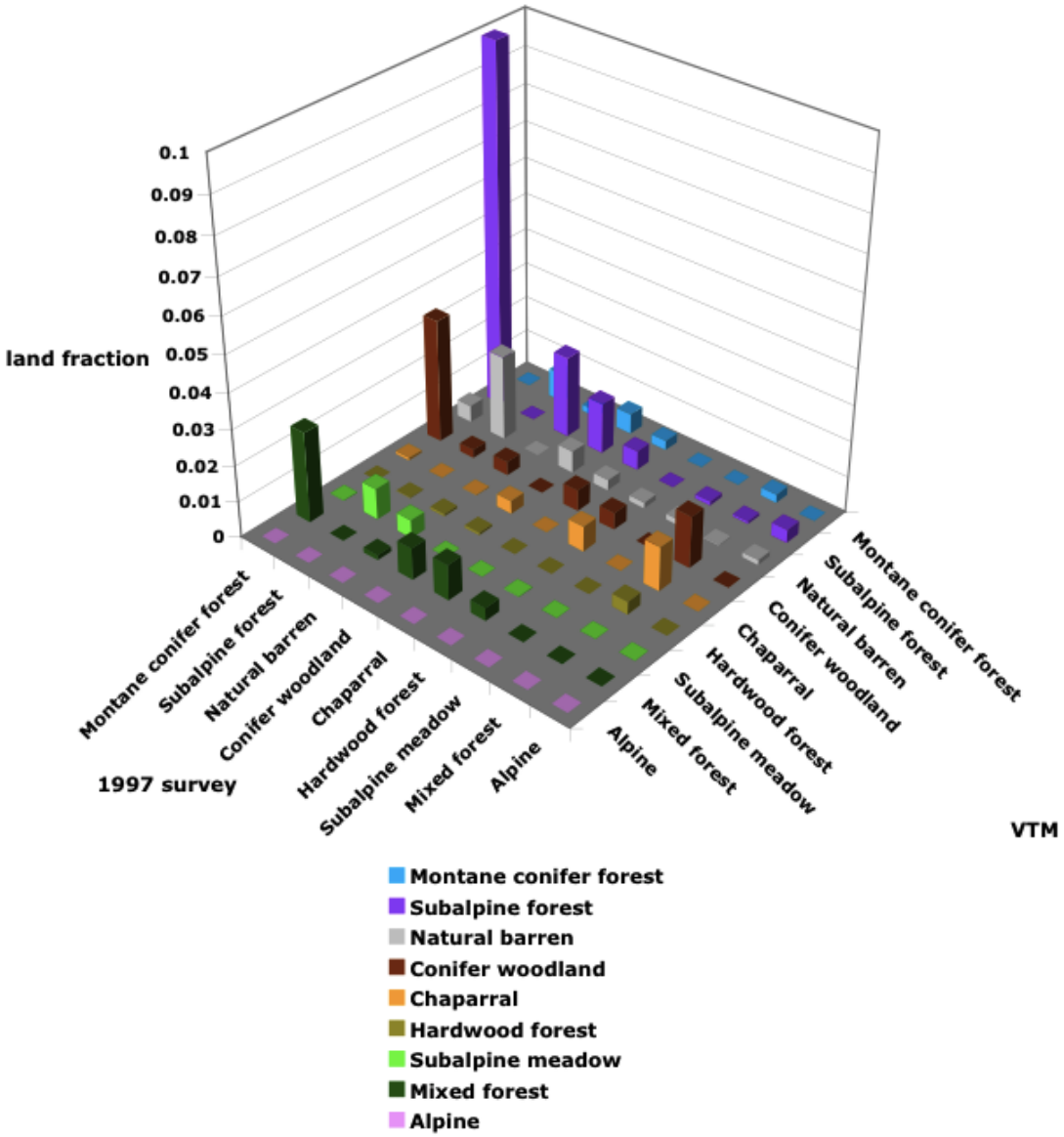

Fig. 2.10 Differences in vegetation type land fractions between the VTM vegetation distribution (Thorne et al. 2006) and the 1997 NPS Survey vegetation distribution (Aerial Information Systems 1997).

the 1997 survey. Maps were made to show, for each time period, which polygons had red fir (*Abies magnifica*), which had lodgepole pine (*Pinus contorta*), and which had both, based on the original species lists for the polygons (fig. 2.11). Visual comparison of these maps shows that the area of overlap between the two species has increased in size, growing towards the northeast, upslope.

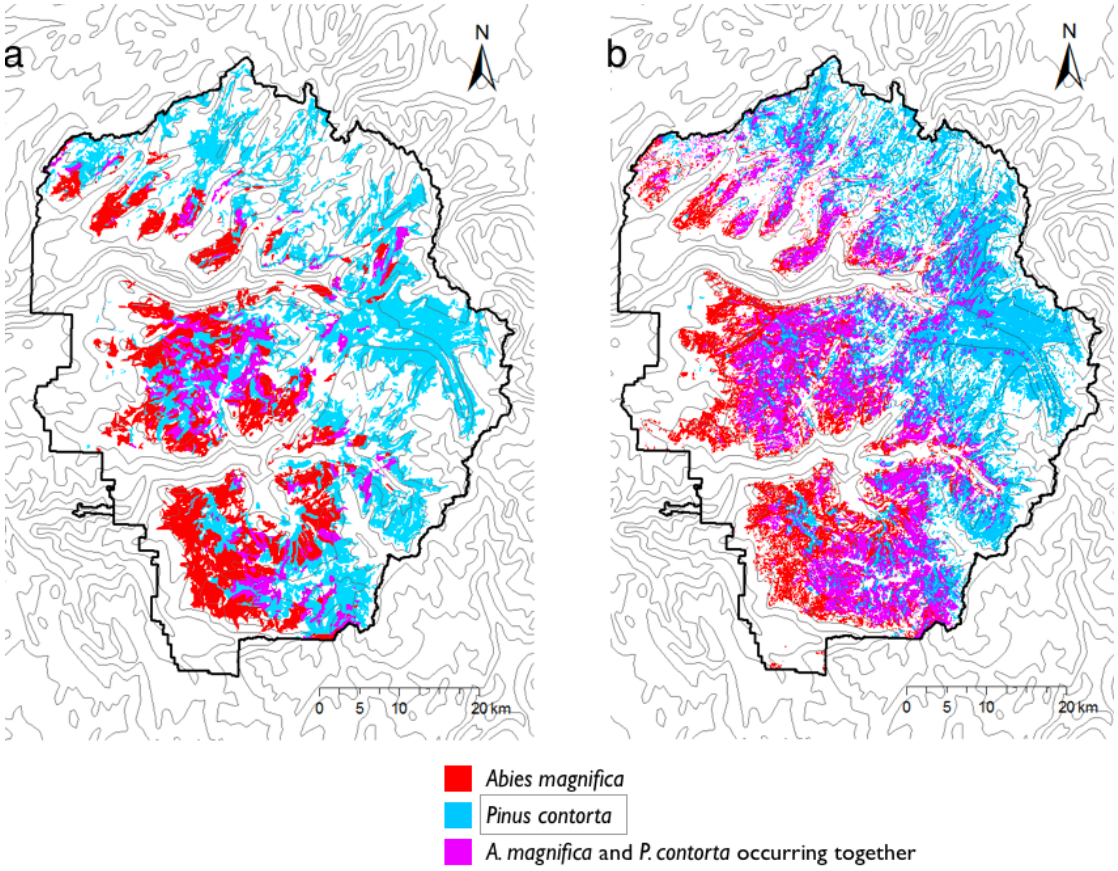

Fig. 2.11 Occurrence of red fir (*Abies magnifica*) and lodgepole pine (*Pinus contorta*) in (a) VTM original map (Thorne et al. 2006) and (b) 1997 NPS Survey original map (Aerial Information Systems 1997).

Comparison of simulated vegetation types to survey vegetation types: 1905—1935

Forty percent of the cells have different vegetation types in the MC1 map of modal vegetation types for 1905—1935, compared to the VTM map (figs. 2.12-14). After adjusting

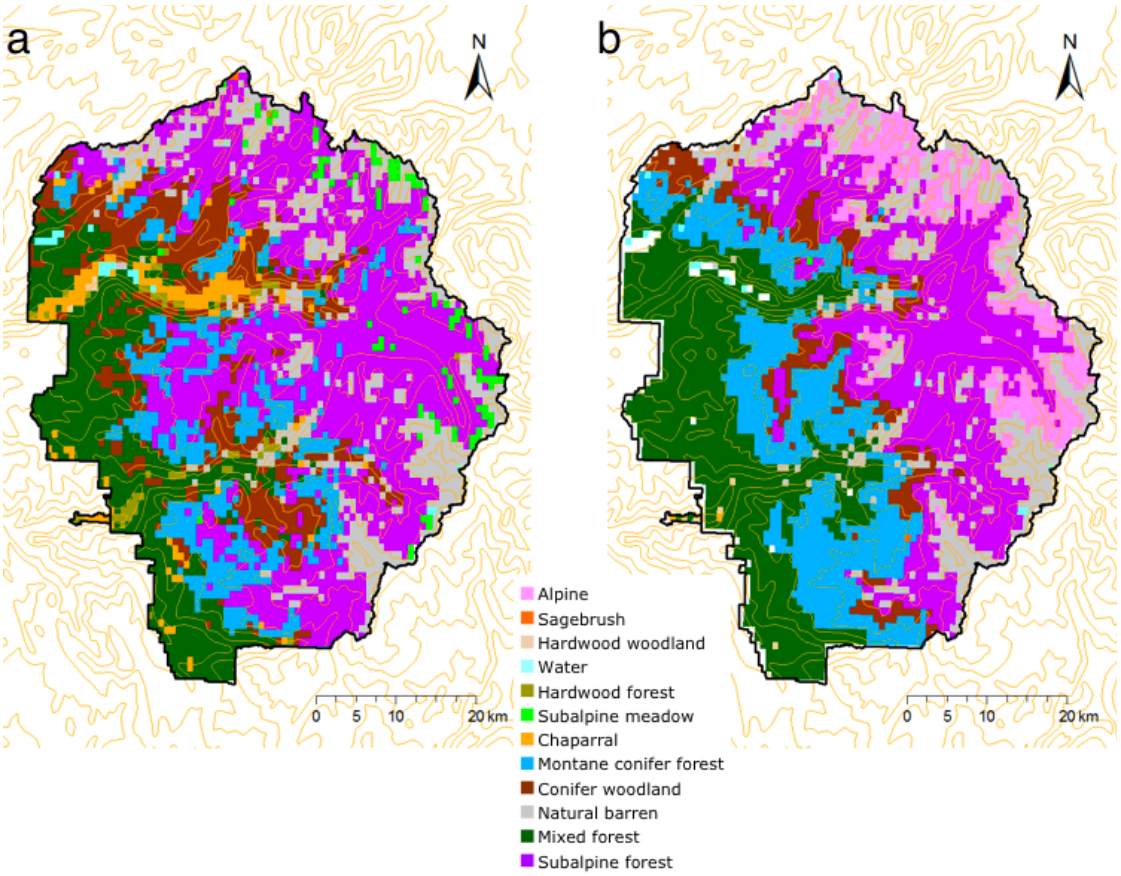

Fig. 2.12 Vegetation distribution maps: (a) VTM survey (Thorne et al. 2006), (b) MC1 modal simulated vegetation for 1905—1935.

for georeferencing error and resampling distortion by removing offsetting changes, there is a remaining difference of 26%.

9.7% percent of the MC1 map for 1905—1935 is classified as alpine, but the VTM map has no alpine vegetation at all. The absence of alpine vegetation in the VTM map does not mean that there was no alpine vegetation at the time of the VTM survey, but is instead a result of the translation of the original VTM vegetation classes into WHR classes. None of the original VTM classes were associated with the WHR alpine class, in the translation used by Thorne et al. (2006). Most of the MC1 alpine cells correspond to VTM subalpine forest cells, and of the rest, nearly all correspond to VTM subalpine meadow cells. None of this difference is attributable to georeferencing inaccuracy.

After allowing for georeferencing inaccuracy, resampling distortion, and the absence of the alpine vegetation class in the VTM map, there is an estimated residual difference of

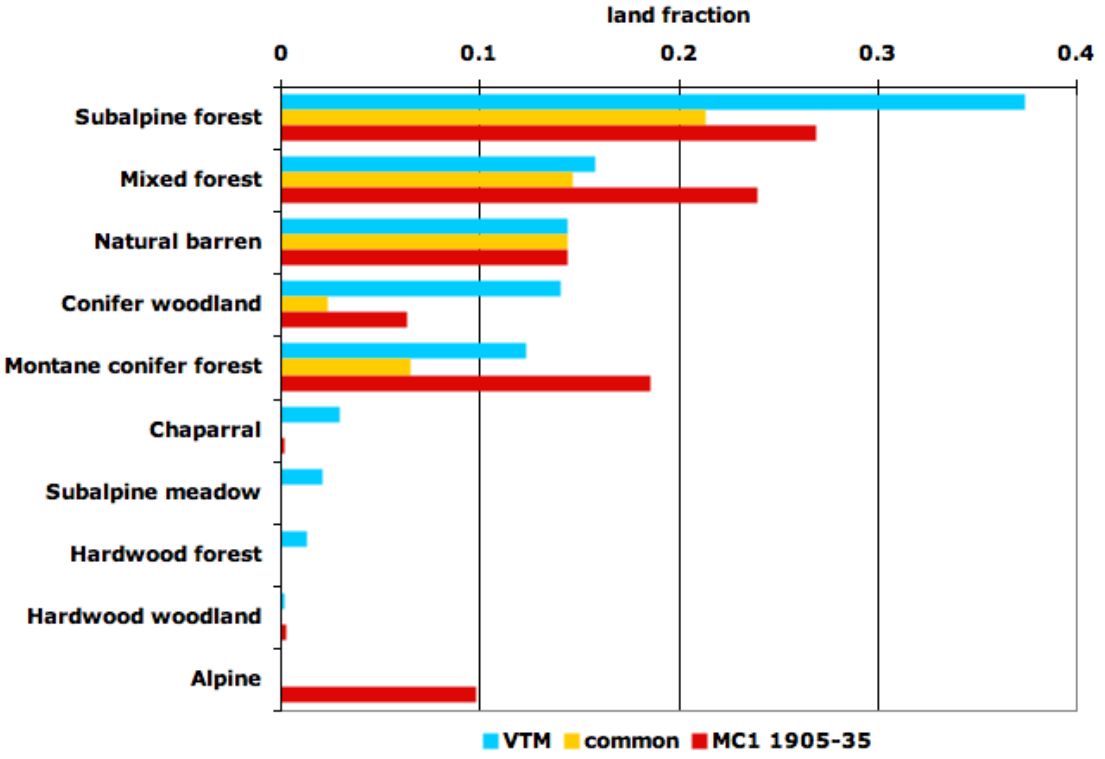

Fig. 2.13 Vegetation land cover fractions within the boundaries of Yosemite National Park included in VTM observed vegetation distribution map (Thorne et al. 2006), in the map of simulated potential vegetation for 1905—1935, and that are common to both maps.

16%. Most of this consists of cells which are identified as conifer woodland on the VTM map, but as forest (5% montane conifer forest, 4% mixed forest, 2% subalpine forest) on the simulated vegetation map (fig. 2.14).

Comparison of simulated vegetation types to survey vegetation types: 1967—1997

Forty-six percent of the cells have different vegetation types in the 1997 survey map than in the simulated map of modal vegetation types for 1967—1997 (figs. 2.15-17). Georeferencing inaccuracies are not expected to have contributed to the differences between the maps. Nevertheless, applying the method described above for estimating the effect of georeferencing inaccuracy reduces the percentage of cells with different vegetation types from 46% to 38%. We interpret the bidirectional switches in this case as resulting from resampling the 46,528 polygons of the 1997 survey into the 4,463 grid cells used by the model MC1.

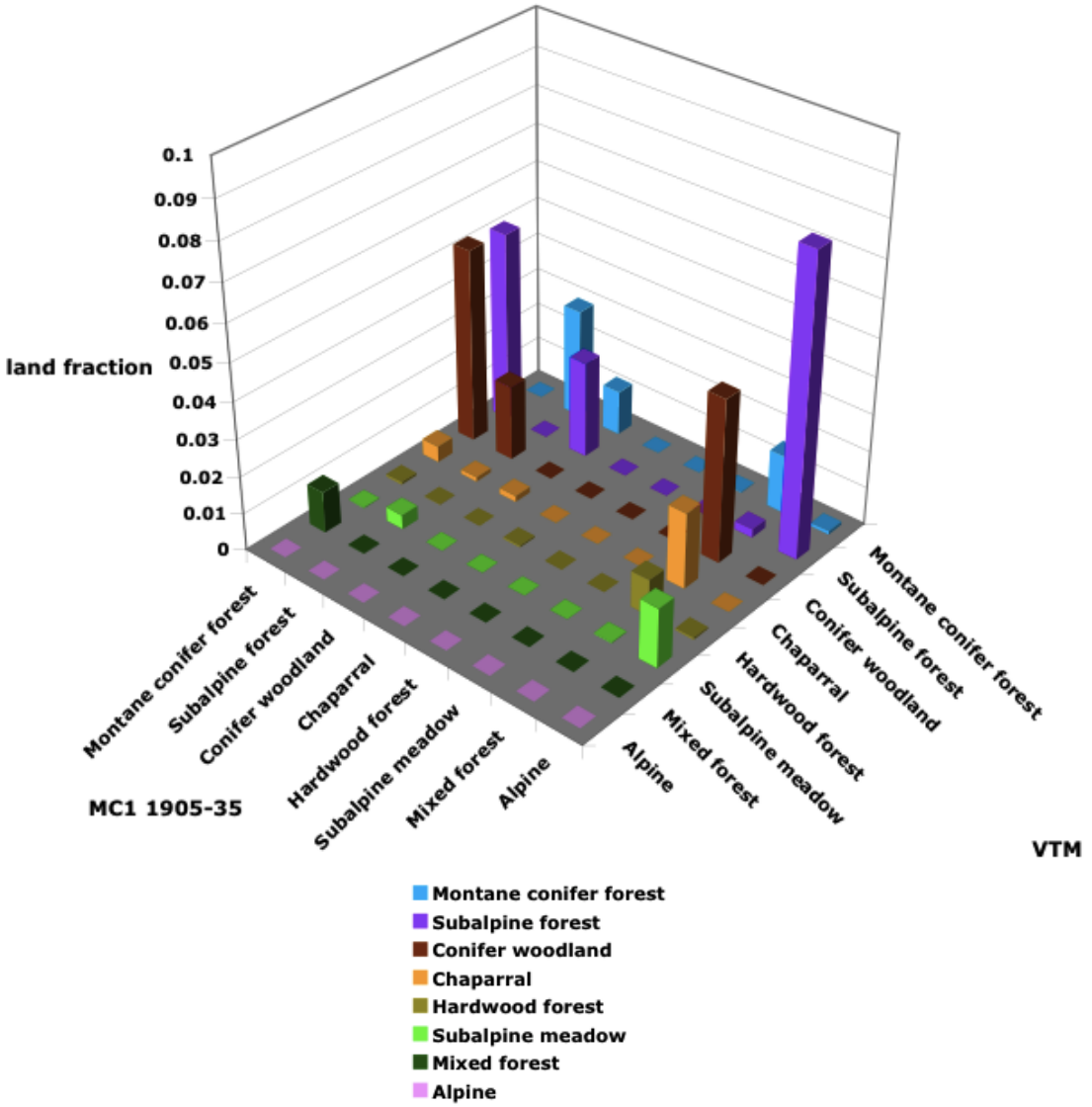

Fig. 2.14 Differences between the observed VTM vegetation distribution (Thorne et al. 2006) and the MC1 simulated vegetation distribution for 1905—1935.

Two kinds of difference account for most of the discrepancy between the 2 maps. 16% of the total area is classified as montane conifer forest in the 1997 survey, while it is classified as another kind of forest in the simulation results (about equally into subalpine forest and mixed forest). 8% of the total area is classified as subalpine forest in the 1997 survey, and classified as alpine in the simulation results. There are 25 other smaller pairwise net differences, summing to 14% of the total area, with a median size of 0.14% of the total area.

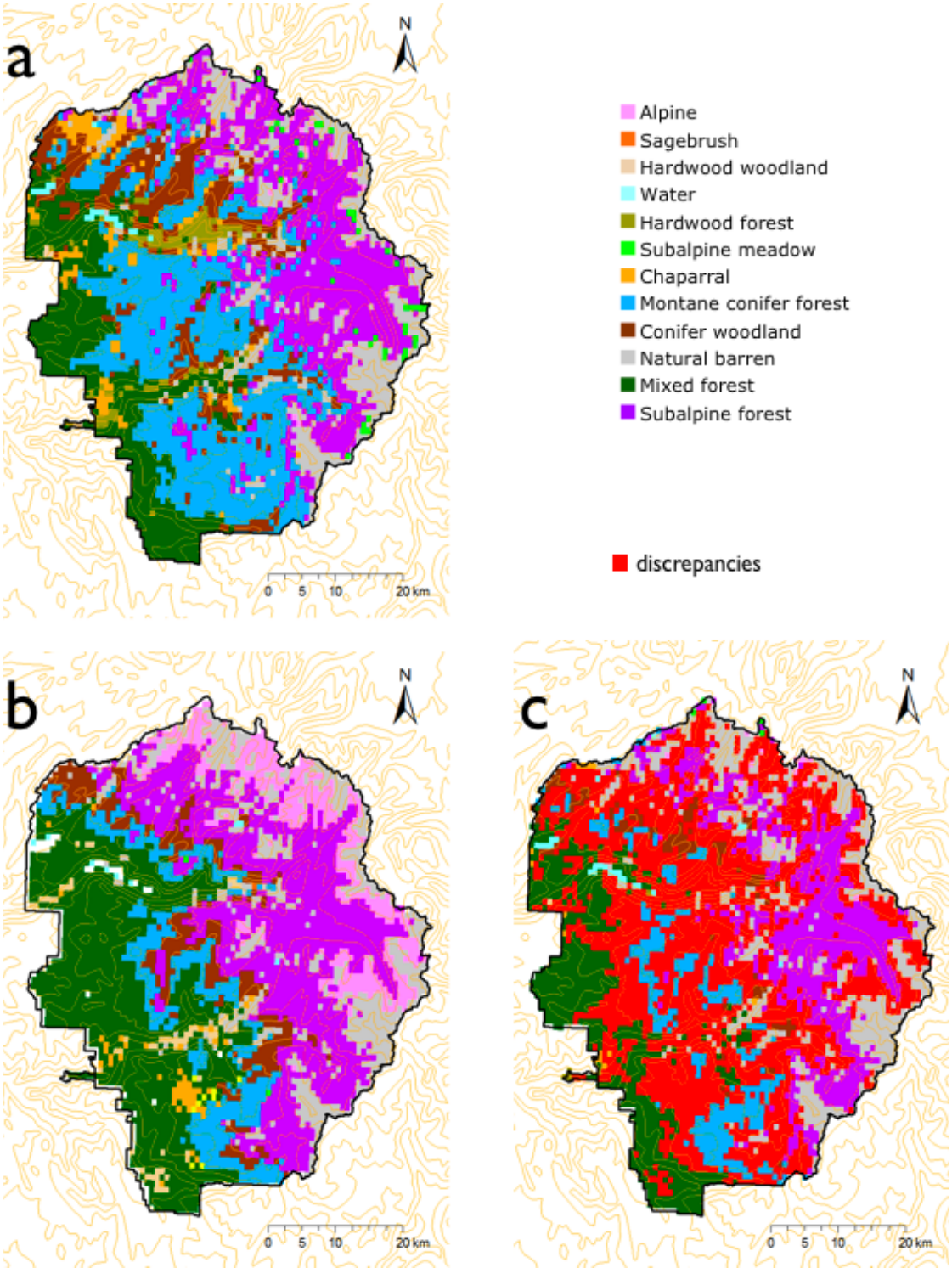

Fig. 2.15 (a) 1997 NPS Survey vegetation map (Aerial Information Systems 1997) and (b) MC1 modal simulated vegetation for 1967—1997, (c) discrepancies between observations and simulation.

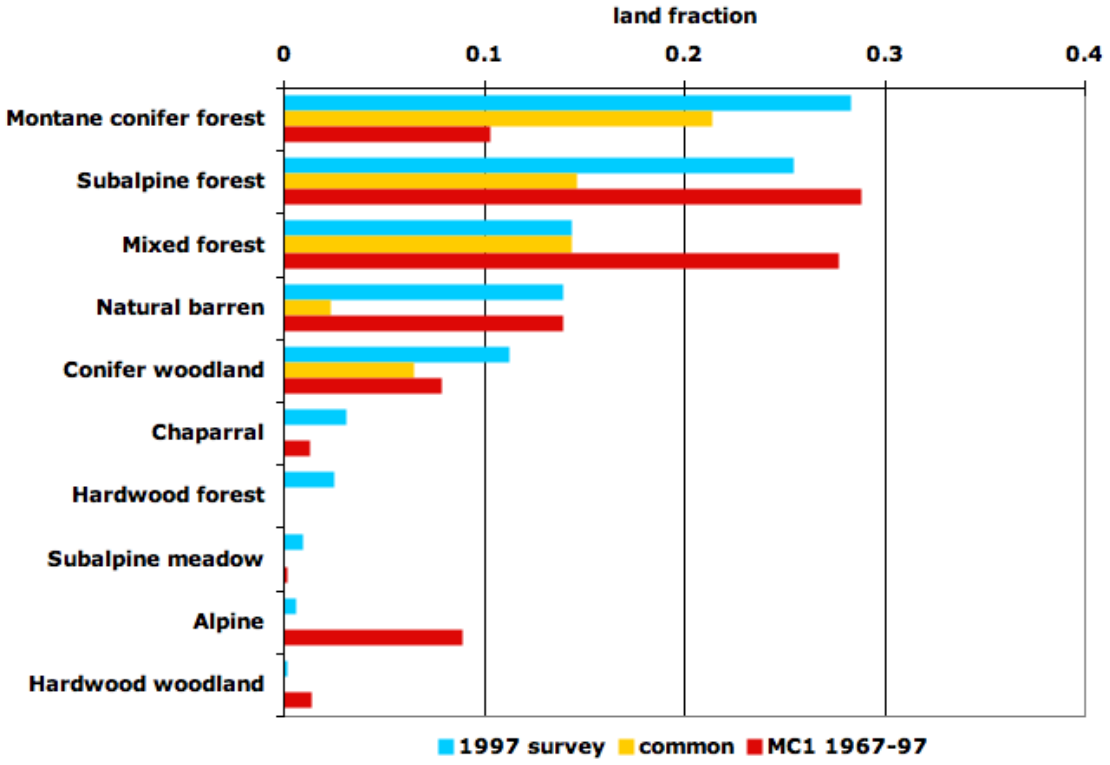

Fig. 2.16 Vegetation land cover fractions within the boundaries of Yosemite National Park included in the 1997 NPS Survey vegetation map (Aerial Information Systems 1997), included in the map of simulated potential vegetation for the 1967—1997 period, and that are common to both maps.

Simulation of vegetation change

Only 12% of the cells have different vegetation types between the simulated vegetation maps for 1967—1997 map versus 1905—1935 (figs. 2.18-20). Only two vegetation type changes amount to appreciably more than one percent of the cells, and both of these are unidirectional. 5.3% of the cells are classified as montane conifer forest on the 1905—1935 map, while they are classified as mixed forest class on the 1967—1997 map. An additional 1.7% of cells are in the montane conifer forest class in 1905—1935, but in the conifer woodland class in 1967—1997. There are no cells in the mixed forest or conifer woodland classes in 1905—1935 that switch to the montane conifer forest class in 1967—1997.

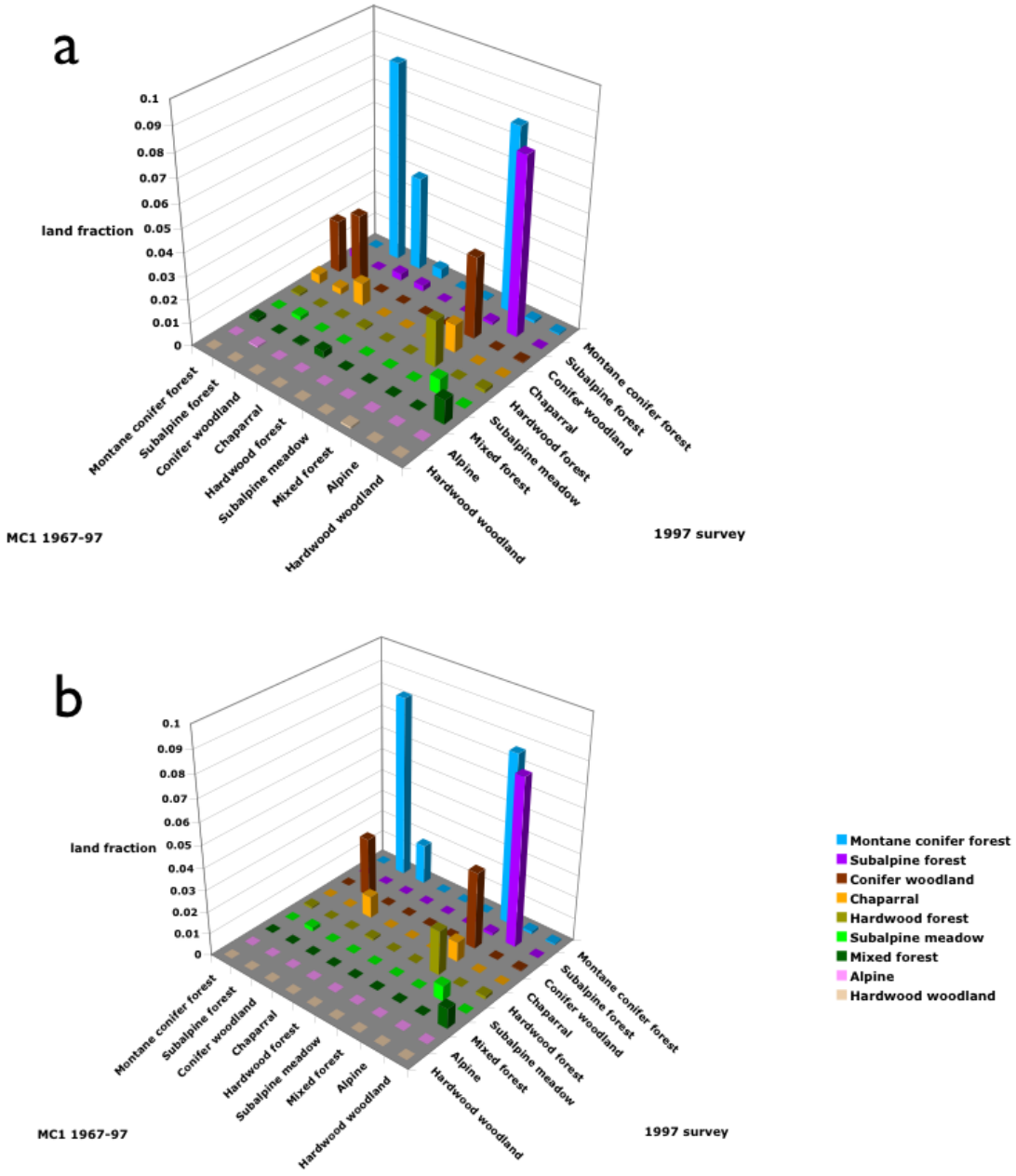

Fig. 2.17 Differences between the 1997 NPS Survey vegetation map (Aerial Information Systems 1997) and the MC1 modal simulated vegetation map for 1967—1997: (a) gross differences; (b) net differences after removing offsetting shifts attributed to the resampling process.

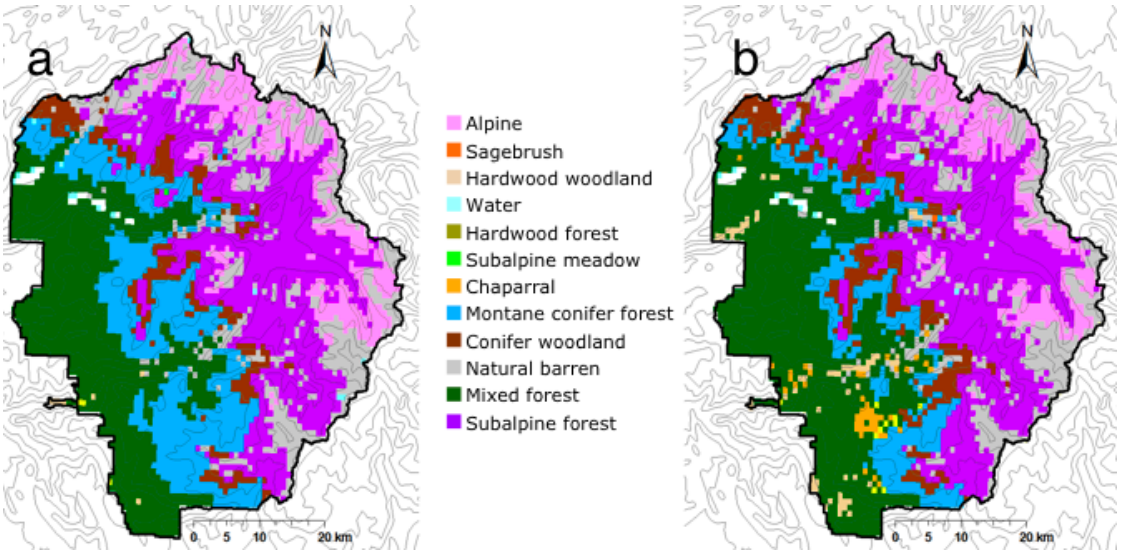

Fig. 2.18 MC1 modal simulated vegetation distributions. (a) 1905—1935, (b) 1967—1997.

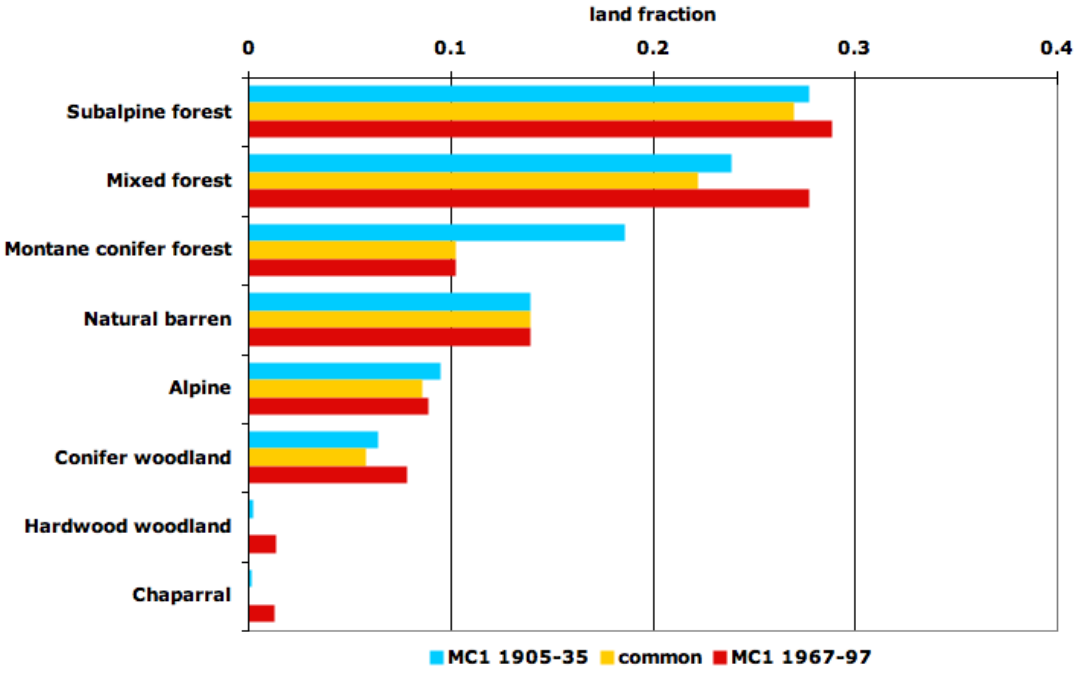

Fig. 2.19 Vegetation land cover fractions within the boundaries of Yosemite National Park included in the maps of simulated vegetation distribution for 1905—1935 and 1967—1997, and that are common to both maps.

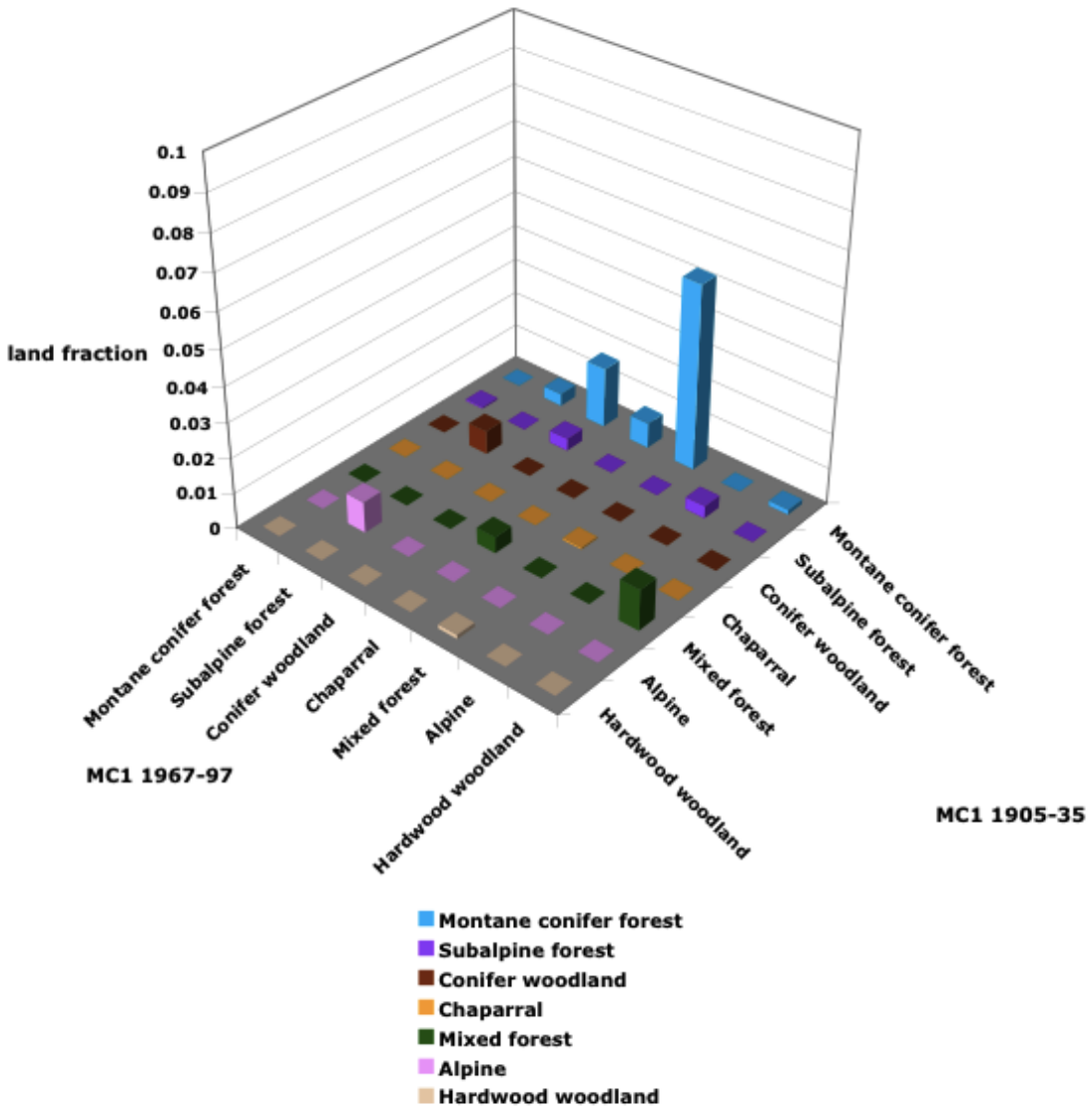

Fig. 2.20 Differences between the simulated vegetation distributions for 1905—1935 and 1967—1997.

Simulation of ecosystem carbon pools and carbon and nitrogen fluxes

Simulated total ecosystem carbon averages 21 kg C m^{-2}, but trends downward by 8% over the 112-year historical period (fig. 2.21a). Live vegetation biomass decreases the most, but litter and belowground soil carbon also decline (fig. 2.21b).

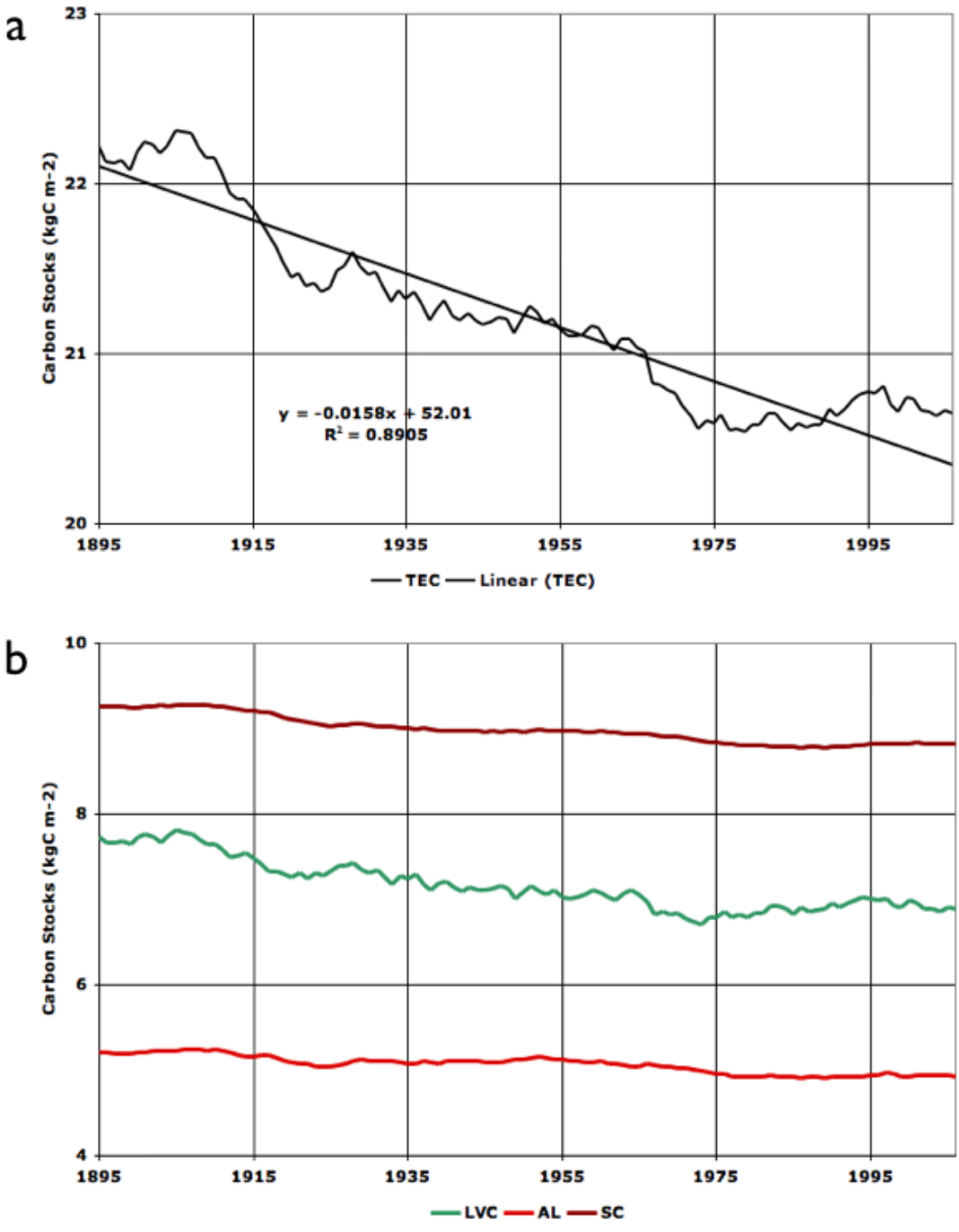

Fig. 2.21 Simulated carbon stocks: (a) total ecosystem carbon (TEC); (b) live vegetation carbon (LVC), aboveground litter, duff, and woody debris (AL), and soil carbon (SC).

Observed and simulated fire

Lee Tarnay of the NPS provided a time series of acres burned from 1977 through 2006 for the NPS Yosemite study in 2008 (Jeanne Panek, University of California, Berkeley, pers. comm.). A comparison to data from the MC1 simulation shows that MC1 simulated far less fire than actually occurred during the 1977-2006 period (fig. 2.22).

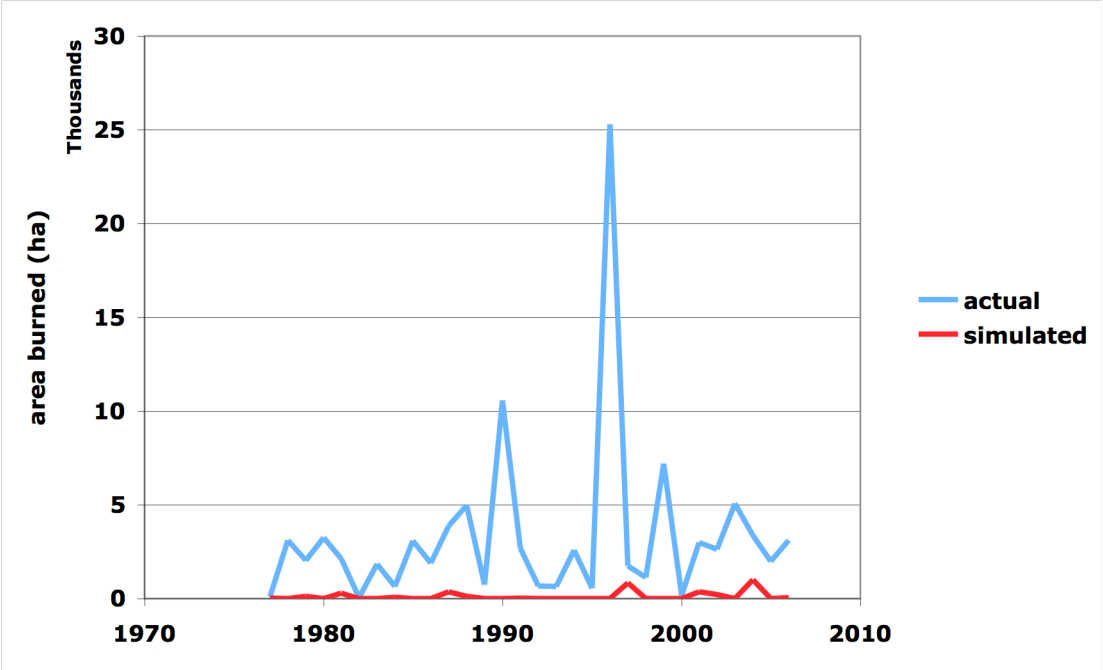

Fig. 2.22 Area burned per year in YNP (actual: Lee Tarnay, pers. comm.).

Discussion

Climate

The absence of a distinct centennial-scale increasing trend in minimum temperatures in the 800 m gridded PRISM climate data for YNP in the 20th century (fig. 2.5b) is inconsistent with other reports in the literature. Moritz et al. (2008) and Millar et al. (2004) reported a 3.7°C increase in the minimum monthly temperature in similar studies. Both studies rely on the temperature record at the Park headquarters in Yosemite Valley. Millar uses that station, together with two other stations, one at Sacramento and one at Mina, Nevada, because of their long, complete records and high synchrony with each other. Mina is 148 km from Park headquarters, and Sacramento is 188 km from Park headquarters. By contrast, the PRISM climate map for Yosemite was created using data from 195 locations located within and outside the Park (Joseph Smith, pers. comm.). The various stations have different periods of record, so the number of stations reporting for any given month is variable. There is another data set, from a network of 40 temperature sensors which began operation in 2002 along an east-west transect across the Park (Lundquist and Cayan 2007), which offers a future prospect of validating the PRISM climate map. The instrumental temperature record at Park headquarters in Yosemite Valley began in 1905. The number of visitors to YNP grew from 5,414 in 1906 to 3,431,514 in 2008 (http://www.nature.nps.gov/-stats/park.cfm).

Comparison to the findings of other researchers

Thorne and colleagues compared VTM maps for the central Sierra Nevada to the 1996 CALVEG National Forest maps (Schwind & Gordon 2001), and found that the two maps differed on 41.8% of the common area (Thorne et al. 2006). The corresponding figure from this YNP study is 38%, but there are several important differences between the two studies. First, this YNP study is limited to the portion of the central Sierra Nevada comprised of the 300,000 ha within the YNP boundaries, while Thorne's comparison covered 1,700,000 ha common to the VTM and CALVEG maps, and specifically excluded YNP[6]. Second, the CALVEG map was prepared in 1996 from satellite imagery, whereas the Yosemite vegetation survey is based on aerial photographs taken in August of 1997. Third, Thorne and colleagues

[6] Current CALVEG maps do include the area within YNP, but within the Park they are based on the 1997 vegetation survey rather than on independent satellite data (Hazel Gordon, personal communication).

compared intersected map polygons from the VTM and CALVEG maps, and used the WHR class to decide whether the intersections were alike or different, whereas we compared 800 m grid cells and used MC1's more aggregated vegetation classes to decide whether corresponding cells were alike or different. Both comparisons are encumbered by the differences in georeferencing accuracy between the VTM maps and the later maps.

Thorne's group reported on vegetation changes in the central Sierra Nevada which they inferred from comparisons of the VTM maps with the CALVEG maps (Thorne et al. 2006, Thorne et al. 2008). Both publications report large decreases in the Ponderosa Pine (PPN) WHR class, and increases in the Montane Hardwood (MHW) and Douglas-Fir (DFR) classes. In the broader study, published in 2006, the Sierra Mixed Conifer (SMC) class also shows a large increase. In the more aggregated MC1 vegetation classes, all of PPN, DFR, and SMC are grouped together in the mixed forest class, so the changes that are most noteworthy in Thorne's reports are not prominent in the Yosemite data. Both YNP and Thorne's study areas are in the central Sierra Nevada, but they do not overlap. The average elevation of YNP is significantly higher than the average elevations of Thorne's study areas. The most prominent result in this Yosemite study, i.e. the increase in montane conifer forest and decrease in subalpine forest from the 1930s to the 1990s, is consistent with the results in Thorne's broader study, which shows a significant increase in the Red Fir (RFR) WHR class and a significant decrease in the Lodgepole Pine (LPN) WHR class, corresponding respectively to the MC1 montane conifer forest and subalpine forest classes. The RFR and LPN classes are not present in meaningful amounts for either time period in the lower elevation Placerville quadrangle study (Thorne et al. 2008).

Muir's descriptions of Yosemite as it was in 1869 paint a picture of open, park-like forests (Muir 1911). Photographic evidence exists of the densification of YNP forests, both in Yosemite Valley and in the high Sierra, between the second half of the 19th century and the turn of the 21st (Klett et al. 2005). Millar and Woolfenden (1999) describe the transition from the end of the Little Ice Age ca. 1860 to the historic climate, including an increase in forest cover at mid-elevations and in meadows. Walker (2000) also recorded an increased density of incense-cedars (*Calocedrus decurrens*) and white fir (*Abies concolor*) at mid-elevations. These reports are consistent with our quantitative results of more montane conifer forest and less of the sparser subalpine forest.

Discrepancy in area burned

MC1 simulates only 3% as much area burned for 1977-2006 as in Lee Tarnay's data for actual area burned during that period (fig. 2.22). The fire model calibration used in this Yosemite study is the same as was used in the statewide California Scenarios 2008 study, and in that earlier study, MC1 simulated more frequent fires than was appropriate, at least in the Central Valley. Investigation of this discrepancy revealed differences between the thresholds used in my version of MC1, for the Buildup Index and the Fine Fuel Moisture Code, and those used in other contemporary versions.

Nitrogen uptake

The simulated demand for nitrogen for growth of vegetation averages 7.4 g N m^{-2} yr^{-1} for 1895-2006. The actual demand is met by a combination of atmospheric deposition, nitrogen mineralization, and biological nitrogen fixation (BNF). Cleveland et al. (1999) estimate BNF in temperate forests at 0.7 - 2.7 g N m^{-2} yr^{-1}. Their global relationship for evapotranspiration (ET) to BNF produces a BNF range of 0.3 to 0.9 g N m^{-2} yr^{-1} for the simulated ET of 265 mm H_2O yr^{-1} for 1895-2006. Fenn et al. (2003) estimate N deposition of 0.1-0.4 g N m^{-2} yr^{-1} over forests in the western U.S. generally, but as much as 1.5 g N m^{-2} yr^{-1} in the southwestern Sierra Nevada, based on measurements in Sequoia National Park. Bytnerowicz and Fenn (1996) estimate wet deposition in the Sierra Nevada at 0.17 g N m^{-2} yr^{-1} but make the point that dry deposition is larger than wet deposition in California. They give a total N deposition rate of 0.62 – 1.08 g N m^{-2} yr^{-1} for a location in Sequoia National Park. Whether or not running the MC1 model in unlimited nitrogen mode is consistent with these estimates of BNF and N deposition depends on how much of the demand for N is met by N mineralization.

The trend in total ecosystem carbon

The observed 20th century vegetation change is consistent with an increase in total ecosystem carbon, but MC1 simulates a decrease. The biggest change evident in the comparison of the VTM map to the 1997 survey map is an increase in montane conifer forest and a decrease in subalpine forest. Montane conifer forests correspond to relatively dense

stands of large red fir trees, while subalpine forests correspond to less dense stands of smaller lodgepole pines. The replacement of subalpine forest by montane conifer forest thus represents a net increase in total ecosystem carbon. Wildfire can remove significant quantities of carbon, but over the long term, the increase in montane conifer forest should result in an increase in total ecosystem carbon. An increasing trend in total ecosystem carbon is also supported by the densification of the forests and infilling of meadows noted by other researchers and observers (e.g. Millar et al. 2004).

Why does MC1 simulate Yosemite as a carbon source in the 20th century? It is not because of too much simulated fire, since MC1 is simulating much less wildfire than it should. The answer lies in the spinup protocol. MC1 is run for 1000 years to establish equilibrium carbon pools. Those pools are used as the initial conditions for the simulation of the historical period. The climate data set used for the spinup run is a detrended, rescaled version of the historical climate record.

The high-pass filter used to eliminate the long-term trend in the spinup and base climates is a bit counterintuitive. It sets the filtered value for a given month equal to the target mean plus the deviation of the actual historical value for that month from the 30-year moving average centered on the given month. This is a legacy from the methods used for the VEMAP project in the late 1990s (Ron Neilson, pers. comm.; Kittel et al. 2004). The target means for the spinup dataset are the means of the first 15 years (1895-1909) of the historical period. Implicit in this protocol is the assumption that the ecosystem carbon pools are in equilibrium with the climate means of 1895-1909 at the beginning of the historical period simulation. But for YNP, 1895-1909 was the wettest part of the 1895-2006 period (figs. 2.5e and 2.23). Vegetation in YNP is water-limited, so the simulated net primary productivity is higher under the wetter spinup climate than under the actual historical climate (fig. 2.24). As a result, the total ecosystem carbon declines over the course of the simulation of the historical period. A reconstruction of winter precipitation anomalies for the Sierra Nevada from tree rings (Lisa Graumlich pers. comm.; Graumlich 1993), juxtaposed to the instrumental record, shows that the 1895-1909 period was anomalously wet relative not only to the 20th century but also to the 19th century as well (fig. 2.25).

In short, my estimate of the initial conditions for the simulation is inaccurate. I used a method for estimating the initial conditions which has been used in many previous studies, at

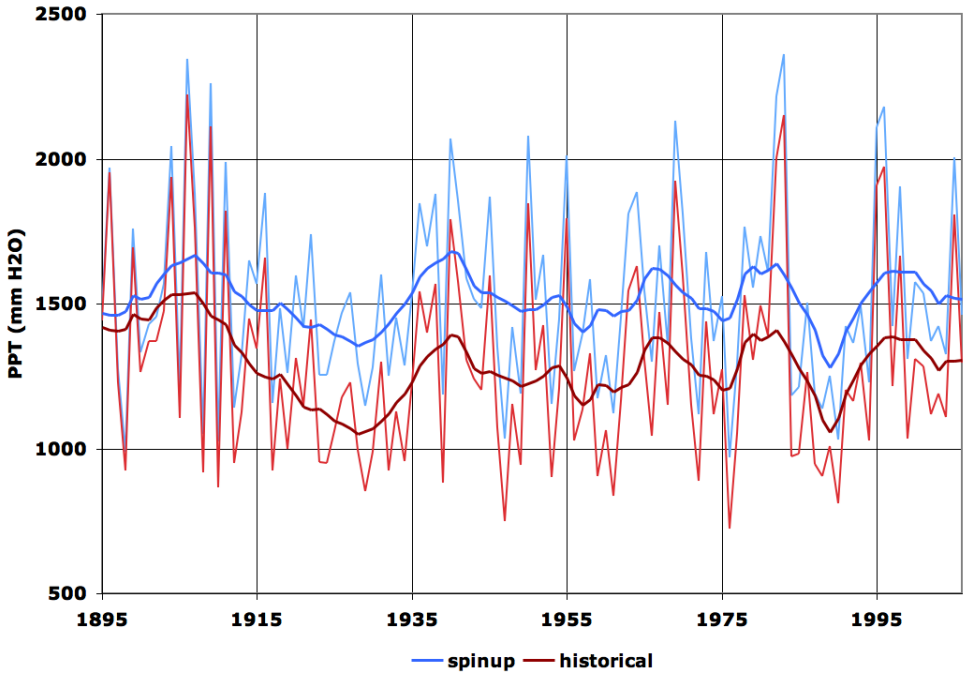

Fig. 2.23 Annual precipitation and 10-year moving averages for the historical and spinup climate data sets. (PRISM climate data, Daly et al. 2008)

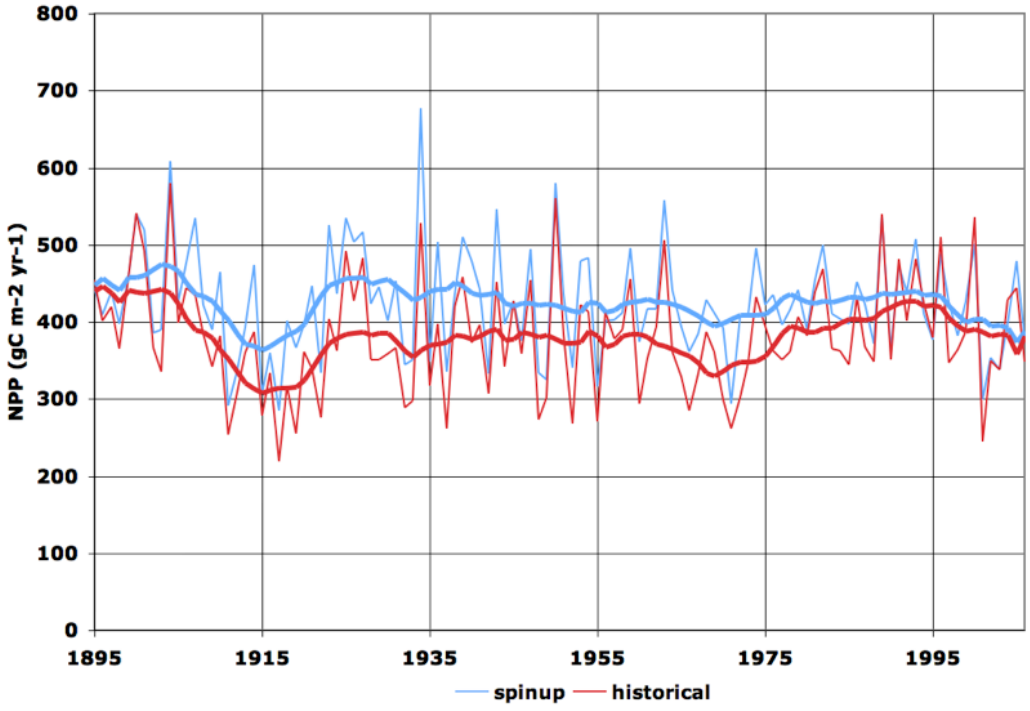

Fig. 2.24 Annual and 10-year moving averages of simulated net primary productivity for the historical and spinup climate data sets.

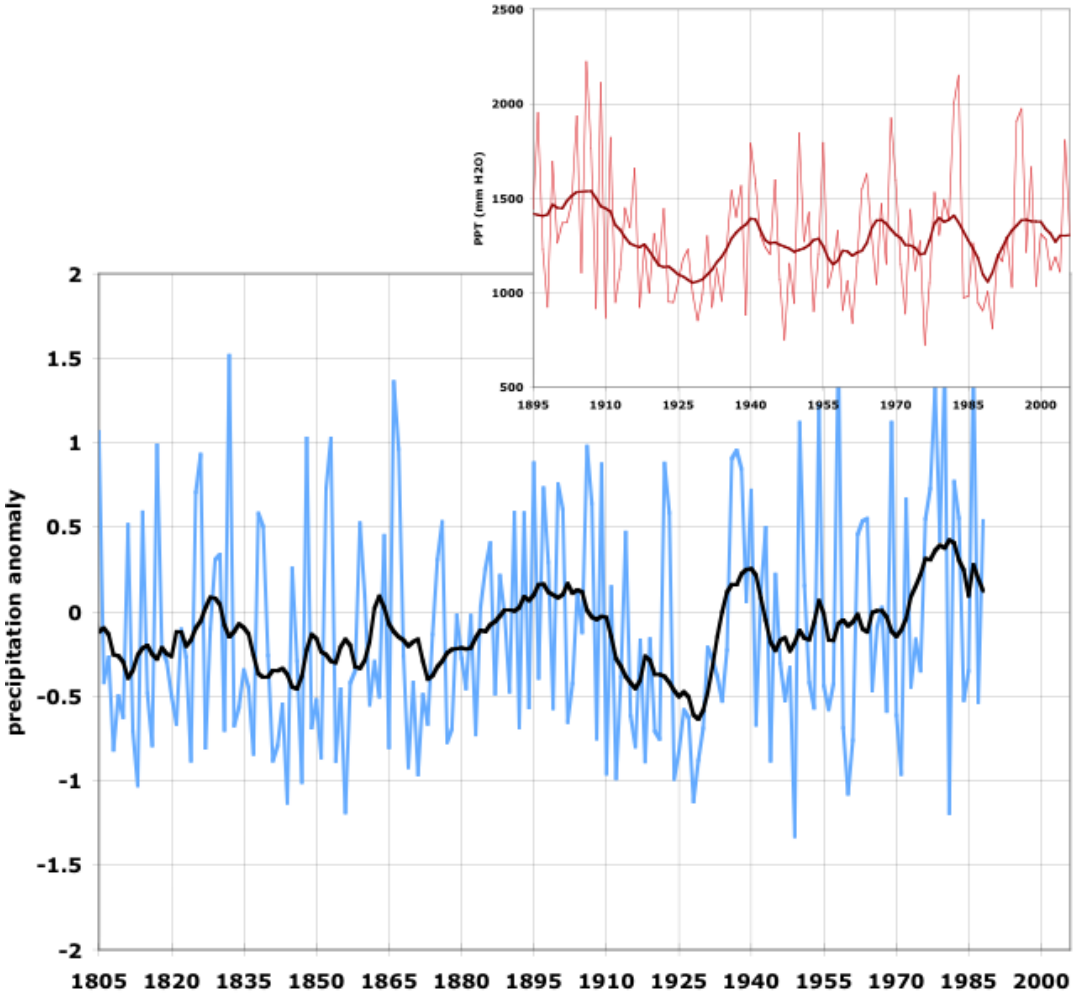

Fig. 2.25 Annual and 10-year moving average winter precipitation anomalies for 1805-1988, relative to the mean of 1928-88, for the Sierra Nevada, reconstructed from tree ring data for years prior to the instrumental record (Graumlich 1993). Inset: Annual precipitation (mm yr^{-1}) and 10-year moving average for Yosemite National Park for 1895-2006 (PRISM climate data, Daly et al. 2008), on the same x-axis as the main graph.

least as far back as the VEMAP project (VEMAP members 1995). For this study, there are two flaws in the method. First, the initial 15 years of the historical record are unrepresentative, both of the period prior to the historical record and of the historical period itself. Second, the climate had changed during the 19th century emergence from the Little Ice Age (Millar & Woolfenden 1999), and there had not been enough time prior to the 1895-1909 reference period for ecosystem carbon pools, composed predominantly of long-lived forest trees, to stabilize.

Role of human land use/land change

MC1 does not simulate human land use. Yosemite's vegetation has been influenced by various forms of human land use over the past 150 years - livestock grazing, timber harvest, fire suppression, tourism (Muir 1911, Beesley 1996). Native Americans shaped the landscape with intentional fires before the arrival of settlers (Woolfenden 1996). None of these influences are included in MC1. Some of the differences between MC1's results for the historical period and the observations made during the historical period undoubtedly arise from the effects of human land use.

Assessment of MC1's hindcast of 20th century vegetation change

MC1 fails to detect the single largest vegetation change between the VTM map and the 1997 Survey map, i.e. the switch of about 10% of the Park area from subalpine forest to montane conifer forest. The two largest changes in the MC1 data add up to only 7% of the Park area - and are *out of*, rather than *into*, the montane conifer forest type. In the observed data, the montane conifer forest class grows from 12% to 28% of the Park area, while in the MC1 data it shrinks from 19% to 10%. Figure 2.26 summarizes the changes between time periods and the differences between observed and simulated vegetation coverage.

How significant is MC1's inability to hindcast the 20th century vegetation changes? First, it is useful to keep in mind that the actual climate change signal in the 20th century is small relative to the expected climate change in the 21st century. Even if it were true that MC1 doesn't accurately simulate the effects of climate changes of the magnitude of those in the 20th century, it is still possible that MC1 may usefully simulate the effects of the larger climate changes expected in the future.

Second, it is likely that the changes simulated by MC1 are out of synchrony with the observed vegetation changes. Most of Yosemite is occupied by long-lived forest species. In the absence of disturbance (e.g. stand replacement fire or large scale beetle kill), turnover from one vegetation type to another takes place over a period similar to the lifespan of the original vegetation, hundreds of years in the case of the tree species common to the Park. Simulations showing an increase in mixed forest at the expense of montane conifer forest may

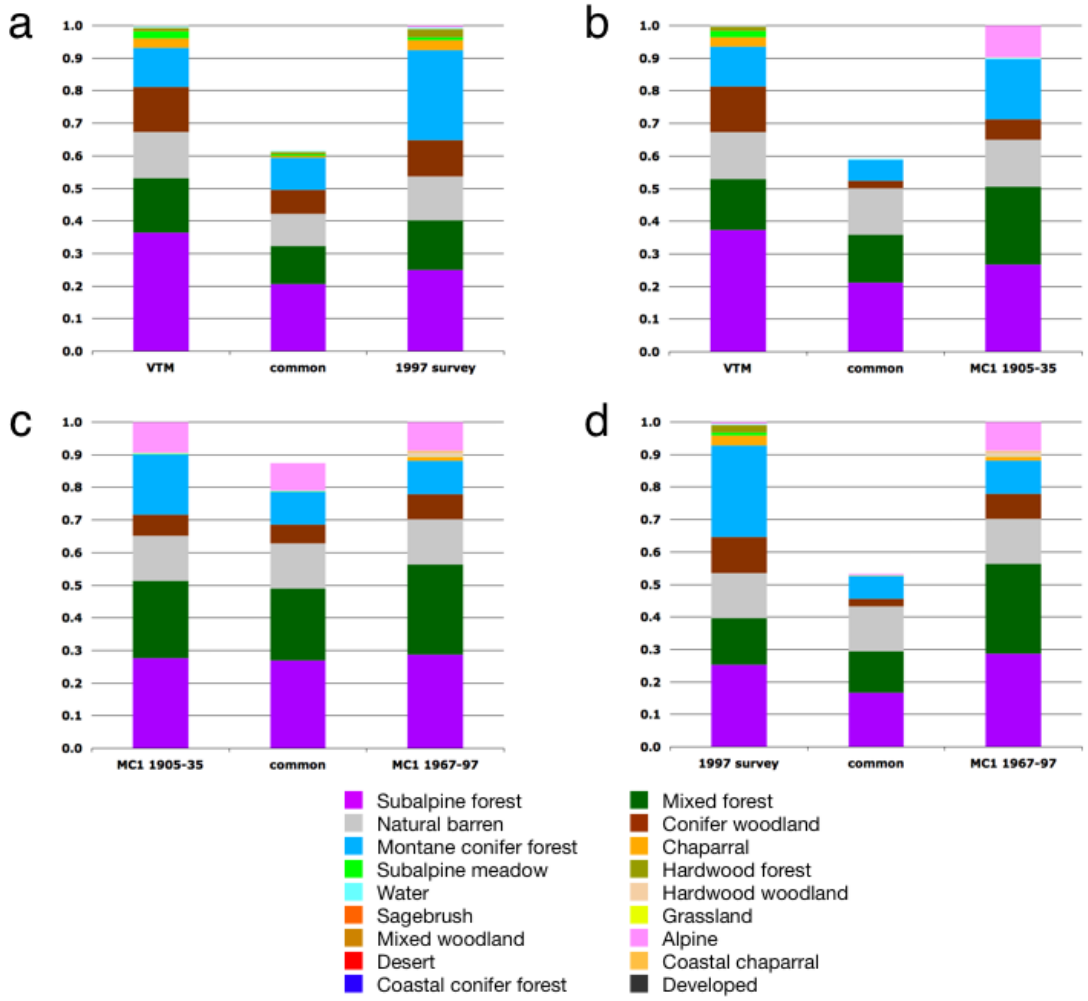

Fig. 2.26 Relative areas in different cover types: (a) VTM compared to 1997 NPS Survey map, (b) VTM compared to modal simulated vegetation distribution for 1905—1935, (c) modal simulated vegetation distribution for 1905—1935 compared to modal simulated vegetation distribution for 1967-1997, (d) 1997 NPS Survey compared to modal simulated vegetation distribution for 1967—1997. The "common" bar represents the relative areas with the same cover type on both maps. (VTM: Thorne et al. 2006; 1997 NPS Survey: Aerial Information Systems 1997)

be interpreted as a projection of changes which would take place in the 21st century if the climate of the 1990s were to persist. Conversely, the observed vegetation change from subalpine forest to montane conifer forest may be a reflection of the centennial scale warming since the end of the Little Ice Age period. Shinneman and Baker (2009), in their study of piñon-juniper woodland in Colorado, speculate that changes during the historic period have

their cause even further back in time, as a continuation of postglacial, early-Holocene expansion. The idea that long-lived forests were still changing in the 20th century as a result of centennial-scale or even millennial-scale climate changes raises doubts about the simulation practice of spinning up to an equilibrium with the climate means of the first 15 years of the historic period. The existence of a set of temperature and precipitation anomalies for the Sierra Nevada going all the way back to 800 A.D. (Graumlich 1993) opens the possibility of spinning up with a climate that actually reflects the MWP and the LIA.

Third, MC1 simulates natural processes and estimates *potential* vegetation, while the observations are of *actual* vegetation produced by a combination of natural and anthropogenic causes. Although Yosemite National Park has been a protected area for more than a century, both the livestock and timber harvest practices of 19th century settlers and the land use habits of earlier native Americans have likely superimposed patterns on the potential vegetation pattern. Moreover, even in the 20th century, Yosemite's protected status has included fire suppression, which is not explicitly simulated by MC1 in this study.

This research project was undertaken with the expectation that the MC1 DGVM would be able to simulate patterns of natural vegetation in YNP which resemble the patterns which were actually observed during the 20th century. That expectation has been fulfilled: the visual resemblance between observed and simulated patterns is apparent in figures 2.12 and 2.15, although there is certainly room for improvement. Quantitative approaches to assessing similarity and difference are taken up in chapter 4. The project had the further aim to test whether the simulation of vegetation change in the 20th century resembled the observed change. The model clearly did not simulate the observed change.

We have gained insight into probable causes of the discrepancies between the observations and the simulations. First is an appreciation for the importance of vegetation persistence at historical rates of climate change - big changes in forest types apparently take centuries rather than decades. Second is the realization that starting up the historical simulation from an equilibrium condition is inappropriate - the vegetation was probably significantly out of equilibrium with the climate at the beginning of the historical period. Third is the recognition that the representation of soil in MC1 is poorly matched to the actual patchiness of soil and bare rock in the high Sierra, and that the soil data used in the simulations is defective. Fourth is the identification of calibration deficiencies in the fire occurrence algorithm. Fifth is the suspicion that accurate simulation of vegetation patterns and dynamics at the landscape scale in complex topography cannot be achieved using gridcells, but will require using patches which are ecologically meaningful (the polygons of the VTM map or the

1997 Survey would be a good place to start). Sixth, human impacts cannot be ignored even for an area which has had protected wilderness status as long as Yosemite.

CHAPTER THREE: PROJECTIONS OF VEGETATION CHANGE IN THE 21ST CENTURY

The MC1 dynamic global vegetation model was used to simulate the vegetation response in Yosemite National Park to three scenarios of 21st century climate. Results indicate that by 2100, the majority of the Park may be dominated by different vegetation types or remnants of 20th century vegetation types not optimally suited for their new environment. In particular, simulations show that subalpine forests will be subject to heat and drought stress and/or undergoing replacement by vegetation types currently found at lower elevations. In the warmest and driest scenario, more than two-thirds of the current forest area in the Park would become more suitable for woodland, shrubland, or grassland.

To forecast with any certainty how vegetation in Yosemite might change because of climate change presents real challenges. First, the answer depends on just how much and in what direction the climate is changing and will continue to change, a subject of intense study by many climate scientists, and on how these changes will manifest themselves at the scale of a topographically complex site such as Yosemite National Park, which is itself a new research issue (Lundquist & Cayan 2007, Daly et al. 2009). Secondly, vegetation patches are small and environmental heterogeneity (soils, aspect, slope) is considerable, a reflection of the dramatic, rugged terrain - a situation that makes it difficult to measure and analyze current ecosystem processes and vegetation assemblages, and consequently to calibrate available simulation models. Thirdly, the vegetation includes species with lifespans ranging from years to millennia, grasses to sequoias, which means that even when the climate changes, there is a landscape legacy that does not disappear instantaneously and needs to be taken into account when projections of vegetation cover are made. Estimating the amount of climate change impact over one century on a species that has already survived many centuries is a challenge.

This study addresses each of those three challenges. First, three future climate scenarios were selected as a sample of the range considered in the most recent IPCC report (IPCC 2007). Secondly, a new, high resolution climatology for the continental U.S. from the PRISM group (Daly et al. 2008) has made possible simulation on a grid with a lattice distance of ~800 meters, finer by at least a factor of ten than most previous studies using DGVMs. This resolution is barely adequate: Yosemite Valley itself is only ~1-2 km in width, while the canyon walls are nearly 1 km high. Finally, we introduce a new simulation protocol in order to gain insight into the fate of areas now occupied by long-lived species.

Methods

Future and alternative climate scenarios

Three future climate data sets were used to simulate the period 2007-2099. They were chosen by National Park Service scientists, during a related study (Panek et al. 2009), to represent a range of possible future climates (table 3.1). The coolest, wettest future was produced by the CSIRO-MK3.0 general circulation model (GCM) (H.B. Gordon et al. 2002) using the SRES B1 emissions scenario (IPCC 2000). The hottest, driest future came from the MIROC 3.2 medium resolution GCM (Center for Climate Systems Research 2004) using the SRES A2 emissions. An intermediate future is represented by the data from the Hadley CM3 GCM (C. Gordon et al. 2000) with SRES A1B emissions. In all cases, temperature increases from 2000 to 2100 (fig. 3.1a). Precipitation tends to decrease towards the end of the 21st century (fig. 3.1b). Vapor pressure deficits also increase (fig. 3.1c). An alternative climate scenario was constructed to represent a stable climate having the interannual variability of the entire 93-year MIROC A2 future climate and the means of its final fifteen years (2085-99).

Table 3.1 Spatially and temporally averaged values for important climate variables from the historical data for 1967—1997 and the three future scenarios for 2069—2099. TMIN/TMAX is the spatial and temporal average of the monthly means of daily minimum/maximum temperatures.

	1967—1997	2069—2099 CSIRO B1	2069—2099 Hadley A1B	2069—2099 MIROC A2
precipitation (mm H_2O yr^{-1})	1299	1202	1082	955
temperature (°C)	5.43	7.29	9.52	10.62
TMIN (°C)	-1.55	+0.15	+2.12	+3.04
TMAX (°C)	12.40	14.43	16.93	18.19
vapor pressure deficit (Pa)	505	572	690	745

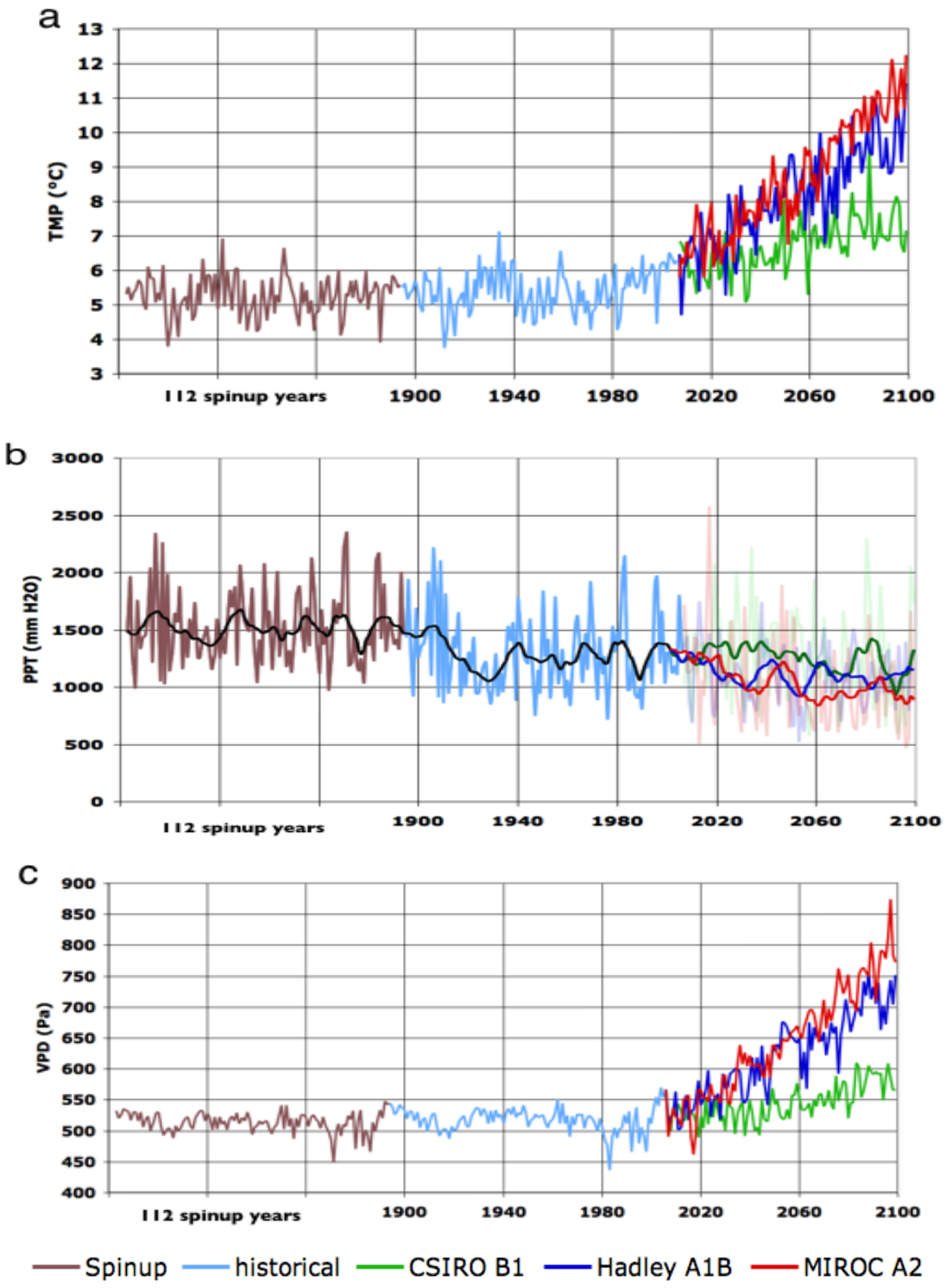

Fig. 3.1 Spinup, historical, and future scenario climate data for Yosemite National Park: (a) mean annual temperature; (b) annual precipitation, with 10-year moving averages; (c) mean annual vapor pressure deficit.

Creating a continuous time series of climate data that combines historical observations and GCM scenarios is difficult because of possible bias in the GCM output. To overcome this problem, a separate long term mean baseline is established for each data set, and the anomalies in the GCM output are assigned to the historical climate baseline.

Downscaling protocols

The downscaling process consists of several steps (Rogers 2009 and Maureen McGlinchy, M.S. student, OSU, Dept. of Forest Ecology and Society, pers. comm.):

1. A one-year, monthly 800 m baseline climatology was constructed from historical climate averages for the period 1971—2000. PRISM historical climate data (Daly et al. 2008) were used by the MAPSS team (USFS PNW Research Station) as a baseline when downscaling the GCM future climate scenarios to the 30 arc-second grid.
2. A one-year, monthly baseline climatology at the GCM's spatial resolution was constructed using GCM output for the period 1971—2000.
3. Time series of climate anomalies for January 2007 through December 2099 at the spatial resolution of the GCM were constructed from the GCM's future climate time series, referenced to the GCM's baseline climatology. Temperature anomalies were calculated by subtracting the baseline climatology values from the future climate values. Precipitation anomalies were calculated by taking the ratio of the future climate value to the baseline climatology value, except when the base climatology value was zero or the ratio is very large, in which case the precipitation anomaly was capped at a maximum ratio of 5 (Rogers 2009).
4. The time series of climate anomalies were downscaled to the 800 m resolution grid using binomial interpolation and applied to the 800m baseline climatology.

The downscaling process was performed on each of the three sets of future climate data to create the three future climate scenarios used in our study.

Future climate scenario characteristics

Under the hottest and driest scenario, differences between the late 21st century and the historical climate of the late 20th century are larger than differences observed between the 1905—1935 and 1967—1997 periods (Chapter 2). Whereas in the 20th century precipitation increased west of the Sierra crest and decreased only east of the crest (fig. 2.7a), precipitation decreased everywhere under the MIROC A2 scenario, by up to 33% in some higher elevation areas (fig. 3.2). Twentieth century maximum temperatures decreased by up to one degree and minimum temperatures generally increased by about a degree (fig. 2.6), resulting in a small reduction in the range of temperatures in the Park. Under the MIROC A2 scenario, both minimum and maximum temperatures are projected to increase everywhere in the Park by up to 6°, but maxima increase more than minima in most locations, resulting in an expansion of the range of temperatures (figs. 3.3a and 3.3b). Vapor pressure deficit in the 20th century exhibited both small increases and decreases (fig. 2.7b), while under the MIROC A2 scenario significant increases are projected in most of the Park (fig. 3.3c).

Simulation protocols

Two simulation protocols were used, here called the “conventional” and “alternative” protocols. The conventional protocol addresses the question: what might the natural vegetation in the Park be as a result of actual historical climate followed by a scenario of future climate? The alternative protocol addresses a different question: what might the equilibrium vegetation be as a result of a climate like that of the final 15 years of the MIROC A2 future scenario?

The conventional protocol uses the values of the MC1 model’s state variables at the end of the historical period as initial conditions for the simulations of three future scenarios. In the alternative protocol, the MIROC A2 future climate for 2007-2099 is used to generate alternative equilibrium (EQ) and spinup climate data sets, by a method analogous to that described in Chapter 2 for generating the conventional EQ and spinup climate data sets from the 112-year historical climate (fig. 3.4). The spinup data sets for both the conventional and alternative protocols were created by detrending and then rescaling the original data sets. The important difference is that whereas the conventional spinup climate is scaled to the

means of the first 15 years of the historical climate, the alternative spinup climate is scaled to the final 15 years of the future climate.

In the conventional protocol, the simulation is conducted in 3 steps: EQ, spinup, and transient (historical or historical+future) runs. The alternative protocol also uses 3 steps, but the third step consists of a 93-year simulation using the alternative spinup climate, whereas the third step for the conventional protocol uses the historical climate (fig. 3.4). For some analyses involving the MIROC A2 scenario, we extended the simulations beyond the 21st century for several additional centuries. We used the alternative spinup climate data set for all extended periods.

To make the analysis more tractable, I divided the 2007-2099 future climate simulation period into three 31-year intervals: the "early 21st century" (2007—2037), the "mid 21st century" (2038-2068), and the "late 21st century" (2069—2099). References to "late 20th century" simulation results pertain to the period 1967—1997.

CO_2 effect and nitrogen availability

The effect of increasing atmospheric CO_2 concentration on photosynthetic productivity is parameterized in the MC1 model. Comparative studies of high and low CO_2 effect carried out by the MAPSS group in the past have used alternative values for the parameters which specify the effect of doubled atmospheric CO_2 concentration on transpiration and on the NPP of C_3 plants. The MAPSS group based their parameter values on an increase of 23% in production in FACE experiments (Norby et al. 2005). In this study, we used the low CO_2 effect parameter values (0.75 for effect on transpiration, and 1.25 for effect on NPP). To address a question about the relative limitations from nitrogen and water, we used the high CO_2 effect parameter values (0.35 for transpiration, 1.65 for NPP) for a few simulations; the results from these runs are labeled as "high CO_2 effect". Since all the simulations were run in MC1's "unlimited nitrogen" mode, we did not simulate nitrogen limitation directly. Instead, we used the "high CO2 effect" to see if, when simulated water use efficiency and production are enhanced under high CO_2, the simulated uptake of nitrogen increases as well.

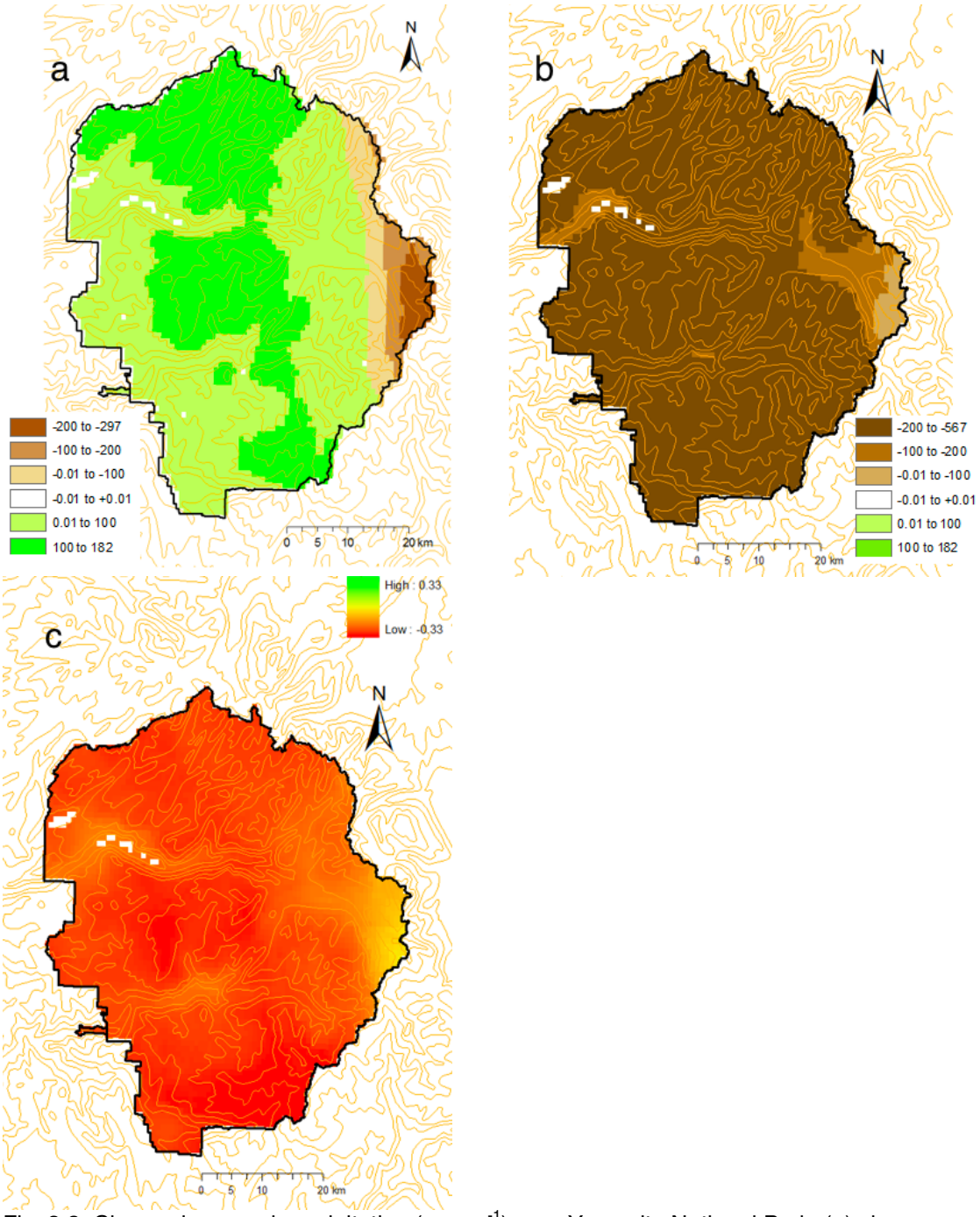

Fig. 3.2 Change in annual precipitation (mm yr^{-1}) over Yosemite National Park: (a) change from 1905—1935 to 1967—1997; (b) change from 1967—1997 to MIROC A2 future climate scenario for 2069—2099, using the same color scale as (a); (c) fractional change from 1967—1997 to MIROC A2 2069—2099.

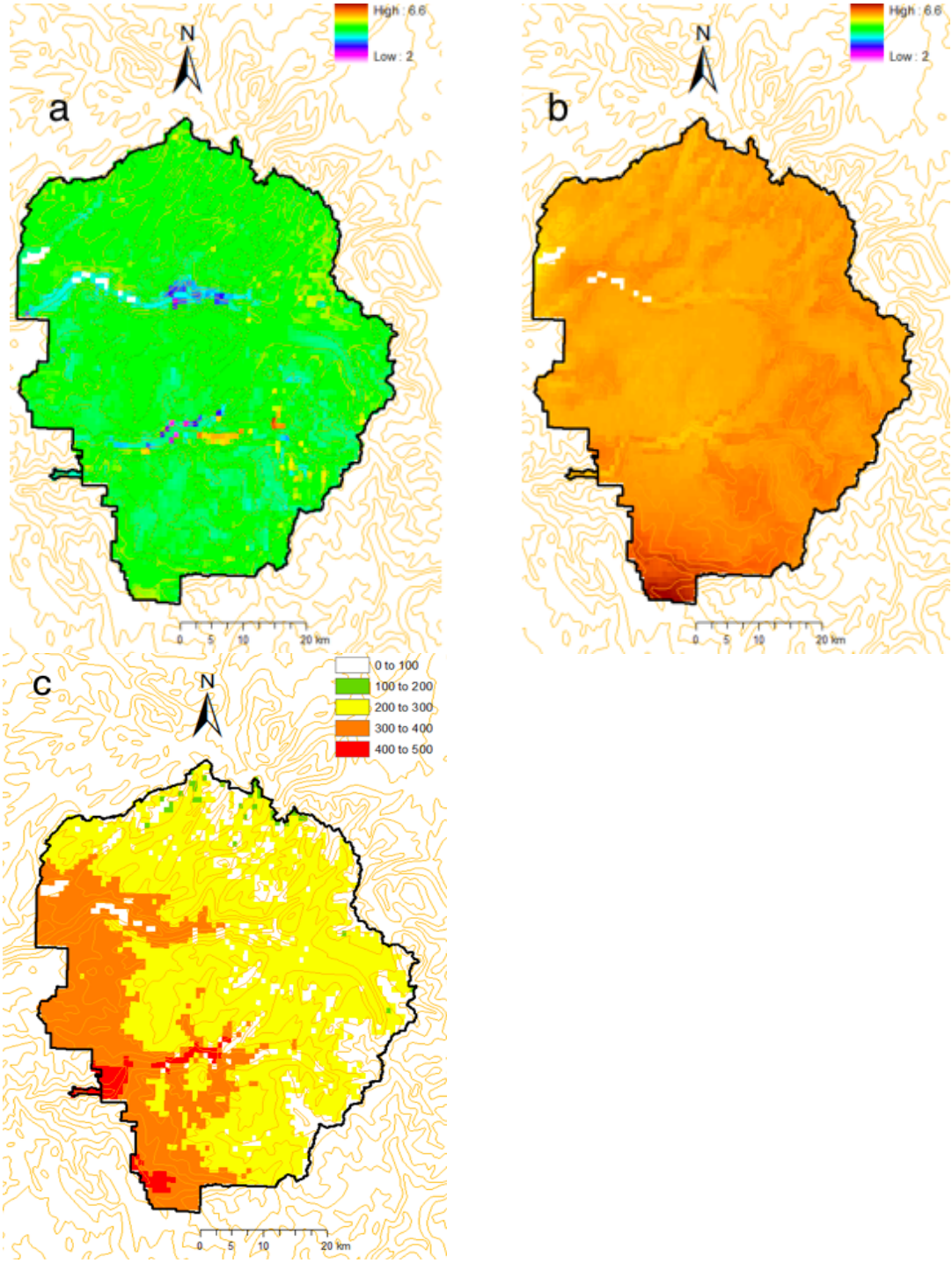

Fig. 3.3 Increases in annual averages of monthly means of daily temperature extremes (TMIN/TMAX, °C) and vapor pressure deficit (Pa) from 1967—1997 to 2069—2099 in the MIROC A2 scenario: (a) TMIN, (b) TMAX, (c) vapor pressure deficit.

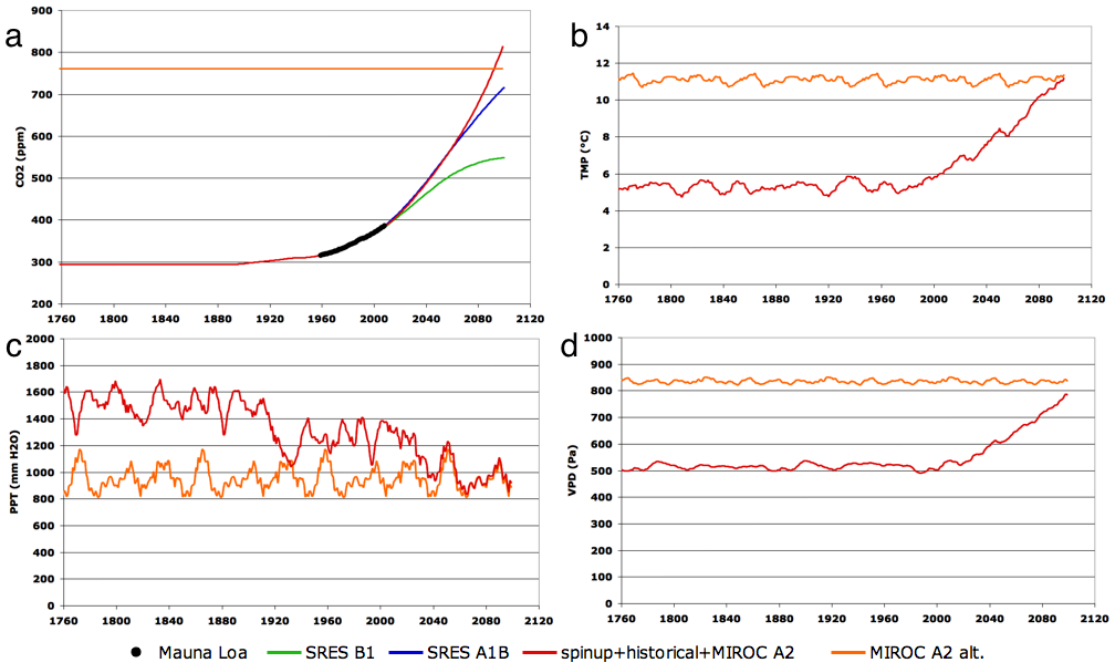

Fig. 3.4 CO_2 and climate data for conventional and alternative simulation protocols: (a) atmospheric CO_2 concentration; (b) 10-year moving average of mean annual temperature in Yosemite National Park; (c) 10-year moving average of annual precipitation; (d) 10-year moving average of annual mean vapor pressure deficit. Mauna Loa: mean annual atmospheric CO_2 concentration measured at Mauna Loa, Hawaii. SRES B1 and A1B: scenario B1 and scenario A1B, Special Report on Emissions Scenarios (IPCC 2007). MIROC A2: spatially averaged mean annual climate variables and CO_2 concentration simulated by the MIROC GCM (Center for Climate Systems Research 2004) under the SRES A2 scenario. MIROC A2 alt.: constant CO_2 concentration and mean annual climate variables corresponding to the average of the last 15 years of the MIROC A2 future scenario.

Fire index

As a measure of the degree to which wildfire is affecting biogeochemical fluxes and carbon stocks, we use the ratio of vegetation carbon consumed by fire to cumulative net primary production, which we call the “fire index”. This formulation of “fire index” was first reported by Panek et al. (2009). Although this ratio may exceed 1 for a particular grid cell in a single year, intrinsically it must be between 0 and 1, and usually much closer to 0 than to 1, when calculated for larger areas and over longer time periods. It is an index of the role of fire when determining the carbon sequestration potential of a site. When carbon losses due to fire and heterotrophic respiration in a given time period are greater than the cumulative net primary production for the period, the site has become a source of carbon.

Results

Potential vegetation changes using the conventional simulation protocol

The maps of modal potential vegetation types for the late 21st century future scenarios differ from the one for the late 20th century: 46% change for the CSIRO B1 scenario, 65% change for the Hadley A1B scenario, and 80% change for the MIROC A2 scenario (fig. 3.5). There is some agreement among the results from the future scenarios: 1) growing degree sums increase sufficiently in all 3 scenarios to eliminate all of the alpine zone; 2) in the Hadley A1B and MIROC A2 scenarios, growing degree sums increase enough to also eliminate the subalpine forest zone, and the leaf area index drops below the woodland/forest LAI threshold (4.7) in areas that were formerly subalpine forest; 3) the montane forest category is greatly reduced, to 3% of the Park area in the CSIRO B1 scenario, and to <1% of the Park area in the other two scenarios; 4) mixed forests become the dominant potential forest type. There are differences between the 3 scenarios: 1) the overall potential forest cover remains unchanged at about two-thirds of the Park area under the CSIRO B1 scenario, but declines to two-fifths under the Hadley A1B scenario, and one-fifth under the MIROC A2 scenario; 2) while forest remains the dominant physiognomic type under the CSIRO B1 scenario, and is still the largest potential type in the Hadley A1B scenario with woodland a close second, the MIROC A2 scenario has more potential woodland, and also more potential grassland, than potential forest (figs. 3.6 & 3.7).

Potential vegetation using the alternative simulation protocol

Despite the use of detrended climate and constant CO_2 in the alternative simulation, the potential vegetation varies markedly across the three 31-year time periods used in the analysis (fig. 3.7). Since the same detrended climate is used for both the spinup and "transient" steps, the pattern of variation within each 99-year transient simulation repeats from one transient simulation to the next (fig. 3.8). During the 31-year period derived from the MIROC A2 data for 2069—2099, the Park vegetation includes mostly woodland (57%) and is

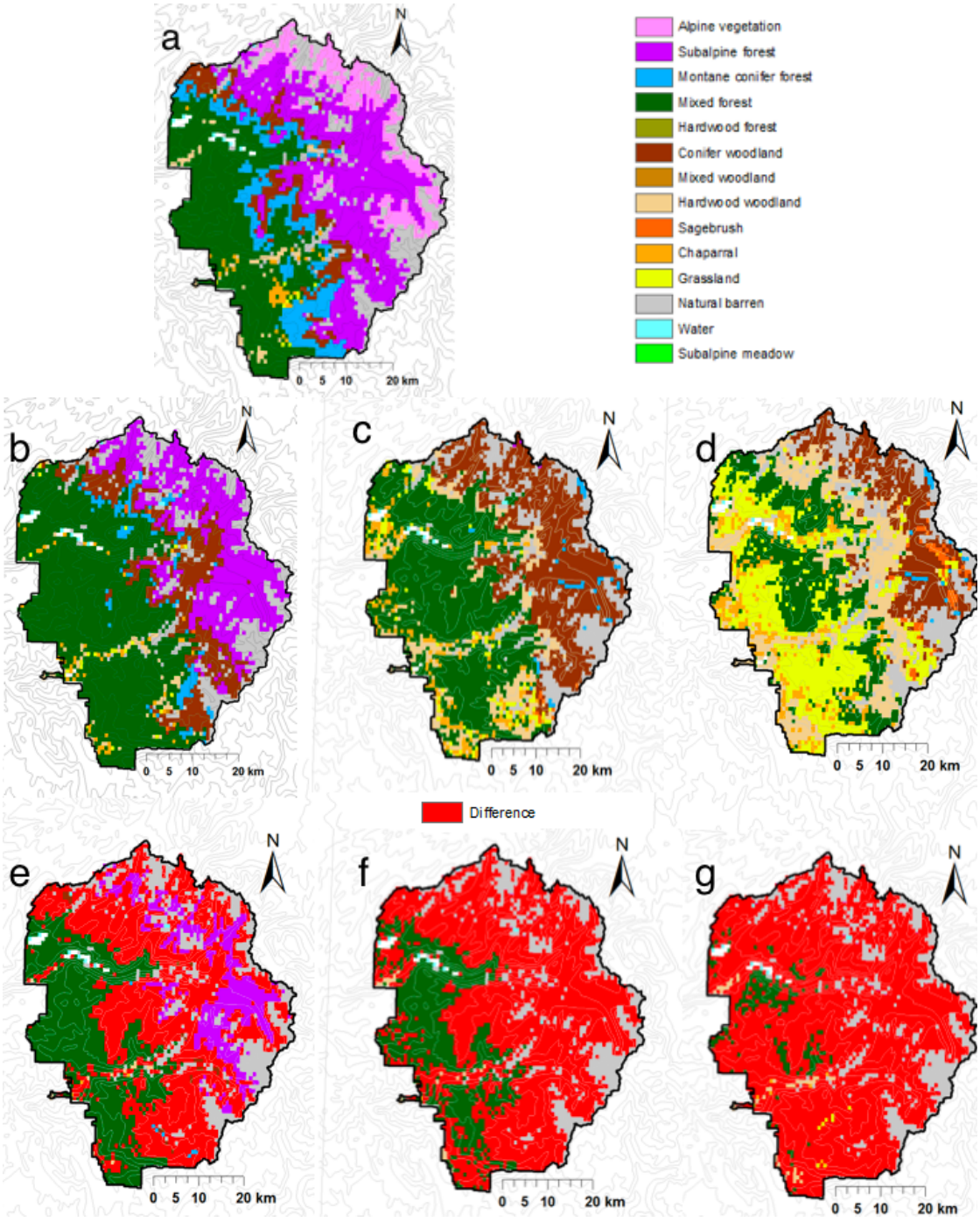

Fig. 3.5 Vegetation maps for 2069—2099 compared to vegetation map for 1967—1997 as simulated by MC1: (a) simulated vegetation map for 1967—97; (b) 2069—2099 under CSIRO B1 scenario; (c) 2069—2099 under Hadley A1B scenario; (d) 2069—2099 under MIROC A2 scenario; (e), (f), (g) locations of differences for CSIRO B1, Hadley A1B, and MIROC A2 scenarios.

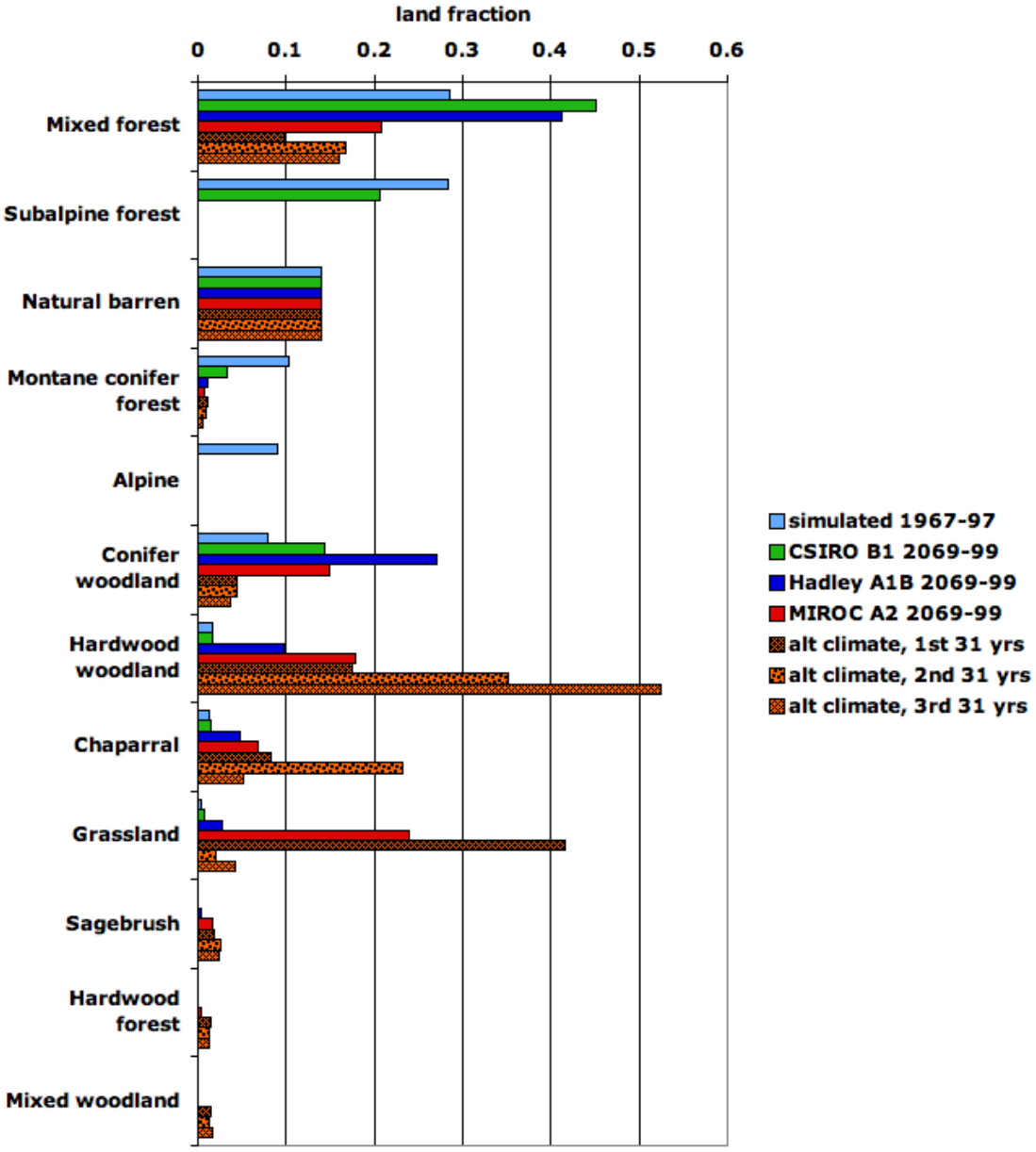

Fig. 3.6 Land fractions associated with simulated potential vegetation types for 1967—1997 and six 31-year simulation periods under different climate scenarios.

CSIRO B1: the CSIRO-MK3.0 general circulation model (H.B. Gordon et al. 2002) using the SRES B1 emissions scenario (SRES, IPCC 2007). Hadley A1B: the Hadley CM3 GCM (C. Gordon et al. 2000) with SRES A1B emissions. MIROC A2: the MIROC 3.2 medium resolution GCM (Center for Climate Systems Research 2004) with SRES A2 emissions. alt climate: alternative spinup climate scaled to the means of the last 15 years of the MIROC A2 scenario.

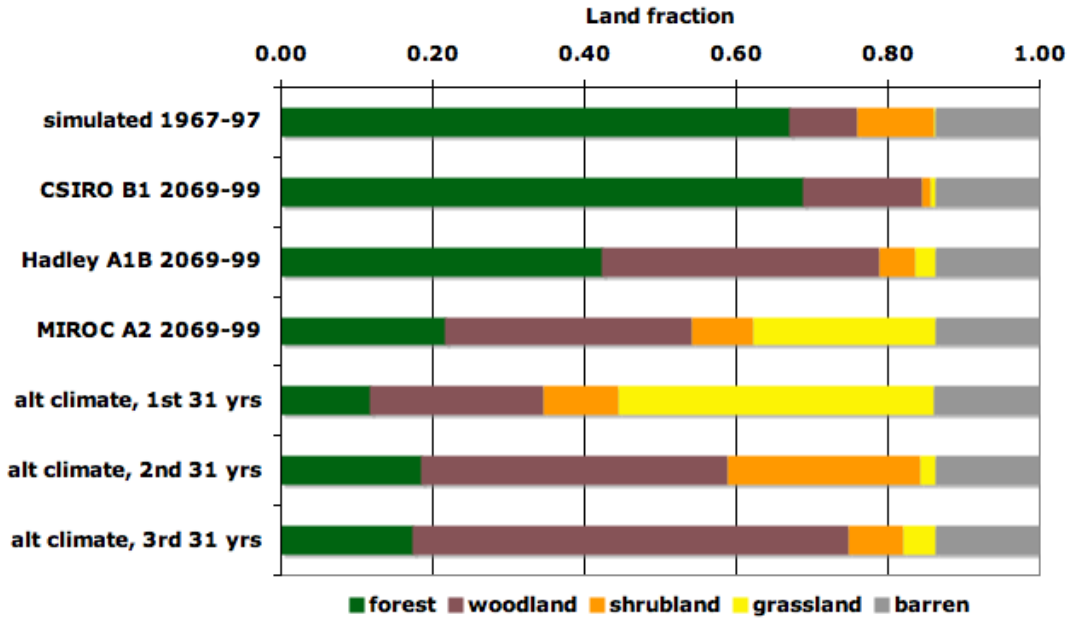

Fig. 3.7 Land fractions associated with simulated potential physiognomic vegetation types for 1967—1997 and six 31-year simulation periods under different climate scenarios. CSIRO B1: the CSIRO-MK3.0 general circulation model (H.B. Gordon et al. 2002) using the SRES B1 emissions scenario (SRES, IPCC 2007). Hadley A1B: the Hadley CM3 GCM (C. Gordon et al. 2000) with SRES A1B emissions. MIROC A2: the MIROC 3.2 medium resolution GCM (Center for Climate Systems Research 2004) with SRES A2 emissions. alt climate: alternative spinup climate scaled to the means of the last 15 years of the MIROC A2 scenario.

subject to large fires. It is followed by a period of relatively little fire where 41% of the Park is dominated by grasslands. During the next period, the Park includes much less grassland area and more shrubland and woodland area, reflecting regrowth after wildfires (fig. 3.7).

Simulated biogeochemical fluxes and wildfire

Interannual variability in simulated net biome production (NBP) increases markedly from the 20th century to the 21st century (fig. 3.9), due to increased wildfire. The increase in interannual variability may be partly an artifact of simulating too little wildfire in the 20th century, but note that simulated wildfire, in terms of area burned, has larger peak annual values in the 21st century under the MIROC A2 scenario than either the simulated or the

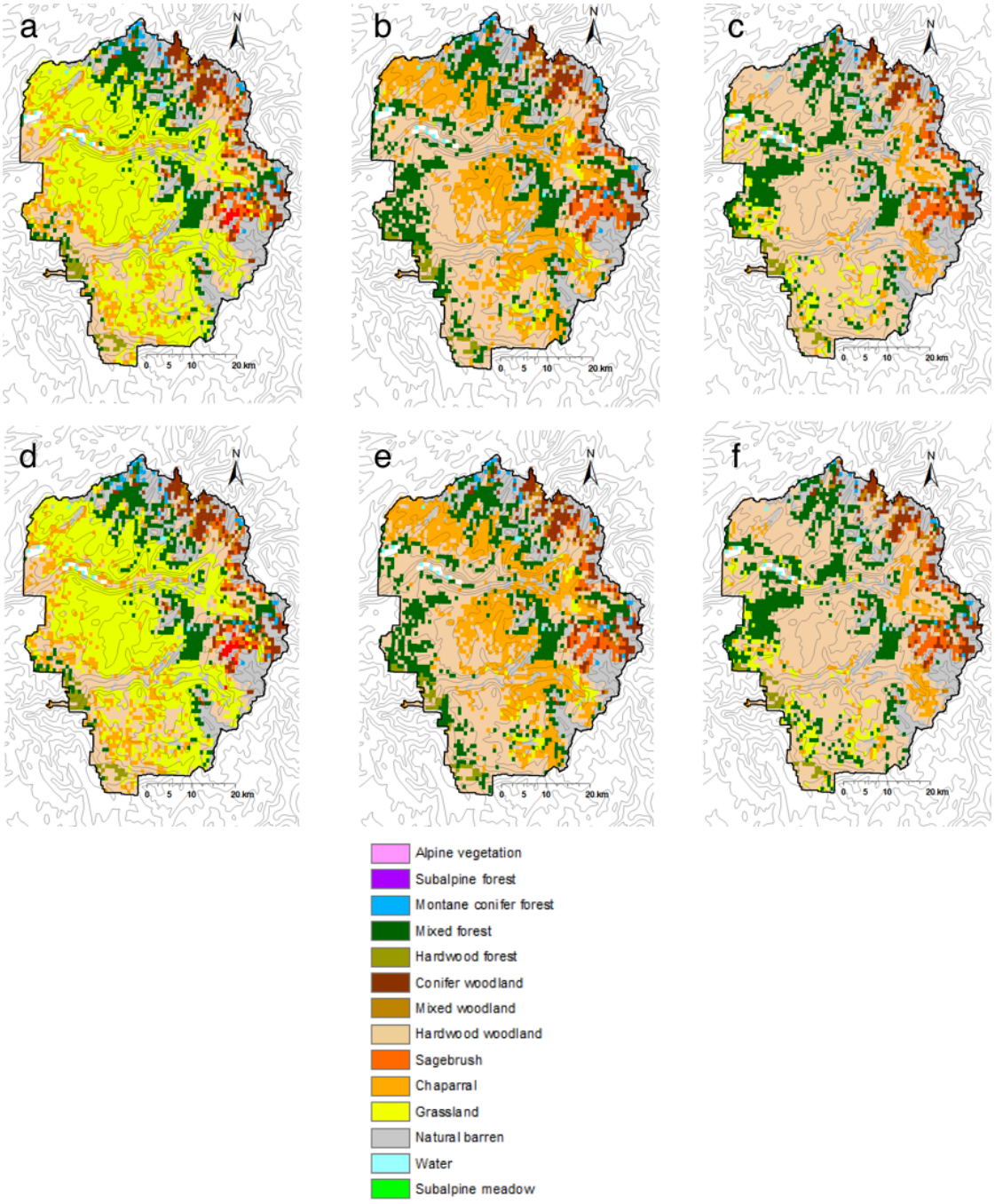

Fig. 3.8 Potential vegetation maps produced for 6 successive 31-year periods for the MIROC A2 scenario using the alternative simulation protocol: (a) and (d) 31-year period derived from MIROC A2 data for 2007—2037; (b) and (e) 31-year period derived from MIROC A2 data for 2038—2068; (c) and (f) 31-year period derived from MIROC A2 data for 2069—2099.

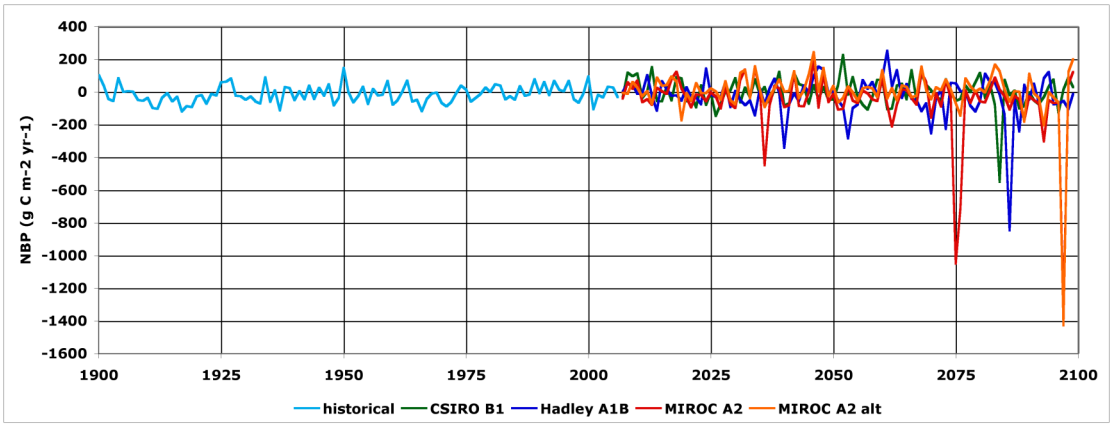

Fig. 3.9 Simulated annual net biome productivity for the historical period (1900-2006 shown), 3 future scenarios (CSIRO B1, Hadley A1B, MIROC A2), and using the alternative protocol with the MIROC A2 scenario (MIROC A2 alt.).

observed values for the 20th century (fig. 3.11). Total ecosystem carbon declines over the course of the 21st century under all 3 scenarios (fig. 3.10), by from 1% (CSIRO B1 scenario) up to 26% (MIROC A2 scenario). Abrupt decreases in total ecosystem carbon in the late 21st century are the result of large simulated fires (fig. 3.11). Under the three future climate scenarios, nitrogen uptake changes little or even decreases relative to the 20th century, while evapotranspiration increases (table 3.2). There is a general increase in biomass consumed by fires under all three future scenarios (table 3.2). Wildfires consume up to 35% of net primary production under the MIROC A2 scenario for the late 21st century, affecting all but the high elevation portions of the Park (fig. 3.12d); under the alternative simulation protocol, only 22% of NPP is consumed, but more of the Park area is affected by fire (fig. 3.12e). Fire index values are smaller and fire is less extensive in the CSIRO B1 and Hadley A1B scenarios (figs. 3.12b and 3.12c). Very little fire was simulated in the late 20th century (fig. 3.12a) in comparison with the simulated fires of the late 21st century,

Simulated ecosystem “memory” of historical climate

A comparison of the trends in NBP (net biome production, i.e. production minus heterotrophic respiration and wildfire consumption) under conventional and alternative protocols highlights the legacy of historical climate on the simulation of future climate

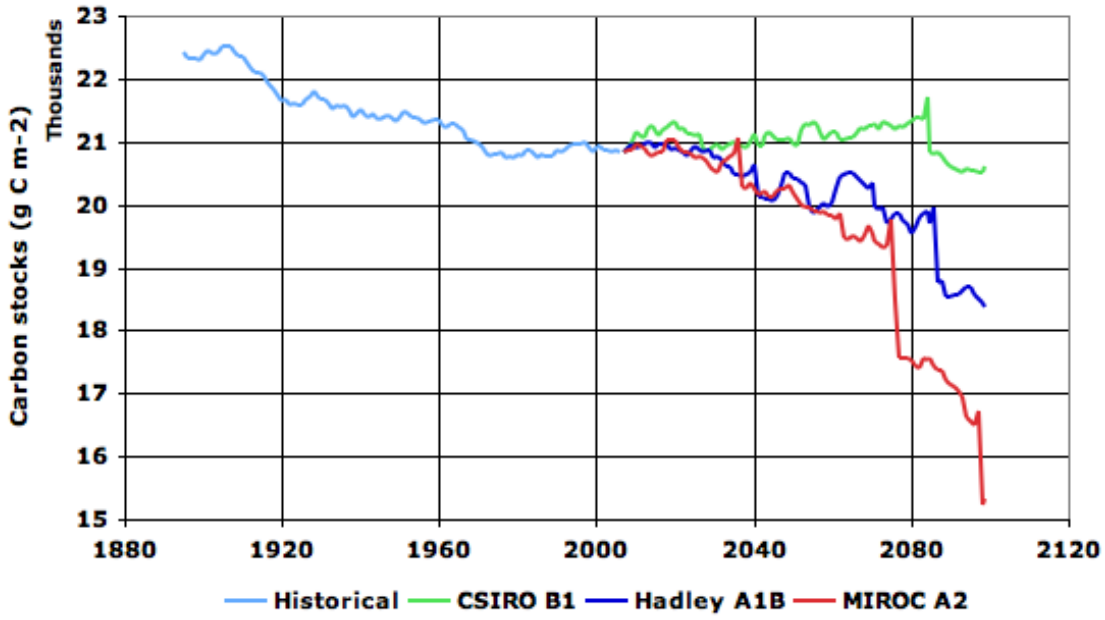

Fig. 3.10 Simulated total ecosystem carbon for the historical period and the three future scenarios.

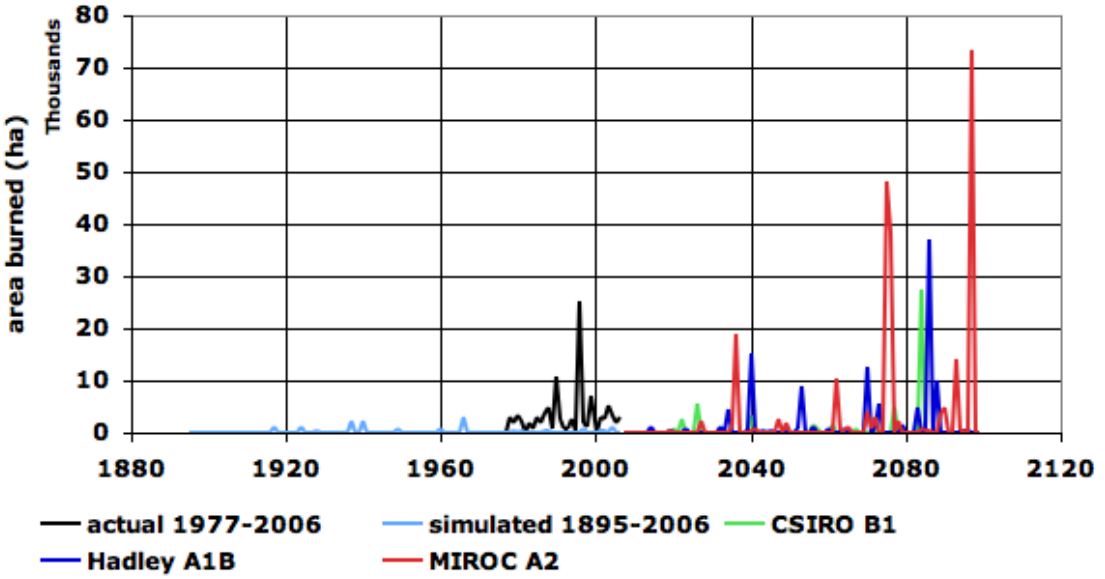

Fig. 3.11 Actual area burned for 1977-2006 and simulated area burned for the historical period and the three future scenarios.

Table 3.2 Simulated biogeochemical fluxes for Yosemite National Park for the historical period and the three future scenarios. B1: the CSIRO-MK3.0 general circulation model (H.B. Gordon et al. 2002) using the SRES B1 emissions scenario (SRES, IPCC 2007). A1B: the Hadley CM3 GCM (C. Gordon et al. 2000) with SRES A1B emissions. A2: the MIROC 3.2 medium resolution GCM (Center for Climate Systems Research 2004) with SRES A2 emissions.

spatially and temporally averaged flux	1895—2006	2007—2037	2038—2068	2069—2099	2007—99
net primary productivity ($g\ C\ m^{-2}\ yr^{-1}$)	323.0	B1: +376 A1B: +343 A2: +350	B1: +385 A1B: +368 A2: +342	B1: +384 A1B: +362 A2: +325	B1: +382 A1B: +358 A2: +339
heterotrophic respiration ($g\ C\ m^{-2}\ yr^{-1}$)	333.6	B1: 368 A1B: 351 A2: 354	B1: 370 A1B: 355 A2: 355	B1: 383 A1B: 375 A2: 346	B1: 374 A1B: 361 A2: 352
net ecosystem productivity ($g\ C\ m^{-2}\ yr^{-1}$)	-10.6	B1: +8 A1B: -8 A2: -4	B1: +15 A1B: +13 A2: -13	B1: +1 A1B: -13 A2: -21	B1: +8 A1B: -3 A2: -13
C in biomass consumed by fire ($g\ C\ m^{-2}\ yr^{-1}$)	2.6	B1: 5 A1B: 5 A2: 15	B1: 4 A1B: 17 A2: 11	B1: 21 A1B: 49 A2: 113	B1: 10 A1B: 24 A2: 46
net biome productivity ($g\ C\ m^{-2}\ yr^{-1}$)	-13.2	B1: +3 A1B: -13 A2: -19	B1: +11 A1B: -5 A2: -24	B1: -20 A1B: -62 A2: -134	B1: -2 A1B: -26 A2: -59
nitrogen uptake by vegetation ($g\ N\ m^{-2}\ yr^{-1}$)	7.4	B1: 7.8 A1B: 6.9 A2: 7.0	B1: 7.9 A1B: 6.7 A2: 6.2	B1: 7.4 A1B: 5.5 A2: 4.6	B1: 7.7 A1B: 6.4 A2: 5.9
evapotranspiration ($mm\ H_2O\ yr^{-1}$)	265	B1: 271 A1B: 271 A2: 276	B1: 271 A1B: 296 A2: 292	B1: 276 A1B: 327 A2: 308	B1: 273 A1B: 298 A2: 292

scenarios (fig. 3.13). NBP under the alternative protocol, from the 19th century thru the 21st century and beyond under the MIROC A2 scenario, oscillates around zero, which we interpret as the system being in equilibrium with the climate. Under the conventional protocol, NBP is negative during both the 20th and 21st centuries. The conventional protocol was extended beyond 2099 using the alternative spinup climate data set. During this extended period, another two centuries elapse before the NBP trace for the conventional protocol converges to

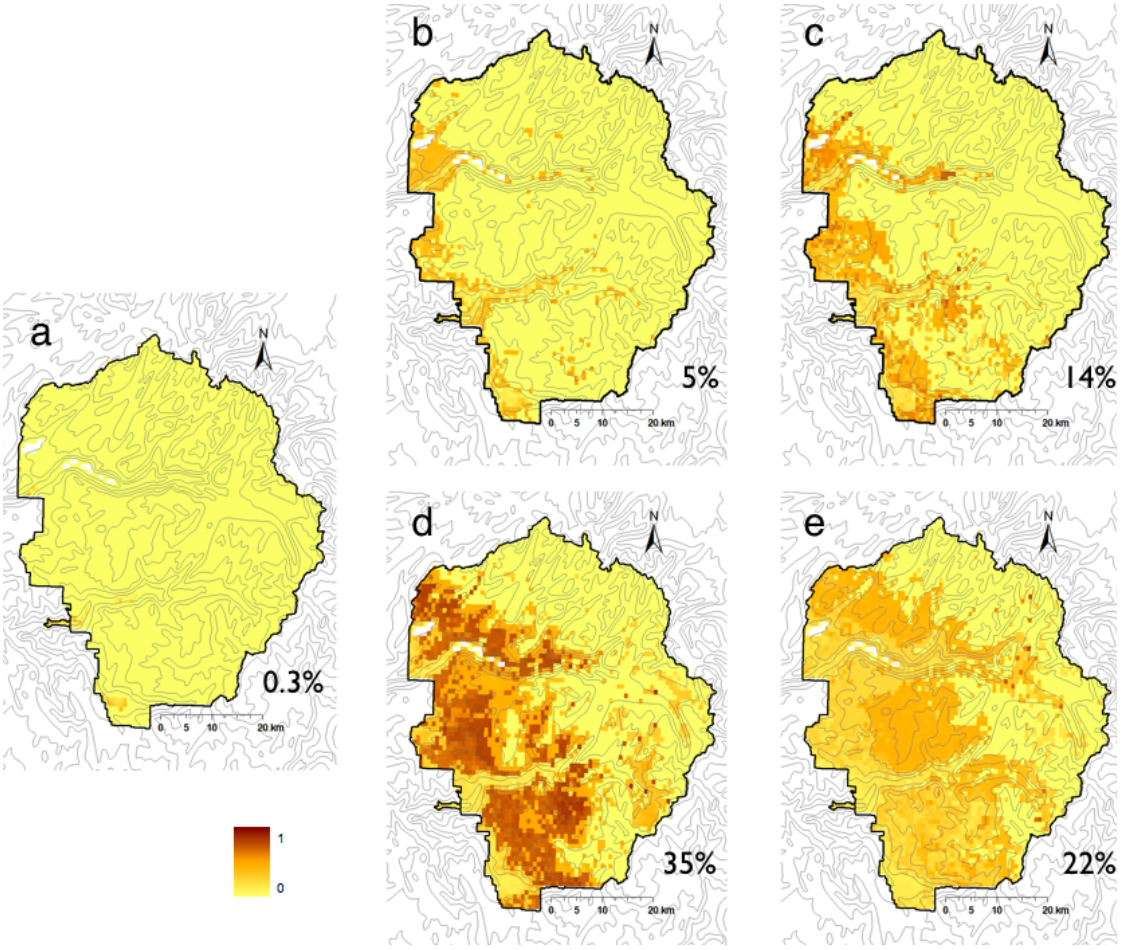

Fig. 3.12 Spatial patterns of the fire index for (a) 1967—1997, (b) 2069—2099 under the CSIRO B1 scenario, (c) 2069—2099 under the Hadley A1B scenario, (d) 2069—2099 under the MIROC A2 scenario, and (e) 2069—2099 under the MIROC A2 scenario using the alternative simulation protocol. Percentage shown in each frame is the fire index value for the Park as a whole. Fire index is defined here as the fraction of NPP consumed by fire.

the NBP trace from the alternative protocol (fig. 3.13), which gives us an estimate of the delay between a change in the environment and our current understanding of vegetation response to gradual change.

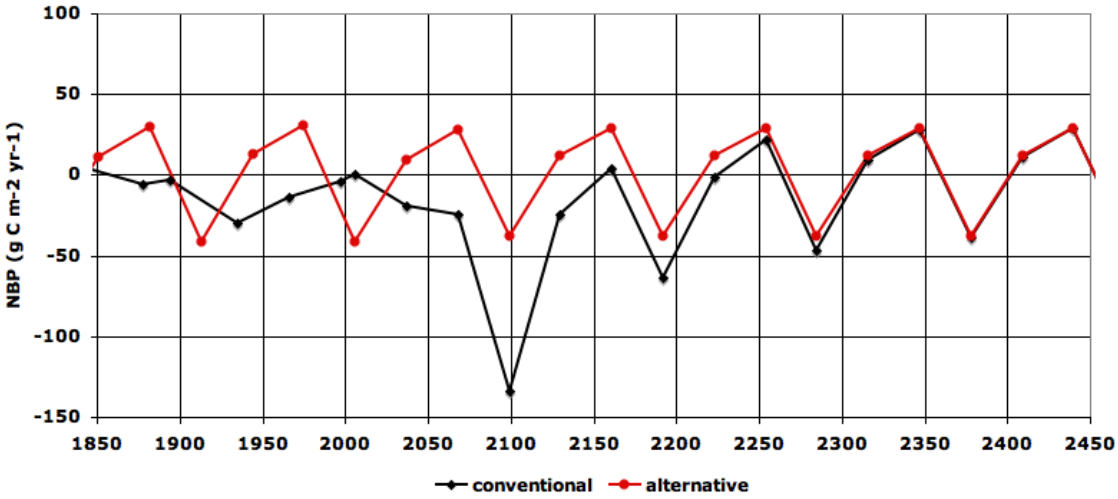

Fig. 3.13 Simulated net biome production in Yosemite National Park under the conventional and alternative simulation protocols, using the MIROC A2 future climate scenario. Data points are averages of annual NBP over time intervals, usually 31 years.

Discussion

Our general conclusion from these simulation results is that, by the end of the 21st century, the vegetation in most of the Park will have changed or, if not yet changed, will be experiencing stressful altered climatic conditions. Changes in vegetation will be mediated by a dramatic increase in wildfire. While considering the results of the MC1 simulations, it is important to keep in mind that MC1 simulates *potential*, rather than actual or predicted vegetation. As the climate changes, the actual vegetation on the landscape may be a combination of long-lived species that established under earlier, different climate conditions, together with younger cohorts of newly establishing species which are better adapted to the new conditions. The rate at which the actual vegetation changes will depend on rates of dispersal and establishment, processes which are not explicitly simulated by the MC1 model. In addition, the actual vegetation at specific locations is also dependent on the local disturbance history. Of all the possible disturbances - windthrow, beetle kill, diseases, timber harvest, grazing, etc. - MC1 simulates only one, wildfire. A result of including wildfire in the model is that a grid cell where conditions are suitable for forest may, in any given year, be classified as grassland, shrubland, woodland, or forest depending on the amount of time and simulated regrowth since the last simulated fire.

Implications of results from the alternative protocol

Under the MIROC A2 scenario, both simulation protocols produce extensive areas of fire at the end of the 21st century. The regular occurrence of large fires in every third 31-year time periods is a constant feature of the alternative protocol simulations when extended for additional centuries. While the amount of wildfire on the centennial scale is plausible, the regularity in its occurrence mainly in every third 31-year time period is likely an artifact of the detrending algorithm used to produce the climate data for the alternative protocol. Even after detrending, the third 31-year period is the warmest and driest of the three periods.

After 2099, an additional 200 simulation years elapse before the NBP values from the conventional and alternative protocols become similar. This persistent "memory" of antecedent transient climate, an emergent property of the simulation, is intuitively consistent with the presence of long-lived species in the real ecosystem. The conventional protocol uses a one-century-long detrended spinup climate scaled to the means of the 15 years 1895-1909 that is poorly suited to capture the effects of the end of the Little Ice Age (mid-nineteenth century) on 20th century vegetation. However an alternative is difficult to come up with since there are few climate records before 1895. Tree ring data could be used to create a more realistic spinup (Dr. Lisa Graumlich, pers. comm.), but this would constitute a separate research project.

Comparison to the findings of other researchers

Ten studies dating back to 1995, over scales from regional to continental and grains from ~800 m to ~50 km, project future vegetation for areas which include Yosemite (table 1.3). These studies all have at least one objective in common, which is to produce insight into the possible vegetation distributions in the late 21st century for their respective areas of interest. For all but the most recent, Yosemite constitutes only a small part of the study area. Emissions scenarios and future climate data sets have evolved during the 14 years since the first of these studies. Not surprisingly, the late 21st century vegetation patterns projected for the Yosemite region vary from study to study, and from those earlier studies to our present study.

All of the earlier studies except the first (VEMAP I: VEMAP Members 1995) use one version or another of MC1. The static biogeography model MAPSS (Neilson 1995) was used

to simulate future vegetation for the conterminous US during VEMAP phase I. For the VEMAP II study both the LPJ (Sitch et al. 2003) and MC1 dynamic global vegetation models were used to simulate vegetation changes across the conterminous US (Bachelet et al. 2003). Late 21st century potential vegetation maps from the MC1 simulations of the "hot and dry" future climate scenario for 5 of these previous studies are shown in fig. 3.14, along with the corresponding map from this study. While there are some similarities between some of the 6 maps, there are many differences.

There are a variety of methodological differences between the studies:

- different grains (3 at 10 km; 1 at 7.5 arc-minutes, ca. 12 km; 2 at 30 arc-seconds, ca. 800 m)
- different vegetation classification schemes (2 studies use VEMAP classes, 1 study uses a global vegetation classification scheme, 2 studies use a scheme developed for the state of California focusing on ecosystem services, and this study uses a recalibration of the "California scheme" specifically for Yosemite)
- different future climate scenarios (PCM IS92a, PCM A1, GFDL A2, and MIROC A2)
- different versions of the MC1 model

Many of the disagreements between the maps can be attributed to those methodological differences. Another source of visual differences between the maps in fig. 3.14 is that they are made from data readily available for the previous studies, and represent slightly different time periods (the single year 2100, the single year 2099, or modal vegetation classes for 2070—99, 2087—96, or 2069—2099). Despite their methodological differences, there is some agreement between these various studies. All of the studies agree on the absence of alpine vegetation zones in YNP in the late 21st century, and all but the earliest one agree on the absence of subalpine zones. All but the current study agree on the persistence of a zone of conifer forest; the current study has a zone of conifer woodland and a sizable adjacent zone of hardwood woodland. All of the studies agree on the existence of a zone of mixed forest west of (downslope from) the conifer zone, although they disagree on the elevational band occupied by the mixed forest. The current study places the upslope edge of the mixed forest at higher elevations than the earlier studies.

The most striking difference between the MIROC A2 map from this study and the maps from the previous studies is the decrease in forests and the increase in woodlands, shrublands, and grasslands. Three changes have been made to the simulation, since the completion of our report for YNP (Panek et al. 2009), which contribute to the decrease in forests. First, known errors in soil depth input data were corrected. The data published in a

Fig. 3.14 Maps of late 21st century potential vegetation distributions for Yosemite National Park from 6 studies. Under each map, the GCM and emissions scenario used in the simulation are shown, along with the year or years to which the map applies. The year in which the study was conducted is shown in parentheses. (a) Lenihan et al. 2006a, (b) Lenihan et al. 2003, (c) Gonzalez et al. 2007, (d) Shaw et al. 2008, (e) Panek et al. 2009, (f) our study. A1, A2, IS92a: IPCC emissions scenarios (IPCC 2000). GFDL: Geophysical Fluid Dynamics Laboratory general circulation model (Manabe et al. 1990, Wetherald et al. 1990). MIROC: Model for Interdisciplinary Research on Climate, version 3.2, medium resolution (Hasumi & Emori 2004). PCM: National Center for Atmospheric Research Parallel Climate Model (Dai et al. 2001, Washington et al. 2000).

Figure 3.14

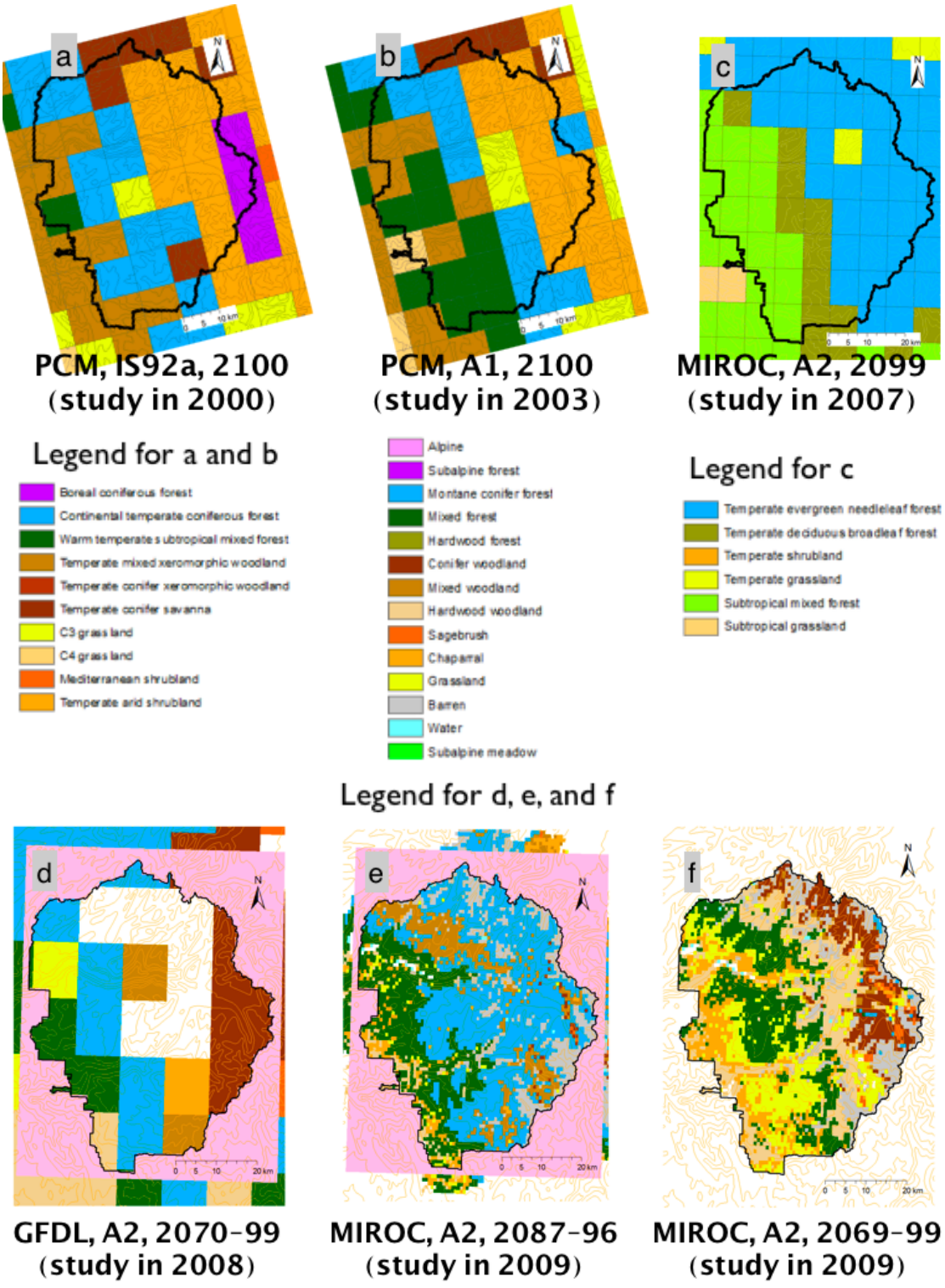
a
b
c
PCM, IS92a, 2100
(study in 2000)
PCM, A1, 2100
(study in 2003)
MIROC, A2, 2099
(study in 2007)
Legend for a and b
Boreal coniferous forest
Continental temperate coniferous forest
Warm temperate subtropical mixed forest
Temperate mixed xeromorphic woodland
Temperate conifer xeromorphic woodland
Temperate conifer savanna
C3 grass land
C4 grass land
Mediterranean shrubland
Temperate arid shrubland
Alpine
Subalpine forest
Montane conifer forest
Mixed forest
Hardwood forest
Conifer woodland
Mixed woodland
Hardwood woodland
Sagebrush
Chaparral
Grassland
Barren
Water
Subalpine meadow
Legend for c
Temperate evergreen needleleaf forest
Temperate deciduous broadleaf forest
Temperate shrubland
Temperate grassland
Subtropical mixed forest
Subtropical grassland
Legend for d, e, and f
d
e
f
GFDL, A2, 2070-99
(study in 2008)
MIROC, A2, 2087-96
(study in 2009)
MIROC, A2, 2069-99
(study in 2009)

report for YNP represented soils which were unrealistically deep over much of the Park. Secondly, the leaf area index threshold used to distinguish conifer woodland from montane conifer forests was raised from 3.75 to 4.7. This change was part of the process of calibrating the model to better match the VTM vegetation distribution. Raising the threshold had the effect of changing the simulated potential vegetation for high elevation areas in the late 21st century from montane conifer forest to conifer woodland. (The biogeography algorithm and associated thresholds are described more fully in chapter 4). Thirdly, errors in the time series of vapor pressure input data were corrected. The older data was biased to significantly higher vapor pressure values. Shallower soils mean lower water holding capacity, and lower vapor pressures mean higher evaporative demand, so the two input data corrections act synergistically to increase water stress. This in turn reduces the carrying capacity of the land. In addition, the decreased vapor pressure allows fuels to become drier in the model, tending to make fires more likely and more intense. The resulting vegetation map suggests a landscape for which the 20th century movement toward denser forests and infilling of high mountain meadows has, in the 21st century, been thrown into rapid reverse, towards a patchwork of more open forests, woodlands, shrublands, and grasslands. I will return to these implications in chapter 5, Conclusions.

CHAPTER FOUR: SIMULATING AND ASSESSING VEGETATION CHANGE

Once per simulation year, the MC1 dynamic global vegetation model derives potential vegetation from first principles. The legacy of the previous time period is carried forward in the form of the previous carbon density for two plant functional types. MC1 tracks carbon separately in woody and herbaceous vegetation, and uses the woody carbon density and climate data to identify what particular vegetation class is appropriate for each gridcell. MC1 does not make use of what the vegetation class was in the previous year.

Year-to-year vegetation change can be decomposed into two parts: interannual variability, and long-term trends. I describe a method to estimate the change associated with the longer-term trend, inspired by "Sorenson's index" as described by Keane (Keane et al. 2009). Sørenson himself was not concerned with temporal change, but with quantifying the similarity between two populations in terms of the species present (Sørenson 1948). He designated his measure of similarity "QS", the quotient of the actual number of common species divided by the possible number of common species.

$$QS = \frac{2c}{a+b} \cdot 100 \qquad \text{eq. 4.1}$$

where

QS = quotient of similarity (%)
a = total number of species in first population
b = total number of species in second population
c = number of species common to both populations

Mueller-Dombois & Ellenberg (1974) use the name "Sørenson's index" for the formula which Sørenson had called QS. Keane et al. (2008) apply Sørenson's concept (and the name "Sorenson's index", designated "SI") to quantifying the similarity of two patterns of vegetation, represented as maps of vegetation classes:

$$SI = 100 \cdot \left(\frac{\sum_{i=1}^{n} \min(A_i, B_i)}{area_{LRU}} \right) \qquad \text{eq. 4.2}$$

where

SI = Sorenson's index
i = index to vegetation class
n = number of vegetation classes
A_i = area of vegetation class *i* in the reference *A*
B_i = area of vegetation class *i* in the simulation output *B*
$area_{LRU}$ = area of the landscape reporting unit

Later, Keane et al. (2009) extend the definition of SI to compare a time series of maps to a single reference map:

$$SI = 100 \cdot \left(\frac{\sum_{j=1}^{m} \sum_{i=1}^{n} \min(A_i, B_{i,j})}{m \cdot area_{LRU}} \right) \qquad \text{eq. 4.3}$$

where

SI, A_j, i, n, and $area_{LRU}$ are as before
j = index to time interval
m = number of time intervals
$B_{i,j}$ = area of vegetation class *i* in the j^{th} map in series *B*

Although the expression "$\min(..., ...)$" suggests taking the minimum value between the total area occupied by vegetation class *i* in the first map (A_i) and the total area occupied by vegetation class *i* in a second map (B_i in eq. 4.2, $B_{i,j}$ in eq. 4.3), the area is actually that part of the study area which is occupied by vegetation class *i* on *both* maps, i.e. the intersection of the parts of both maps occupied by vegetation class *i* (Keane et al. 2008).[7] I used a further generalization of equation 4.3 to compare a reference *series* of vegetation maps with a second series. I use the method to quantify the difference between simulated vegetation patterns for different time intervals, e.g. between the simulated vegetation patterns for 1967—1997 and those for 2069—2099. In this use it is a measure of the vegetation change over time. I also use it to compare a single map of observed vegetation patterns with a series of simulated vegetation patterns, e.g. between the 1997 NPS Survey and the simulated vegetation patterns for 1967—1997. The latter use represents a special case where the reference "series" consists of just one map. In this second use, it is a measure of the departure of the simulation from the observations.

In this chapter I only report results from simulating the historical period and the MIROC A2 future climate scenario. It is likely given current atmospheric CO_2 concentrations that the actual future trajectory of greenhouse gas concentrations will lie above the A2 emission scenario (Raupach et al. 2007), therefore I chose to document only the MIROC A2 scenario as it is the closest scenario to projected trends.

[7] The published form of this equation (Keane et al. 2009) inadvertantly omits the *i* subscript from the $B_{i,j}$ term (Robert Keane, pers. comm.).

Methods

Biogeography rules (Table 4.1)

A set of biogeography rules in the MC1 model use climate and the leaf area index of woody vegetation to determine potential vegetation type. The rules are applied hierarchically. At the top level, growing degree-day sums are used to distinguish zones of alpine and subalpine vegetation from other areas. Next, for all areas except the alpine and subalpine zones, temperature thresholds are used to determine the type of any woody vegetation, distinguishing between needleleaf woody vegetation, broadleaf woody vegetation, and a mixture of the two. (In the alpine and subalpine zones, woody vegetation is assumed to be always needleleaf.) At the third level, leaf area index (LAI) of the woody vegetation is used to determine the physiognomy of the vegetation, separating forests, woodlands, shrublands, and grasslands. Finally, minimum mean monthly temperature is used to distinguish between different types of woodland and between different types of shrubland. For Yosemite, the MC1 biogeography rules distinguish among twelve potential vegetation types, designated *alpine vegetation, subalpine forest, subalpine meadow, montane conifer forest, mixed forest, hardwood forest, conifer woodland, mixed woodland, hardwood woodland, chaparral, sagebrush*, and *grassland*.

Temperature and LAI data used in the biogeography rules are smoothed to reduce the effect of interannual variability. The smoothing is carried out on annual time series of same month data. For example, the smoothed value of the mean temperature for the month of February is calculated as:

$$TMP_{smooth}[Feb_{curr}] = e^{-1/\tau} \cdot TMP_{smooth}[Feb_{prev}] + (1 - e^{-1/\tau}) \cdot TMP_{raw}[Feb_{curr}] \quad \text{eq. 4.4}$$

where

$TMP_{smooth}(month)$ = smoothed value of average temperature for the given month (°C)
$TMP_{raw}(month)$ = unsmoothed value of average temperature for the given month (°C)
Feb_{curr} = index to value of TMP_{raw} and TMP_{smooth} for February in the current simulation year
Feb_{prev} = index to value of TMP_{raw} and TMP_{smooth} for February in the previous simulation year
τ = 10 (yr)

In the exponent ($-1/\tau$) of the exponential term, both the numerator and the denominator have units of years; thus the exponential term itself ($e^{-1/\tau}$) is unitless. The denominator, τ, represents an estimate of the characteristic response time of the vegetation type to changing climatic conditions. Woodward describes τ as the time required to change by 63.2% (= $1 - e^{-1}$) towards a new value after a step change in conditions (Woodward 1987 p.20). During the

original development of the MC1 model, alternative values for τ were explored; τ = 10 years was chosen as the value which produced the most realistic simulations of vegetation change (D. Bachelet, pers. comm.).

An annual temperature index (TI) is calculated for use in distinguishing between needleleaf, broadleaf, and mixed areas of woody vegetation, hereafter called domains. TI is

Table 4.1 Summary of biogeography rules. Potential vegetation types are shown in boldface. TI: temperature index; gdd: growing-degree-day sum; LAI: woody leaf area index; minT: lowest monthly average of daily minimum temperatures.

High Elevation	gdd ≤ 1300	**alpine**		
	1300 < gdd ≤ 1900	LAI < 1.0	**subalpine meadow**	
		LAI ≥ 1.0	**subalpine forest**	
Forest	gdd > 1900			
		TI ≤ -8 needleleaf	-8 < TI ≤ 45 mixed	TI > 45 broadleaf
		montane conifer forest	**mixed forest**	**hardwood forest**
	LAI >	4.7	4.7	4.75
Woodland	LAI ≤	4.7	4.7	4.75
	minT ≤ 0 °C	**conifer woodland**	**hardwood woodland**	
	minT > 0 °C	**mixed woodland**		
	LAI >	2.0	2.5	3.0
Shrubland	LAI ≤	2.0	2.5	3.0
	minT ≤ 0 °C	**sagebrush**	**chaparral**	
	minT > 0 °C	**chaparral**		
	LAI >	0.2	1.0	0.1
Grassland	LAI ≤	0.2	1.0	0.1
		grassland		

unitless, and varies between -100 and +100 in proportion as the lowest smoothed monthly mean temperature varies between -15°C and +18°C. Gridcells with values of TI below -8 are in the needleleaf domain; gridcells with values of TI above +45 are in the broadleaf domain; and gridcells with values of TI between -8 and +45 are in the mixed domain.

A growing degree-days (gdd) sum, referenced to 0°C, is calculated from the smoothed monthly average temperatures. It is used to distinguish alpine vegetation (≤1300 gdd) and subalpine vegetation (> 1300 and ≤ 1900 gdd) from other types of vegetation. Subalpine forests are further distinguished from subalpine meadows using a projected woody LAI threshold of 1.0 (m^2 leaf m^{-2} ground).

When the growing degree-days sum is > 1900 gdd, a combination of woody vegetation domain (i.e. needleleaf, broadleaf, or mixed), projected woody LAI, and mininum monthly mean temperature are used to distinguish among the remaining nine vegetation types. The forest/woodland LAI threshold was calibrated to 4.7 for the needleleaf and mixed domains, and 4.75 for the broadleaf domain. For the needleleaf domain, the woodland/shrubland LAI threshold was calibrated to 2.0; conifer woodland results where the minimum monthly mean temperature is ≤ 0°C, otherwise the vegetation class is mixed woodland. For the mixed domain, the woodland/shrubland threshold was calibrated to 2.5; for the broadleaf domain, the threshold is 3.0. In both those cases, the woodland vegetation class is hardwood woodland. The shrubland/grassland LAI threshold is 0.2 for the needleleaf domain, 1.0 for the mixed domain, and 0.1 for the broadleaf domain. Shrublands in the broadleaf and mixed domains are classified as chaparral. In the needleleaf domain where the minimum monthly mean temperature is below freezing, shrubland is classified as sagebrush, otherwise it is classified as chaparral. The sagebrush type corresponds to the LSG Low Sage and SGB Sagebrush classes in the WHR scheme (table 2.3). LSG corresponds to Küchler's Sagebrush Steppe; and SGB includes both his Sagebrush Steppe and his Juniper Shrub Savanna (de Becker & Sweet 2008). The chaparral type corresponds to CRC Chamise - Redshank Chaparral, MCH Mixed Chaparral, and MCP Montane Chaparral (table 2.3). All three of those WHR classes correspond to Küchler's Chaparral class (de Becker & Sweet 2008).

Leaf area index is related to the size of the live carbon stock in woody vegetation through the equation

$$LAI = \frac{C}{C_k + C} \cdot lai_{max} \qquad \text{eq. 4.5}$$

where

LAI = projected leaf area index of woody vegetation (m^2 leaf m^{-2} ground)
C = live coarse wood carbon (g C m^{-2})
lai_{max} = 10 (projected m^2 leaf m^{-2} ground)
C_k = 2000 (g C m^{-2})

The LAI values compared to the biogeography thresholds are smoothed maximum annual LAI values. The smoothing algorithm is similar to the one described above for temperature data (eq. 4.4), except that after a fire is simulated, only the maximum annual LAI values for years after the year of the fire are used in the smoothing calculation.

MC1's biogeography algorithm was calibrated for this study by adjusting the values of four thresholds to obtain a better match between the modal simulated potential vegetation map for 1905—1935 and the VTM map. I began the calibration process using a version of MC1 which had been used in an earlier study of the entire state of California at a grain of 12km (Shaw et al. 2008). I made these changes:

- the TI threshold between the needleleaf and mixed domains was lowered from +20 to -8
- the gdd threshold for subalpine vegetation types was lowered from 2000 to 1900
- the forest/woodland LAI threshold for the needleleaf domain was raised from 3.75 to 4.7
- the forest/woodland LAI threshold for the mixed domain was raised from 4.25 to 4.7.

Calibration of the LAI threshold values was carried out through an ad hoc process of adjusting values, repeating the simulation, and then evaluating the effect by visual appraisal of the resulting vegetation map, compared to the VTM map, and by recalculating measures of similarity between the maps. Threshold values not adjusted in this study were obtained from the calibration done for the California Scenarios 2008 study (Panek et al. 2008).

Difference index

I introduce a "map series difference index" (MSDI), as a measure of the difference in vegetation between a reference time series of gridded vegetation maps and a second time series of gridded vegetation maps. Differences between vegetation patterns in two time series of maps arise both from interannual variation *within* a single time series and from longer-term trends *between* time series. MSDI has a maximum of +1 and a minimum of $-(1 + 1/n)$, where n is the length of the time series. Negative values indicate that the interannual variability within the two time series is more significant than the longer-term trends between the two time series. Positive values indicate that the longer-term trend is more significant than the interannual differences.

Building on Keane's work, and as a preliminary step to defining the difference index, I define a "map series similarity index" (MSSI) as a way of quantifying how *similar* two map

series are to each other. In the definition, the *match* term replaces the inner summation in Keane's formulas (eqs. 4.2 and 4.3). The *match* term is the fraction of gridcells for which the attribute of interest is the same in spatially corresponding gridcells in the two maps I compare. In the definition of MSSI, I replaced the outer summation in Keane's formulas, which represents the comparison of each map in the time series with the reference map, by a double summation, which represents the comparison of *every* map in each time series with *every* map in the other time series. MSSI, like Sorenson's index, ranges in value from 0 (no similarity) to 1 (complete similarity). In the case where the reference "series" is just a single map, the definition of MSSI is equivalent to the definition of Sorenson's index in equation 4.3.

$$MSSI(A,B) = \frac{\sum_{tb=1}^{nb}\sum_{ta=1}^{na} match(ta,tb)}{na \cdot nb} \qquad \text{eq. 4.6}$$

$$match(ta,tb) = \frac{\sum_{j=1}^{ncols}\sum_{i=1}^{nrows}\left(A_{ta}[i,j] \equiv B_{tb}[i,j]\right)}{nrows \cdot ncols} \qquad \text{eq. 4.7}$$

where

A, B = time series of maps to be compared
MSSI = map series similarity index
na, nb = the lengths of time series A and B
ta, tb = indices to time series A and B
match(ta, tb) = the fraction of gridcells in map A_{ta} having the same value for the attribute of interest as the corresponding gridcells in map B_{tb}
nrows, ncols = the numbers of rows and columns in the map grid
i, j = row and column indices
$\left(A_{ta}[i,j] \equiv B_{tb}[i,j]\right)$ is 1 when the cell attribute values are the same, 0 otherwise

MSSI, when used to compare the maps in a time series of maps with each other, is a measure of the interannual variability *within* a single time series. I make use of that characteristic to define the difference index MSDI in a way that helps distinguish differences arising from interannual variation from differences arising from longer-term trends.

$$MSDI(A,B) = MSSI(A,A) + MSSI(B,B) - MSSI(A,B) - 1 \qquad \text{eq. 4.8}$$

where

A, B, MSSI are as before
MSDI = map series difference index

A rationale for the form of MSDI and derivation of its properties are given in the Appendix.

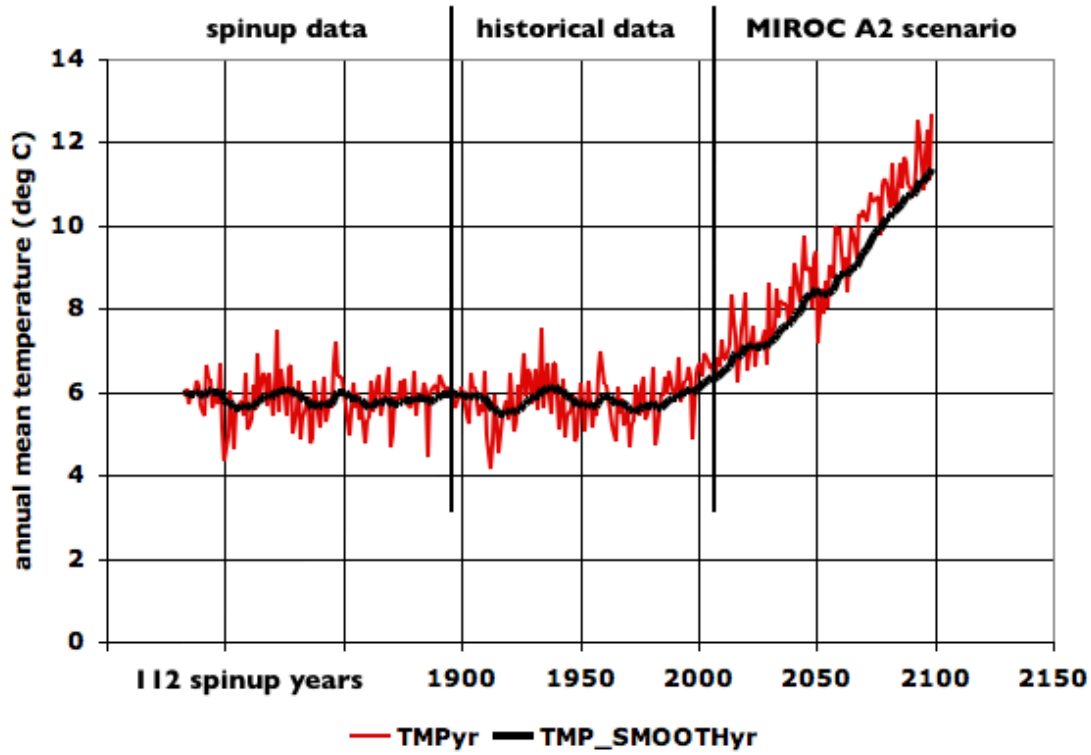

Fig. 4.1 Unsmoothed and smoothed mean annual temperature time series for Yosemite National Park, using detrended, rescaled spinup data, PRISM historical data for 1895-2006 (Daly et al. 2008), and MIROC A2 scenario data for 2007-2099 (Center for Climate Systems Research 2004, IPCC 2000).

Results for the historical period and the MIROC A2 future scenario

Smoothing

Smoothing of temperature data and woody leaf area index values reduces the amplitude of interannual variability substantially (eq. 4.4, fig. 4.1). As a result, changes in the growing degree-day sum, temperature index, and minimum mean monthly temperature which have the potential to produce changes in vegetation type are more closely associated with longer-term trends than with interannual variability. When there is a well-defined long-term trend, as in the rising temperatures of the MIROC A2 scenario, the smoothing algorithm also introduces a lag of 10 years between the unsmoothed temperatures and the smoothed temperatures (fig. 4.1).

Calibration

The calibration reduced the differences between the simulated potential vegetation maps and the VTM map. Before the biogeography thresholds were adjusted, the simulated potential vegetation map for 1935 differed from the VTM map on 69% of the gridcells, and the MSDI value for the comparison of the VTM map to the series of annual simulated potential vegetation maps for 1905—1935 was 0.62. After the thresholds were changed, the difference between the simulated potential vegetation map for 1905—1935 and the VTM map was reduced to 40%, and the MSDI value was reduced to 0.33.

The calibration also reduced the differences between the simulated potential vegetation maps for 1967—1997 and the 1997 NPS Survey map, but by lesser amounts. Before the thresholds were adjusted, the simulated potential vegetation map for 1997 differed from the 1997 survey map on 67% of the gridcells, and the MSDI value for the comparison of the 1997 survey map to the series of annual simulated potential vegetation maps for 1967—1997 was 0.62. After the thresholds were changed, the difference between the simulated potential vegetation map for 1967—1997 and the 1997 survey map was reduced to 46%, and the MSDI value was reduced to 0.38.

Simulated vegetation changes

Simulations using the 20th century climate indicate that alpine and subalpine zones, together with the unvegetated areas, occupied nearly half of the Park area (fig. 4.2a-4.2c). Under the MIROC A2 scenario, temperatures increase sufficiently in the early 21st century to eliminate all of the alpine zone and shift the subalpine zone upslope towards the northeast (fig. 4.2d). By the late 21st century, the subalpine zone too has disappeared (fig. 4.2f).

Outside the alpine/subalpine zones, the Park area is split between an upslope part which is cold enough to fall in the needleleaf domain, and a downslope part which is warm enough to fall in the mixed domain (fig. 4.3). The ratio of needleleaf domain area to mixed domain area varies from period to period over the 20th and 21st centuries. Beginning in the late 20th century, the boundary between the two areas advances upslope, from west to east. From the early 20th century through the early 21st century, the needleleaf domain, characterized by montane conifer forest and conifer woodland, is bounded on the upslope side

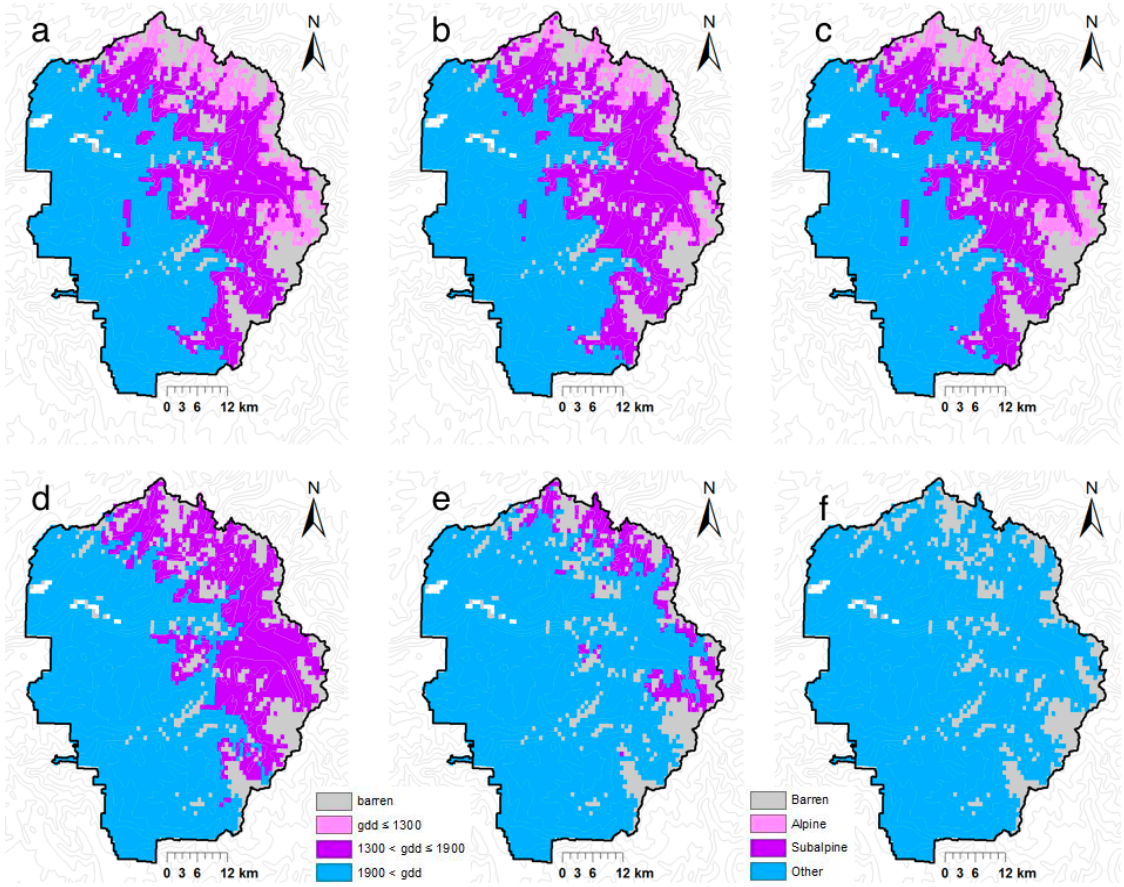

Fig. 4.2 Maps of average growing degree-day (0°C) sums and corresponding climate zones for six 31-year periods, using PRISM historical data for 1895-2006 (Daly et al. 2008), and MIROC A2 scenario data for 2007-2099 (Center for Climate Systems Research 2004, IPCC 2000): (a) 1905—1935, (b) 1936—1966, (c) 1967—1997, (d) 2007—2037, (e) 2038—2068, (f) 2069—2099.

by the subalpine zone (figs. 4.3a-4.3d and 4.2a-4.2d). This boundary with the subalpine zone moves into the highest parts of the Park in the middle 21st century (fig. 4.3e), and by the late 21st century the subalpine zone has disappeared and the needleleaf domain extends clear across the Sierra crest, while the mixed domain occupies all of the middle elevation and most of the lower elevation areas, comprising the majority of the Park (fig. 4.3f). At lower elevations, there are a few small areas that are warm enough to fall in the broadleaf domain (fig. 4.3f).

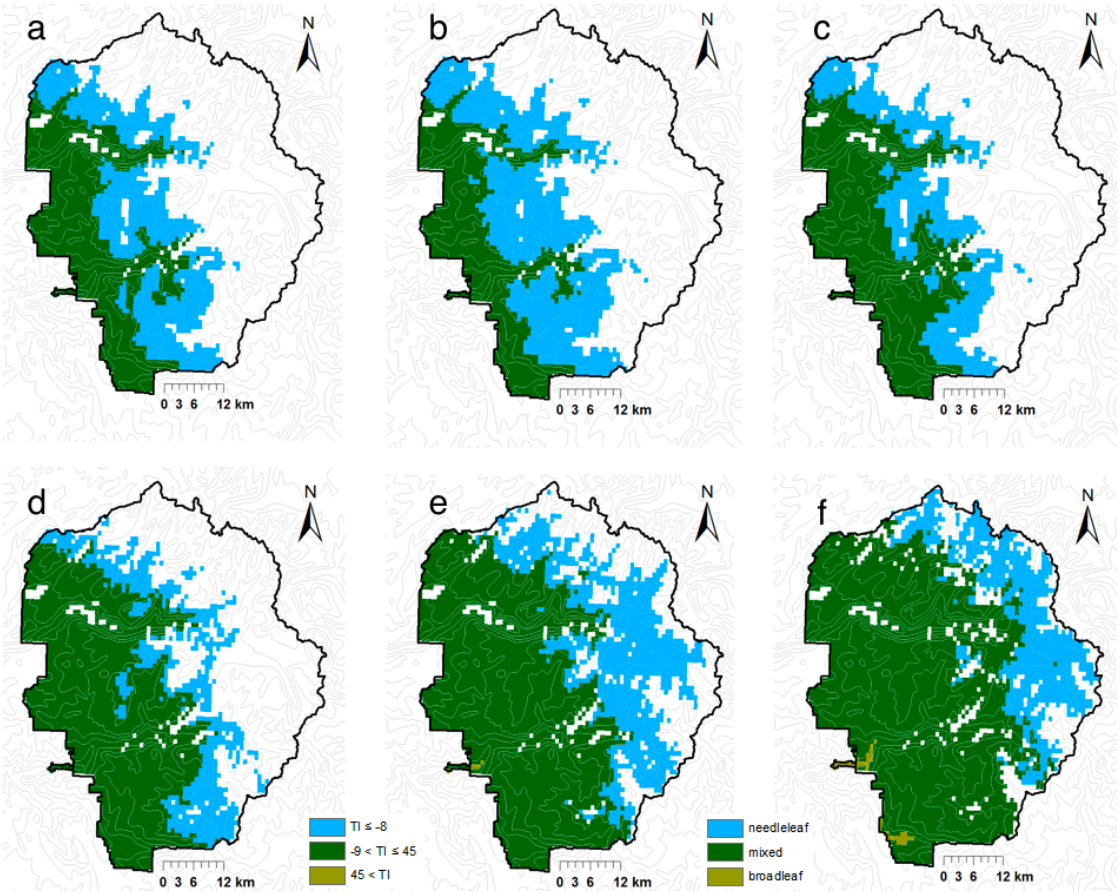

Fig. 4.3 Maps of temperature index (TI) and corresponding woody vegetation type for vegetated areas outside the alpine and subalpine zones, for six 31-year periods, using PRISM historical data for 1895-2006 (Daly et al. 2008), and MIROC A2 scenario data for 2007-2099 (Center for Climate Systems Research 2004, IPCC 2000): (a) 1905—1935, (b) 1936—1966, (c) 1967—1997, (d) 2007—2037, (e) 2038—2068, (f) 2069—2099.

The simulated leaf area index in most of the area outside the alpine and subalpine zones is high enough to warrant a forest classification throughout the 20th century and the early 21st century (fig. 4.4a-4.4d). By mid 21st century, the subalpine zone shrinks to a small area along the Sierra crest. The simulated LAI in the high elevation part of the Park which had previously been in the subalpine zone is below the forest/woodland threshold (fig. 4.4e), resulting in reclassification of that area as conifer woodland. Low leaf area indices, some low enough to fall below the woodland/shrubland threshold or even below the shrubland/grassland

threshold, also appear in the southwestern part of the Park and in Yosemite Valley and the Poopenaut Valley area below Hetch Hetchy reservoir (fig. 4.4e). In the late 21st century, average LAIs have fallen below the forest threshold into the woodland, shrubland, and grassland ranges in most of the Park. The decline in LAIs is associated with a spike in simulated wildfire and a sharp drop in ecosystem carbon in the 2070s (figs. 3.11 and 3.10). The sequence of modal simulated potential vegetation maps shown in fig. 4.5 is the result of the changes in growing degree-day sums, temperature index, and leaf area index shown in figs. 4.2, 4.3, and 4.4. Visually, the three 20th century maps (figs. 4.5a-4.5c) are relatively similar to each other, while the three 21st century maps (figs. 4.5d-4.5f) are increasingly

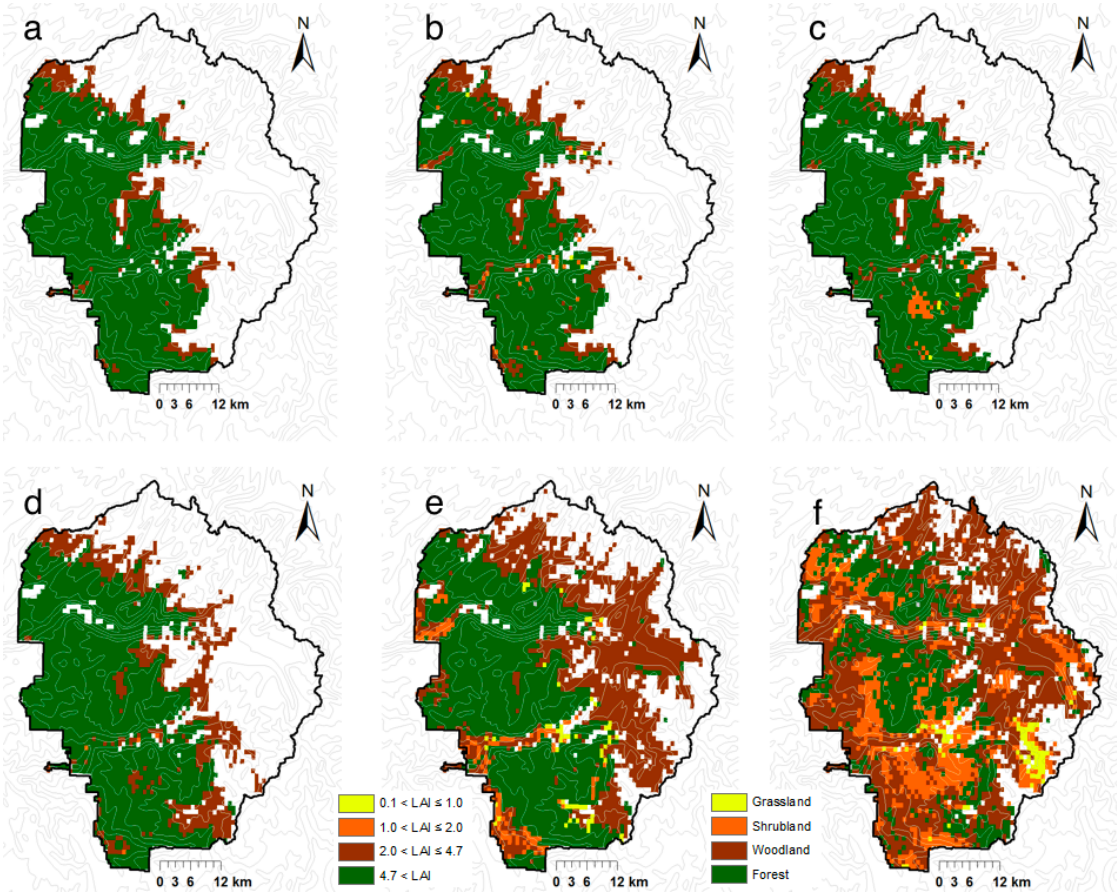

Fig. 4.4 Maps of simulated leaf area index of woody vegetation (LAI, projected m^2 leaf m^{-2} ground) and approximate corresponding physiognomic type for vegetated areas outside the alpine and subalpine zones, for six 31-year periods, using PRISM historical data for 1895-2006 (Daly et al. 2008), and MIROC A2 scenario data for 2007-2099 (Center for Climate Systems Research 2004, IPCC 2000): (a) 1905—1935, (b) 1936—1966, (c) 1967—1997, (d) 2007—2037, (e) 2038—2068, (f) 2069—2099.

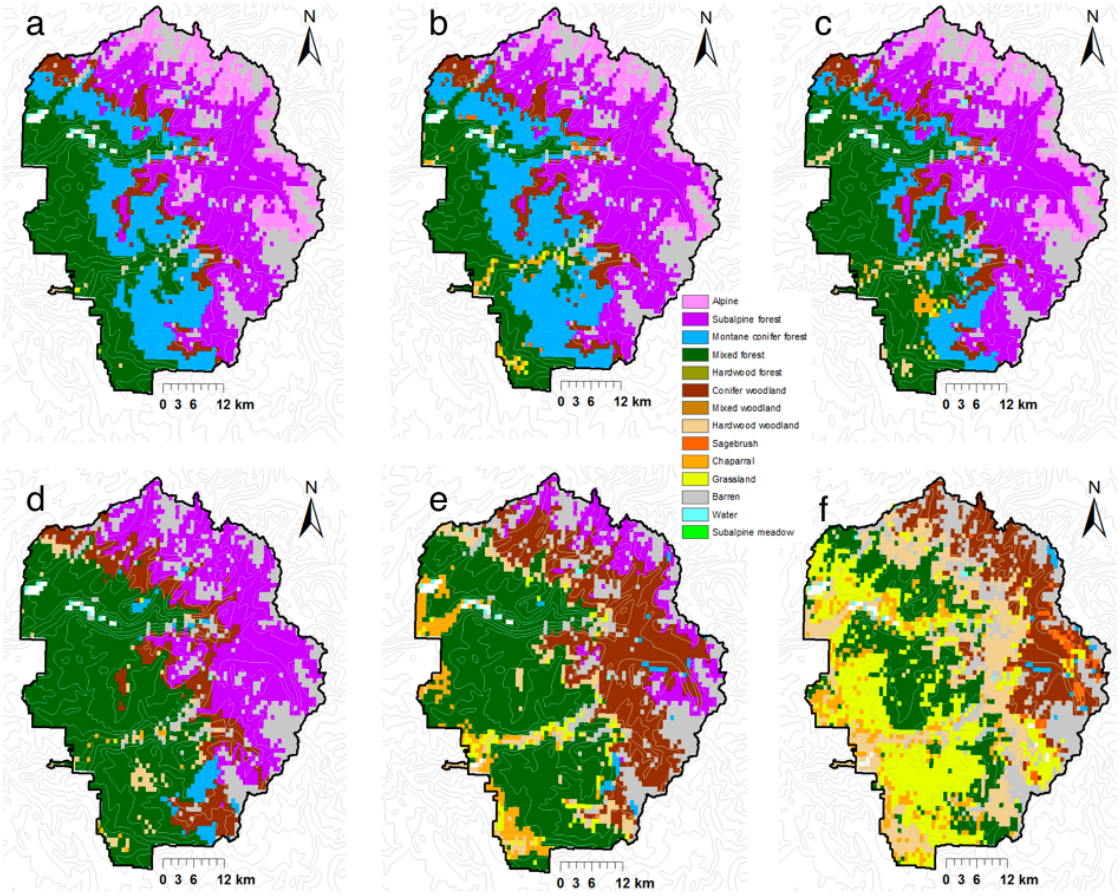

Fig. 4.5 Maps of modal simulated potential vegetation types for six 31-year periods, using PRISM historical data for 1895-2006 (Daly et al. 2008), and MIROC A2 scenario data for 2007-2099 (Center for Climate Systems Research 2004, IPCC 2000): (a) 1905—1935, (b) 1936—1966, (c) 1967—1997, (d) 2007—2037, (e) 2038—2068, (f) 2069—2099.

different from the 20th century maps, as well as quite different among themselves. The first big change is apparent in the map for the early 21st century (fig. 4.5d): the area which was previously classified as montane conifer forest has been reclassified as mixed forest, representing an eastward extension of mixed forest to higher elevations. Most of the area below the subalpine zone but still cold enough to be in the needleleaf domain (see fig. 4.3d) has leaf area indices which are below the forest/woodland threshold (see fig. 4.4d) and so is

classified as conifer woodland rather than montane conifer forest in fig. 4.5d. Two additional significant differences are visible in the mid 21st century map (fig. 4.5e). At high elevation, the subalpine zone disappears almost completely (see also fig. 4.2e), and is replaced by conifer woodland because the simulated LAI is below the forest/woodland threshold (see fig. 4.4e). At the lowest elevations and in the Yosemite and Poopenaut Valleys, significant areas of chaparral and grassland appear in the mid 21st century map (fig. 4.5e) for the first time, corresponding to areas of low LAI (fig. 4.4e). Finally, the late 21st century map of potential vegetation (fig. 4.5f) bears little resemblance to the 20th century maps. The alpine, subalpine, and montane conifer forest zones are gone. The highest elevations are occupied by conifer woodland. Just below the conifer woodland (including part of the Tuolumne Meadows area) is a belt of hardwood woodland, then mixed forest and large areas of grassland. At the lowest elevations and in the Yosemite and Poopenaut Valleys, the dominant potential vegetation types are chaparral and hardwood woodland.

Some of the modal potential vegetation types in the southwestern part of the Park in figures 4.5e and 4.5f are inconsistent with the average leaf area indices in figures 4.4e and 4.4f. LAIs characteristic of shrubland appear in places mapped as having potential vegetation of grassland. This inconsistency is an artifact of displaying the temporal *average* value for LAI, which is a continuous variable, while displaying the *modal* value for the potential vegetation type, a categorical variable. Much of the affected area converts from mixed forest to grassland in the 2070s as a result of simulated wildfires. Although the LAI is below the shrubland/grassland threshold for the majority of the 2069—2099 period, which results in grassland as the modal vegetation type, the high LAIs associated with the forests prior to the simulated fires, when averaged with the low grassland LAIs, produce an average LAI which is above the shrubland/grassland threshold.

The warmer and drier climate of the late 21st century in the MIROC A2 scenario affects the seasonal pattern of simulated vegetation growth, but not in ways that result in different vegetation types. A comparison of climographs for 1967—1997 and 2069—2099 shows that, in the projected climate for the late 21st century, the mean monthly temperature for the Park never falls below freezing, whereas in the late 20th century the mean temperature was below freezing in all three winter months (fig. 4.6a and 4.6b). The milder winters result in earlier snowmelt (fig. 4.6c) and increased net primary productivity for the forests in fall and winter months, while the reduction in simulated NPP due to drought in the summer months is exacerbated (fig. 4.6d and 4.6e).

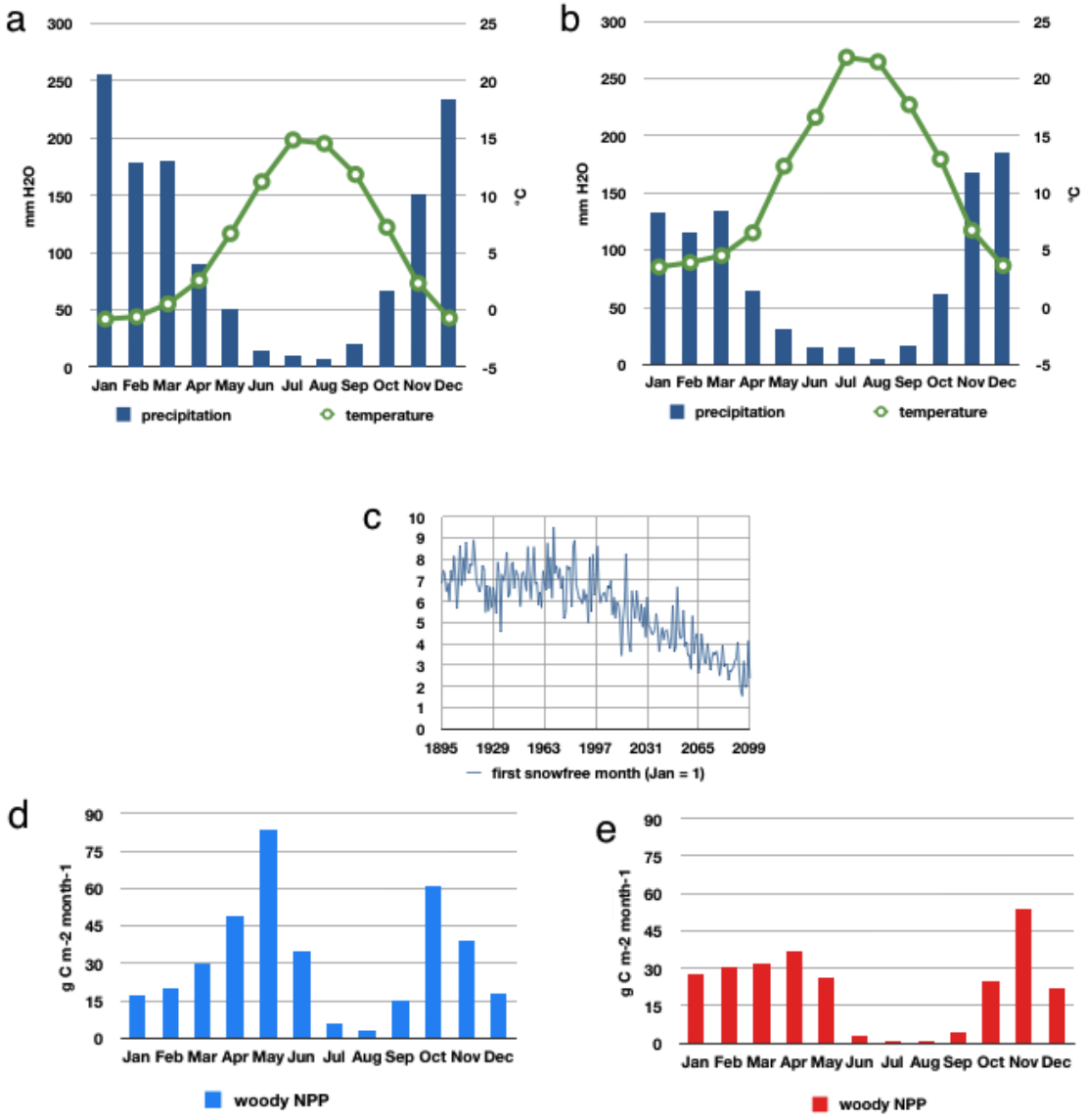

Fig. 4.6 Comparison of late 20th century to late 21st century seasonality under the MIROC A2 future climate: a) climograph for 1967—1997, b) climograph for 2069—2099, c) spatial average of simulated first snowfree month for 1895—2099, d) seasonality of simulated net primary production for woody vegetation for 1967—1997, e) seasonality of simulated net primary production for woody vegetation for 2069—2099.

Map series difference index

I compared the values of Sorenson's index and the map series difference index with simple percentage match and difference values, as measures of the correspondence between simulated potential vegetation and observed vegetation (table 4.2). MSDI values are given in table 4.3 for all pairwise comparisons of the 6 series of annual maps underlying the modal potential vegetation maps in fig. 4.5. Of particular interest are the MSDI values for the six series compared with themselves, along the diagonal of table 4.3. As expected from the definition of MSDI (eq. 4.8), these values are all negative, since the only differences arise from interannual variability. The magnitudes of the first 4 values fall within a narrow range (0.05 - 0.09), but the final 2 values, corresponding to the mid and late 21st century, increase sharply in magnitude. The magnitude of the final value (0.21) is more than double the magnitude of any of the values corresponding to the 20th century and the early 21st century. MSDI values for the off-diagonal comparisons range from 0 to 0.55. When expressed as percentages, all the MSDI values are smaller than the percentage difference between the modal potential vegetation maps for the corresponding 31-year periods. The MSDI value is much smaller than the percentage difference in comparisons involving 2069—2099, the period with the greatest interannual variability.

Discussion

The calibrated values of the TI threshold between the needleleaf and mixed domains and the gdd threshold for the subalpine zone are plausible compared to other versions of MC1, but the forest/woodland LAI thresholds for the needleleaf and mixed domains are higher than in previous versions. The original values of all of these thresholds were the values used in simulations for the California Scenarios 2008 study (Shaw et al. 2008). The TI index did not have analogous threshold values in versions of MC1 prior to that used for the California Scenarios 2008 study, but it is related to a temperature index from the Century model. Cardinal values of Century's TI include -100 for pure evergreen needleleaf, and +100 for pure deciduous broadleaf, so using the range -8 to +45 as the mixed domain is consistent. In regard to the gdd threshold, there was a version of MC1 prior to the California Scenarios 2008 study which used 1600 as the subalpine gdd threshold (Gonzalez et al. 2007). The original version of MC1 did not use gdd thresholds (Daly et al. 2000). As to the forest/woodland LAI

Table 4.2 Measures of similarity and difference between vegetation surveys and simulated potential vegetation. VTM (Thorne et al. 2006) is compared with simulated potential vegetation for 1905—1935. The 1997 Survey (Aerial Information Systems 1997) is compared with simulated potential vegetation for 1905—1935, 1936—1966, and 1967—1997. SI: Sorenson's index (*sensu* Keane et al. 2009). MSDI: map series difference index. SI and MSDI result from comparisons of a single survey map with a series of 31 annual maps of simulated potential vegetation. % match and % difference result from comparisons of a single survey map with a single map of the modal simulated potential vegetation for the 31 year period. Simulations for 1905—1997 were made using PRISM historical climate data (Daly et al. 2008).

	measures of similarity		**measures of difference**	
	% match	SI	% difference	MSDI
sim. 1905—1935 vs. VTM	60%	0.59	40%	0.33
sim. 1905—1935 vs. 1997 Survey	60%	0.59	40%	0.33
sim. 1936—1966 vs. 1997 Survey	63%	0.63	37%	0.32
sim. 1967—1997 vs. 1997 Survey	54%	0.55	46%	0.38

thresholds, in the original version of MC1 and in the MAPSS static biogeography model, an LAI threshold of 3.75 was used to distinguish between forests and other physiognomic vegetation types, regardless of leaf form (Daly et al. 2000, Neilson 1995). Woodward used an LAI of 3 as the level above which trees are dominant, but did not distinguish woodland from forest (Woodward 1987 p.84). I increased the woodland/forest thresholds to 4.7 for the needleleaf (originally 3.75) and mixed (originally 4.25) domains, in an effort to get MC1 to produce more woodland potential vegetation, so as to better match the VTM survey map. In light of other considerations, this may be a case of getting the right answer for the wrong reasons. I will return to this point at the end of the chapter.

Simulated potential vegetation types for the 20th century failed to reproduce the observed vegetation shift from subalpine forest to montane conifer forest. With the details of the biogeography algorithm and the MSDI metric provided in this chapter, a better understanding of the differences between the simulation and the observations is possible. In

Table 4.3 Map series difference indices when comparing two series of maps of annual simulated potential vegetation type. Simulations for 1905-1997 were made using PRISM historical climate data (Daly et al. 2008). Simulations for 2007-99 were made using the climate data from the MIROC A2 scenario (Center for Climate Systems Research 2004, IPCC 2007). Percentages in parentheses are the percentage of cells that do not match in a comparison of the modal potential vegetation types.

	1905—1935	**1936—1966**	**1967—1997**	**2007—2037**	**2038—2068**	**2069—2099**
1905—1935	-0.09 (0%)					
1936—1966	0.01 (11%)	-0.05 (0%)				
1967—1997	0.00 (12%)	0.05 (18%)	-0.07 (0%)			
2007—2037	0.23 (40%)	0.26 (39%)	0.20 (36%)	-0.08 (0%)		
2038—2068	0.45 (68%)	0.50 (70%)	0.46 (63%)	0.29 (36%)	-0.12 (0%)	
2069—2099	0.50 (83%)	0.55 (84%)	0.49 (80%)	0.41 (73%)	0.11 (59%)	-0.21 (0%)

chapter 2, I quantified the simulated change between the early 20th century and the late 20th century by calculating the percentage of gridcells with different modal potential vegetation types, comparing a single map of modal simulated vegetation type for 1905—1935 with a single map of modal simulated potential vegetation type for 1967—1997. 12% of the cells were different. The MSDI metric, on the other hand, produces a value of 0.00 for the comparison of the 1905—1935 series of simulated potential vegetation maps to the 1967—1997 series of simulated potential vegetation maps. Since MSDI can take on values less than zero, a value of zero does not mean there is no difference between the two series, but means instead that the portion of the difference attributable to a trend has the same amplitude as the portion of the difference attributable to the interannual variability of the two series. In the analysis of simulated change in chapter 2, a small trend of 5% of the cells switching from montane conifer forest to mixed forest was noted. A close inspection of figures 4.3a and 4.3c shows that the location of the needleleaf/mixed threshold (TI = -8) moves eastward a small

amount between the 1905—1935 period and the 1967—1997 period; the mixed domain expands at the expense of the needleleaf domain. This detail connects the trend in potential vegetation to underlying increases in the spatially explicit historical temperature data.

There is less difference between the 1936—1966 simulated potential vegetation map series and the 1997 NPS Survey (MSDI = 0.32) than there is between the 1967—1997 simulated potential vegetation map series and the 1997 NPS Survey (MSDI = 0.38) (table 4.2). Comparison of the observed vegetation maps with the growing degree-day sum maps (fig. 4.7) suggests why this might be so. In the early 20th century observed map (fig. 4.7d) subalpine forest vegetation appears to be in disequilibrium with the growing-degree-day sum map for the same period (fig. 4.7f): there is more subalpine forest and less montane conifer forest in the VTM survey map than would be expected based on the growing-degree-day sum map. In the map made from observation 60 years later (fig. 4.7e), the area of subalpine forest has shrunk to approximately the same extent and position of the subalpine zone in the growing-degree-day sum maps for any of the three 20th century periods (figs. 4.7f-4.7h). While the 1936—1966 simulated potential vegetation map is the best match to the 1997 survey map, note that even the 1905—1935 potential vegetation map matches the 1997 survey better than the 1967—1997 potential vegetation map. I conclude that the vegetation was out of equilibrium with the climate in the early 20th century, and that by the late 20th century it had changed to a state better adapted to the climate of the mid and early 20th century.

In the mid 19th century, the Little Ice Age (LIA) was ending (Millar & Woolfenden 1999). Presumably the subalpine zone in YNP had extended further west to lower elevations during the LIA, compared to its location in the 20th century. On that presumption, we can interpret the larger-than-expected area of subalpine forest in the VTM survey map as remnant forests from the colder climate of the Little Ice Age. If a climate time series for the period prior to 1895 suitable for input to the MC1 model can be reconstructed from Dr. Graumlich's tree-ring-based climate anomaly data (Graumlich 1993), we could test this interpretation.

Under the MIROC A2 scenario, the pace of simulated vegetation change accelerates in the mid and late 21st century. MSDI values resulting from comparisons with any 20th century period double from the early to the mid 21st century, and increase still further in comparisons with the late 21st century (table 4.3). Interannual variability in the late 21st century more than doubles in comparison with any period in the 20th century (table 4.3, diagonal). Two kinds of change are apparent. The largest change in the mid 21st century is associated with the disappearance of the subalpine zone. Most of the upper elevation

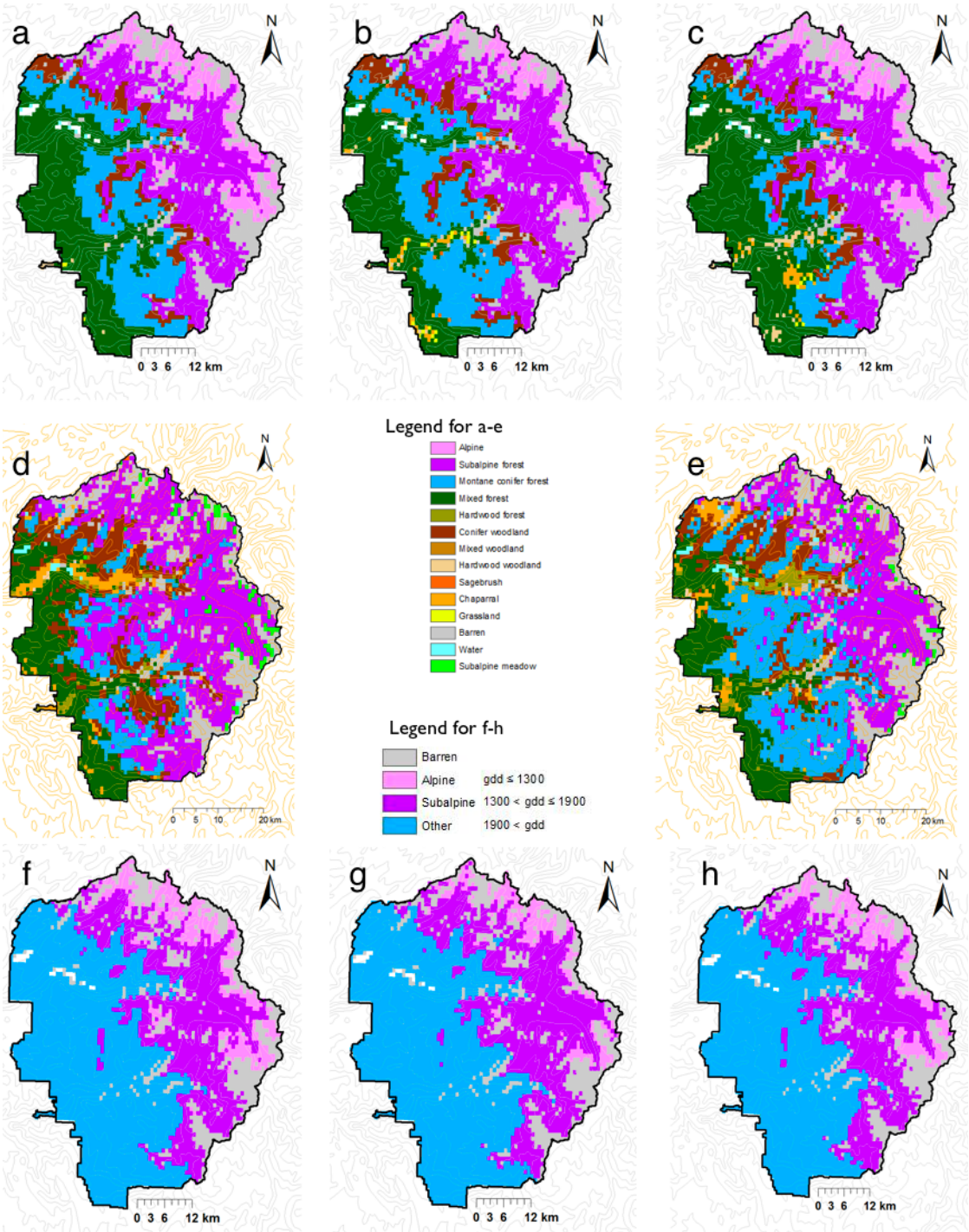

Fig. 4.7 VTM and 1997 NPS Survey vegetation maps compared to maps of modal simulated potential vegetation and growing-degree-day sums. Modal simulated vegetation types (a-c) and growing-degree-day sums (f-h): (a) & (f) 1905—1935, (b) & (g) 1936—1966, and (c) & (h) 1967—1997. Survey maps: (d) VTM survey (Thorne et al. 2006), (e) 1997 NPS Survey (Aerial Information Systems 1997).

portions of the Park cross over a growing-degree-day sum threshold in one 31-year period, which results in a wholesale change in the simulated potential vegetation (figs. 4.2e and 4.5e). The MSSI metric, when applied to compare a time series of maps with itself, is a measure of interannual variability. By this measure, the interannual variability is also up, but by less than 50%. The largest change in the late 21st century is associated with a large increase in simulated wildfire (figs. 3.12d and 4.5f). This has the added effect of raising interannual variability to a level nearly 3 times higher than the average for the three 20th century periods. The calibration of the fire submodel in these simulations can still be improved, and a better calibration may change the timing and strength of simulated wildfire.

The association of increased interannual variability in simulated potential vegetation types with increased simulated fire seems likely, however, to be a constant feature of the simulations. For this case, the MSDI metric offers an advantage over a simple %-difference calculation. A simulated fire can reduce the live vegetation carbon from forest levels to grassland levels. As the simulation continues and the vegetation grows back, the biogeography algorithm will simulate first grassland, then shrubland, then woodland, and finally forest dominance. Transiting this series of successional states shows up as an increase in interannual variability. The MSDI metric is less “flashy” than a simple percentage difference between maps of modal potential vegetation in this situation. For example, the percentage difference between the 1967—1997 and 2038—2068 modal potential vegetation maps is 63%. The MSDI value for the comparison of the two underlying 31-year series of potential vegetation maps is 0.46. The percentage difference increases to 80% for the comparison between the 1967—1997 and 2069—2099 periods, but the MSDI value only increases slightly, to 0.49.

I return now to the subject of calibration. My calibrated value for the forest/woodland LAI threshold for conifers, 4.7, is well above the value, 3.75, used in earlier studies. I raised the value in order to force MC1 to produce more woodland potential vegetation, so as to reduce one of the sources of difference between the VTM map and the simulated potential vegetation maps for the early 20th century. It is, however, implausible that there is any real sense in which conifer woodlands have significantly higher LAIs in Yosemite than in other locations. Moreover, there are several other possible causes for differences between the VTM map and the simulated potential vegetation maps:

1. The soil data used in the simulations may err on the side of soils that are too deep, and hence capable of supporting forests where in reality there are woodlands.
2. The simulated potential vegetation type may be temporally out of synchrony with the actual vegetation type; woodlands may have been recorded by Wieslander’s crews in

locations capable of supporting forests given the climate of the 20th century, as a result of harsher climatic conditions in earlier times.

3. MC1 may have simulated a much lower level of wildfire than actually occurred in the late 19th and early 20th century.

These alternatives suggest ways to redo and improve the study, a topic which will be addressed in the final chapter.

CHAPTER FIVE: CONCLUSIONS

What we did and what we found

The dynamic global vegetation model MC1 was used to simulate the distribution of potential vegetation for the 20th and 21st centuries in Yosemite National Park. Climate data for the 20th century at a monthly timestep and 30 arc-second grain, provided by the PRISM group, were used to estimate the extent of the changes in climate during the historical period. Actual changes in vegetation distribution between 1935 and 1997 were inferred from a comparison of historical vegetation surveys and compared to simulation results. Simulations were also run using three potential future climate scenarios. Simulated distributions of potential vegetation for the late 21st century under each future climate scenario were compared to simulation results for the late 20th century. Time trends in carbon and nitrogen fluxes and pools were examined.

Based on the comparison of the 1935 and 1997 surveys, about 25% of the actual vegetation of the Park changed between the 1930s and 1997. Half of that change consisted of subalpine forests being replaced by montane conifer forests. In terms of California Wildlife Habitat Relationship classes, one-tenth of the Park area changed from the lodgepole pine class to the red fir class. Subalpine forests, dominated by lodgepole pine (*Pinus contorta*), are characteristically shorter and less dense than montane conifer forests, that are dominated by red fir (*Abies magnifica*). Changes in climate between the 1930s and 1997, inferred from the PRISM climate data, are small compared to changes projected by the future climate scenarios. On a spatially averaged basis, twentieth century changes in climate are generally favorable to forest growth, as they include a small increase in precipitation (6%), a small increase in minimum winter temperature (+0.6°C) and decrease in maximum summer temperature (-0.4°C). However, the PRISM data shows considerable spatial variation within the Park in both the magnitude and sign of these changes. Nevertheless, the spatially-averaged climate changes together with the observed change in vegetation distribution are consistent with an increase in ecosystem carbon stocks. A recent study of U.S. forest biomass by Blackard et al. (2008) provides the data required to make quantitative estimates of carbon stocks in the Park for the late 20th century. However, since quantitative estimates of carbon stocks for the Park in 1935 are not available, we were not able to quantify the change in carbon stocks based on observations.

Simulated vegetation change in the 20th century amounted to only about half the area of the observed change, and did not reproduce the observed shift from subalpine forest to montane conifer forest. The single largest category of simulated change was the shift from montane conifer forests to mixed forests, over 5% of the Park area. Simulated net biome productivity was negative, and the simulated ecosystem carbon pools declined by 8% over the historical period. This result seems to be an artifact of the spinup protocol, which generates initial conditions consistent with the climate means of the first 15 years of the historical climate data. Those years, 1895-1909, were unusually wet compared to the entire 112-year historical period, 1895-2006. Work is in progress, but not yet completed, to calculate initial conditions based on temperature and precipitation anomalies for the previous 1000 years derived from tree ring studies.

Simulated changes in potential vegetation between the late 20th and late 21st centuries affected half of the Park under the CSIRO B1 scenario, two-thirds of the Park under the Hadley A1B scenario, and four-fifths of the Park under the MIROC A2 scenario. A large number of wildfires are simulated in the late 21st century. Yosemite National Park is simulated as a carbon source by the end of the 21st century under all 3 scenarios, and for the entire 21st century under 2 of the 3 scenarios. Only under the mildest scenario, CSIRO B1, is the Park a carbon sink, and then only during early and mid 21st century.

The simulation under the MIROC A2 scenario using the conventional simulation protocol produces a potential vegetation map for the late 21st century where only 25% of the Park is forested, 25% is dominated by grasslands, and the rest is dominated by woodlands. We used an alternative simulation protocol to project conditions in the Park under a stable climate using the means of the late 21st century MIROC A2 climate, and the interannual variability of the entire 93-year MIROC A2 scenario. Under those conditions, about 15% of the Park remains forested. The other vegetated portions display high interdecadal variability, changing from grasslands to shrublands to woodlands, and then back to grasslands again as a result of large wildfires occurring mostly during the final third of the 93-year climate data sequence.

What it means

In the latter part of this century, it is likely that a combination of rising temperatures, declining precipitation, and resulting extensive wildfires could convert the vegetation in much

of Yosemite National Park from closed canopy forest to open woodland, shrubland, or even grassland. It is likely that the landscape would exhibit obvious signs of ecosystem stress: drought-stressed remnant forests and large areas of fire scarred and early regrowing post-disturbance vegetation. Remaining forests would likely include many more broadleaf trees than middle and high elevation Yosemite forests do now. Mature, healthy landscapes physiognomically similar to the potential vegetation simulated under these future conditions can be found today in the California coast range (fig. 5.1).

Results from our simulations remain uncertain because the magnitude of the simulated trends and the location of future forests depend on the reliability of the scenario one chooses. Differences between our current results and the 2009 report to the National Park Service (Panek et al. 2009) are attributable to corrections to the input data, and to improved calibration. During the course of this study we have also identified opportunities for further improvements in soil data inputs, spinup protocol, fire model calibration, future climate scenarios, analysis methods, and in the logic of the MC1 model itself.

What next

Next steps for simulations of Yosemite vegetation

Some important questions remain at the end our study. Will there be refugia for alpine and subalpine species when their environment has changed? Will the existing old Sequoias in the Park's Tuolumne and Mariposa Groves, which grew up before and persisted through both the Medieval Warm Period and the Little Ice Age, still be alive and healthy in 2100? Will their progeny be able to grow, if not in the locations of the present groves, at least somewhere in the Park?

There are a number of things we could do to improve our estimate of future conditions in the Park:

Fig. 5.1 Current vegetation in Yosemite National Park and an illustration of projected future vegetation. a) Yosemite Valley from Yosemite Falls trail on February 7, 2009 (photo by author); b) Mount Diablo in the California coast range (photo from WikiMedia Commons).

1. Improve the calibration of the fire model to better reproduce the Park's fire history.
2. Recalibrate the biogeography model, once the fire model calibration has been improved.
3. Incorporate the latest soil survey data, i.e. data from the CA790 survey on the Natural Resources Conservation Service website (http://soils.usda.gov/).
4. Create new future climate scenarios using the A1FI emission scenario more closely aligned with current anthropogenic emissions, and using a "politically relevant aggressive mitigation scenario", E1 (Lowe et al. 2009).
5. Create a new spinup climate dataset based on Dr. Lisa Graumlich's reconstruction of precipitation and temperature anomalies for the last 1000 years in the Sierra Nevada.
6. Move from gridcells to polygons representing ecologically meaningful units of analysis.
7. Add the capability of assimilating actual vegetation and disturbance history.
8. Use additional models, especially those capable of simulating processes and ecosystem services not included in MC1, e.g. unsaturated flow and wildlife habitat models.
9. Incorporate into MC1 any relevant improvements which have been made to the Century model since the creation of MC1.

An agenda at the global scale

It is generally recognized that we also need to consider how vegetation change will affect climate - that GCMs and DGVMs should be coupled and run together, rather than sequentially. Large changes, perceived however imperfectly many decades in advance, can be used to inform strategies to minimize negative impacts and take advantage of opportunities associated with changes in climate.

Reducing the spatial scale at which GCM/DGVMs run can make results more relevant to management questions. Current developments in the climate modeling community include the use of nested models with regional climate models (RCMs) simulating local climate and detailed vegetation processes, allowing land surface feedbacks to the atmosphere. DGVMs and GCMs were created to run at coarse spatial scale originally to make them feasible using then available computing power. Computing power constraints have relaxed. It is feasible to run RCMs at finer spatial resolution, ~10s of km instead of 100s of km (Mearns et al. 2009). There are the beginnings of understanding of how synoptic scale climate changes manifest themselves in local microclimates (Daly et al. 2009, Lundquist & Cayan 2007). As the

Yosemite study has shown us, the spatial grain of our DGVM simulations has decreased to the point where it is feasible to use analysis units that have ecological and climatological meaning, vegetation/soil/topographical/ownership polygons instead of gridcells. Just as RCMs are differentiated from GCMs, DGVMs calibrated regionally deserve to be called by a new name - perhaps simply DVMs, as long as they include small scale processes. Our expectations for such DVMs should be higher: for the region of calibration, the DVM should be able to hindcast observed conditions fairly accurately, it should be able to assimilate real data on land cover and disturbance history, and it should be able to take into account topographical detail such as soil data, slope, aspect, etc. The RCM/DVM toolkit would be appropriate for looking at what may happen in 10 to 40 years, rather than 100 years out. It should produce results which are relevant for deciding how to manage public lands, and which can inform policy discussions.

So what?

Our study is not the first to produce potential vegetation maps for the future which are dramatically different from the vegetation maps of the late 20th century. The maps of the conterminous U.S. in the VEMAP I paper show vegetation type changes across broad regions (VEMAP members 1995); that study used simulation results from three static biogeography models. The VEMAP II study used two dynamic global vegetation models, MC1 and LPJ, and produced equally remarkable contrasts between maps for 1990 and maps for 2095 (Bachelet et al. 2003). The Lynx study used MC1 to simulate potential vegetation for all of North America north of Mexico under 9 different future climates, and included a striking map showing the degree of agreement between the 9 cases on vegetation shifts relative to 1961—1990 (Gonzalez et al. 2007). MC1 was used also in regional studies of Alaska (Bachelet et al. 2005) and the Pacific Northwest (Rogers 2009); in each case the vegetation maps for the future are substantially different from the corresponding maps for the present.

The knowledge we gain from our global and regional simulations has the power to be as transformative, on a global scale, as the understanding of the mosquito's role in spreading yellow fever was for the tropics. Those of us who are privileged to use simulation tools to look into the future have a responsibility to communicate what we see. To live up to that responsibility, it is necessary to go beyond publishing in scientific journals. Active researchers can play a role in a long term program of educating the public. There are amazing new tools

coming into existence for visualizing our data: Data Basin (http://databasin.org/), GoogleEarth, the proposed “alternative future mobile theater” (John Bolte, pers. comm.), virtual reality technology. My hope is that the results from this research will be communicated, using these new tools or others like them, to non-specialist members of the public.

BIBLIOGRAPHY

Aerial Information Systems (1997). *Yose_1997veg_final_poly* [computer map, Arc coverage] 1997. Yosemite National Park: National Park Service.

Aerial Information Systems (2007). *Yosemite National Park and Environs Comprehensive Mapping Classification and Photo Interpretation Report*. Unpublished final report prepared for Yosemite National Park. 304 p.

Bachelet D, Lenihan JM, Daly C, Neilson RP (2000). Interactions between fire, grazing and climate change at Wind Cave National Park, SD. *Ecological Modeling* 134, 229-244.

Bachelet D, Neilson RP, Lenihan JM, Drapek RJ (2001a). Climate change effects on vegetation distribution and carbon budget in the United States. *Ecosystems* 4, 164-185.

Bachelet D, Lenihan JM, Daly C, Neilson RP, Ojima DS, Parton WJ (2001b). MC1: A Dynamic Vegetation Model for Estimating the Distribution of Vegetation and Associated Ecosystem Fluxes of Carbon, Nutrients, and Water—technical documentation. Version 1.0. *General Technical Report* PNW-GTR-508. U.S. Department of Agriculture, Forest Service, Pacific Northwest Research Station, Portland, OR. 95 pages.

Bachelet D, Neilson RP, Hickler T, Drapek RJ, Lenihan JM, Sykes MT, Smith B, Sitch S, Thonicke K (2003). Simulating past and future dynamics of natural ecosystems in the United States. *Global Biogeochemical Cycles* 17 (2), 1045.

Bachelet D, Lenihan JM, Neilson RP, Drapek RJ (2005). Simulating the response of natural ecosystems and their fire regimes to climatic variability in Alaska. *Canadian Journal of Forest Research* 35, 2244-2257.

Bachelet D, Lenihan J, Drapek R, Neilson R (2008). VEMAP vs VINCERA: A DGVM sensitivity to differences in climate scenarios. *Global and Planetary Change* 6, 38-48.

Barbour M, Major J, editors (1995). *Terrestrial Vegetation of California.* California Native Plant Society, Sacramento CA.

Beesley D (1996). Reconstructing the Landscape: An Environmental History, 1820-1960. Chapter 1 in *Sierra Nevada Ecosystem Project: Final report to Congress*, vol. II, *Assessments and scientific basis for management options.* University of California, Davis, Centers for Water and Wildland Resources.

Blackard JA, Finco MV, Helmer EH, Holden GR, Hoppus ML, Jacobs DM, Lister AJ, Moisen GG, Nelson MD, Riemann R, Ruefenacht B, Salajanu D, Weyermann DL, Winterberger KC, Brandeis TJ, Czaplewski RL, McRoberts RE, Patterson PL, Tymcio RP (2008). Mapping U.S. forest biomass using nationwide forest inventory data and moderate resolution information. *Remote Sensing of Environment* 112, 1658-1677.

Boer GJ, Flato GM, Ramsden D. (2000). A transient climate change simulation with greenhouse gas and aerosol forcing: projected climate change in the 21st century. *Climate Dynamics*, 16, 427-450.

Brovkin V, Bendtsen J, Claussen M, Ganopolski A, Kubatzki C, Petoukhov V, Adreev A (2002). Carbon cycle, vegetation, and climate dynamics in the Holocene: Experiments with the CLIMBER-2 model. *Global Biogeochemical Cycles* 16(4), 1139, 20 pp.

Brovkin V, Ganopolski A, Svirezhev Y (1997). A continuous climate-vegetation classification for use in climate-biosphere studies. *Ecological Modelling*, 101, 251-261.

Buonomo E, Jones R, Huntingford C, Hannaford J (2007). On the robustness of changes in extreme precipitation over Europe from two high resolution climate change simulations. *Quarterly Journal of the Royal Meteorological Society* 133, 65-81.

Bytnerowicz A, Fenn ME (1996). Nitrogen deposition in California forests: a review. *Environmental Pollution* 92(2), 127-146.

California Department of Fish and Game (2004). The California wildlife habitat relationships system. California Department of Fish and Game, Sacramento, CA. http://www.dfg.ca.gov/whdab/html/wildlife_habitats.html

Center for Climate Systems Research (2004). K-1 model developers: K-1 coupled model (MIROC) description, Tech. Rep. 1, Center for Climate System Research, University of Tokyo, www.ccsr.u-tokyo.ac.jp/kyosei/hasumi/MIROC/tech-repo.pdf.

Christensen JH, Christensen OB, Lopez P et al. (1996). The HIRHAM4 Regional Atmospheric Climate Model. *DMI Science Report 96–4.* Danish Meteorological Institute, Copenhagen, Denmark.

Cleveland CC, Townsend AR, Schimel DS, Fisher H, Howarth RW, Hedin LO, Perakis SS, Latty EF, Von Fischer JC, Esleroad A, Wasson MF (1999). Global patterns of terrestrial biological nitrogen (N_2) fixation in natural ecosystems. *Global Biogeochemical Cycles* 13(2), 623-645.

Collins WD, Bitz CM, Blackmon ML, Bonan GB, Bretherton CS, Carton JA, Chang P, Doney SC, Hack JJ, Henderson TB, Kiehl JT, Large WG, McKenna DS, Santer BD, Smith RD (2006). The Community Climate System Model Version 3 (CCSM3). *Journal of Climate* 19, 2122-2143.

Cox PM (2001). Description of the TRIFFID Dynamic Global Vegetation Model. *Technical Note 24.* Hadley Centre, Met Office.

Cox PM, Betts RA, Collins M, Harris PP, Huntingford C, Jones CD (2004). Amazonian forest dieback under climate-carbon cycle projections for the 21st century. *Theoretical and Applied Climatology* 78, 137-156.

Cox PM, Betts RA, Jones CD, Spall SA, Totterdell IJ (2000). Acceleration of global warming due to carbon-cycle feedbacks in a coupled climate model. *Nature* 408, 184-187.

Cramer W, Bondeau A, Schaphoff S, Lucht W, Smith B, Sitch S (2004). Tropical forests and the global carbon cycle: impacts of atmospheric carbon dioxide, climate change and rate of deforestation. *Philosophical Transactions of the Royal Society of London, Series B, Biological Sciences* 359, 331-343.

Cramer W, Bondeau A, Woodward FI, Prentice IC, Betts R, Brovkin V, Cox PM, Fischer V, Foley JA, Friend AD, Kucharik C, Lomas MR, Ramankutty N, Sitch S, Smith B, White A, Young-Molling C (2001). Global response of terrestrial ecosystem structure and function to CO2 and climate change: results from six dynamic global vegetation models. *Global Change Biology* 7, 357-373.

Daly C, Neilson RP, Phillips DL (1994). A statistical-topographic model for mapping climatological precipitation over mountainous terrain. *Journal of Applied Meteorology* 33, 140–158.

Daly C, Bachelet D, Lenihan JM, Neilson RP, Parton W, Ojima D (2000). Dynamic simulation of tree–grass interactions for global change studies. *Ecological Applications* 10, 449–469.

Daly C, Halbleib M, Smith JI, Gibson WP, Doggett MK, Taylor GH, Curtis J, Pasteris PP (2008). Physiographically sensitive mapping of climatological temperature and precipitation across the conterminous United States. *International Journal of Climatology*. Published online in Wiley InterScience (www.interscience.wiley.com) DOI: 10.1002/joc.1688

Daly C, Conklin DR, Unsworth MH (2009). Local atmospheric decoupling in complex topography alters climate change impacts. *International Journal of Climatology* 29, in press. http://dx.doi.org/10.1002/joc.2007

de Becker S, Sweet A (2008). Crosswalk between WHR and California Vegetation Classifications. California Department of Fish and Game. http://www.dfg.ca.gov/biogeodata/cwhr/pdfs/CrosswalkWHR_CalVegClassifications.pdf

Delworth TL, Stouffer RJ, Dixon KW, Spelman MJ, Knutson TR, Broccoli AJ, Kushner PJ, Wetherald RT (2002). Review of simulations of climate variability and change with the GFDL R30 coupled climate model. *Climate Dynamics*, 19(7), 555-574.

Delworth TL, Rosati A, Stouffer RJ, Dixon KW, Dunne J, Findell K, Ginoux P, Gnanadesikan A, Gordon CT, Griffies SM, Gudgel R, Harrison MJ, Held IM, Hemler RS, Horowitz LW, Klein SA, Knutson TR, Lin S-J, Milly PCD, Ramaswamy V, Schwarzkopf MD, Sirutis JJ, Stern WF, Spelman MJ, Winton M, Wittenberg AT, Wyman B (2006). GFDL's CM2 Global Coupled Climate Models. Part I: Formulation and simulation characteristics. *Journal of Climate* 19, 643-674.

Döscher R, Willén U, Jones C et al. (2002). The development of the coupled regional ocean-atmosphere model RCAO. *Boreal Environmental Research* 7, 183–192.

Esser G, Hoffstadt J, Mack F, Wittenberg U (1994). *High-Resolution Biosphere Model (HRBM) – Documentation Model Version 3.00.00*. Mitteilungen ausdem Inst. fur Pflanzenokolgieder Justus-Liebig-Univ. Giessen, vol.2, Giessen, Germany. 70 pp.

Fenn ME, Baron JS, Allen EB, Rueth HM, Nydick KR, Geiser L, Bowman WD, Sickman JO, Meixner T, Johnson DW, Neitlich P. (2003). Ecological Effects of Nitrogen Deposition in the Western United States. *BioScience* 53(4), 404-420.

Fites-Kaufman JA, Rundel P, Stephenson N, Weixelman DA (2007). Montane and Subalpine Vegetation of the Sierra Nevada and Cascade Ranges. Chapter 17 in *Terrestrial Vegetation of California,* 3rd ed., Barbour MG, Keeler-Wolf T, Schoenherr AA, eds., University of California Press, pp. 456-501.

Flato GM, Boer GJ, Lee WG, McFarlane NA, Ramsden D, Reader MC, Weaver AJ (2000). The Canadian Centre for Climate Modeling and Analysis Global Coupled Model and its Climate. *Climate Dynamics*, 16, 451-467.

Foley JA, Prentice IC, Ramankutty N, Levis S, Pollard D, Sitch S, Haxeltine A (1996). An integrated biosphere model of land surface processes, terrestrial carbon balance, and vegetation dynamics. *Global Biogeochemical Cycles* 10(4), 603-628.

Friedlingstein P, Cox P, Betts R, Bopp L, von Bloh W, Brovkin V, Cadule P, Doney S, Eby M, Fung I, Bala G, John J, Jones C, Joos F, Kato T, Kawamiya M, Knorr W, Lindsay K, Matthews HD, Raddatz T, Rayner P, Reick C, Roeckner E, Schnitzler K-G, Schnur R, Strassmann K, Weaver AJ, Yoshikawa C, Zeng N (2006). Climate—Carbon Feedback Analysis: Results from the C^4MIP Model Intercomparison. *Journal of Climate* 19, 3337-3353.

Friend AD, White A (2000). Evaluation and analysis of a dynamic terrestrial ecosystem model under preindustrial conditions at the global scale. *Global Biogeochemical Cycles* 14(4), 1173-1190.

Gomberg P (2007). *How to Make Opportunity Equal: Race and Contributive Justice.* Blackwell Publishing, Oxford, United Kingdom. 184 pages.

Gonzalez P, Neilson RP, McKelvey KS, Lenihan JM, Drapek RJ (2007). *Potential Impacts of Climate Change on Habitat and Conservation Priority Areas for Lynx canadensis (Canada Lynx)*. A report to the US Forest Service and NatureServe, from The Nature Conservancy, October 2, 2007. 19 pages.

Gordon C, Cooper C, Senior CA, Banks HT, Gregory JM, Johns TC, Mitchell JFB, Wood RA (2000). The simulation of SST, sea ice extents and ocean heat transports in a version of the Hadley Centre coupled model without flux adjustments. *Climate Dynamics* 16, 147-168.

Gordon HB, Rotstayn LD, McGregor JL, Dix MR, Kowalczyk EA, O'Farrell SP, Waterman LJ, Hirst AC, Wilson SG, Collier MA, Watterson IG, Elliott TI (2002). The CSIRO Mk3 Climate System Model [Electronic publication]. Aspendale: CSIRO Atmospheric Research. CSIRO Atmospheric Research technical paper no. 60. 130 p. (http://www.cmar.csiro.au/e-print/open/gordon_2002a.pdf)

Graumlich LJ (1993). A 1000-Year Record of Temperature and Precipitation in the Sierra Nevada. *Quaternary Research* 39, 249-255.

Hakkarinen C, Smith JB (2006). Climate change scenarios. Chapter 4 in *The Impact of Climate Change on Regional Systems*, Smith JB and Mendelsohn R, eds. Edward Elgar, Cheltenham, UK.

Hansen J, Fung I, Lacis A, Rind D, Lebedeff S, Ruedy R (1988). Global climate changes as forecast by Goddard Institute for Space Studies three-dimensional model. *Journal of Geophysical Research*, 93, 9341-9364.

Hasumi H, Emori S (eds.) (2004). K-1 coupled model (MIROC) description. Center for Climate System Research, University of Tokyo, Tokyo, Japan.

Haxeltine AI, Prentice IC, Cresswell ID (1996). A coupled carbon and water flux model to predict vegetation structure. *Journal of Vegetation Science* 7, 651-666.

Haxeltine A, Prentice IC (1996). BIOME3: An equilibrium terrestrial biosphere model based on ecophysiological constraints, resource availability, and competition among plant functional types. *Global Biogeochemical Cycles* 10(4), 693-709.

Hudson DA, Jones RG (2002) Simulations of Present-Day and Future Climate Over Southern Africa using HadAM3H. *Hadley Centre Technical Note 39*. Hadley Centre for Climate Prediction and Research, Met Office, Bracknell, UK.

IPCC (1994). *Climate Change 1994—Radiative Forcing of Climate Change and an Evaluation of the IPCC IS92 Scenarios.* Cambridge University Press, Cambridge and New York.

IPCC (2000). *Special Report on Emissions Scenarios.* Nakicenovic N, Swart R, eds. Cambridge University Press, Cambridge, UK. 570 pages.

IPCC (2007). *Climate Change 2007: The Physical Science Basis. Contribution of Working Group I to the Fourth Assessment Report of Intergovernmental Panel on Climate Change*. Solomon S, Qin D, Manning M, eds.

Jacob D (2001) A note to the simulation of the annual and interannual variability of the water budget over the Baltic Sea drainage basin. *Meteorology and Atmospheric Physics* 77, 61–73.

Johns TC, Carnell RE, Crossley JF et al. (1997). The second Hadley Centre coupled ocean-atmosphere GCM: Model description, spinup and validation. *Climate Dynamics* 13, 103-134.

Johns TC, Gregory JM, Ingram WJ, Johnson CE, Jones A, Lowe JA, Mitchell JFB, Roberts DL, Sexton DMH, Stevenson DS, Tett SFB, Woddage MJ (2003). Anthropogenic climate change for 1860 to 2100 simulated with the HadCM3 model under updated emissions scenarios. *Climate Dynamics* 20, 583-612.

Joos F, Prentice IC, Sitch S, Meyer R, Hooss G, Plattner G-K, Gerber S, Hasselmann K (2001). Global warming feedbacks on terrestrial carbon uptake under the Intergovernmental Panel on Climate Change (IPCC) emission scenarios. *Global Biogeochemical Cycles* 15(4), 891-907.

Keane RE, Holsinger LM, Parsons RA, Gray K (2008). Climate change effects on historical range and variability of two large landscapes in western Montana, USA. *Forest Ecology and Management* 254, 375-389.

Keane RE, Hessburg PF, Landres PB, Swanson FJ (2009). The use of historical range and variability (HRV) in landscape management. *Forest Ecology and Management* 258, 1025-1037.

Keeler-Wolf T (2007). The History of Vegetation Classification and Mapping in California. Chapter 1 in *Terrestrial Vegetation of California*, 3rd edition, Barbour MG, Keeler-Wolf T, Schoenherr A, eds. University of California Press, Berkeley CA.

Keeley JE (2004). VTM plots as evidence of historical climate change: goldmine or landmine? *Madroño* 51, 372-378.

Kelly M, Allen-Diaz B (2005). Digitization of a Historic Dataset: The Wieslander California Vegetation Type Mapping Project. *Madroño* 52, 191-201.

Kern JS (1995). Geographic patterns of soils water-holding capacity in the contiguous United States. *Soil Science Society of America* 59(4), 1126-1133.

Kern JS (2000). Erratum for Geographic patterns of soils water-holding capacity in the contiguous United States. *Soil Science Society of America* 64(1), 382-382.

Kittel TGF, Rosenbloom NA, Royle JA, Daly C, Gibson WP, Fisher HH, Thornton P, Yates DN, Aulenbach S, Kaufman C, McKeown R, Bachelet D, Schimel DS, VEMAP2 Participants (2004) VEMAP phase 2 bioclimatic database. I. Gridded historical (20th century) climate for modeling ecosystem dynamics across the conterminous United States. *Climate Research* 27, 151–170.

Klett M, Solnit R, Wolfe B (2005). *Yosemite In Time*. Trinity University Press, San Antonio TX. 140 pages.

Kucharik CJ, Foley JA, Delire C, Fisher VA, Coe MT, Lenters JD, Young-Molling C, Ramankutty N, Norman JM, Gower ST (2000). Testing the performance of a Dynamic Global Ecosystem Model: Water balance, carbon balance, and vegetation structure. *Global Biogeochemical Cycles* 14(3), 795-825.

Lenihan JM, Drapek RJ, Bachelet D, Neilson RP (2003). Climate change effects on vegetation distribution, carbon stocks, and fire regimes in California. *Ecological Applications* 13 (6), 1667–1681.

Lenihan JM, Drapek R, Neilson R (2006a). Terrestrial Ecosystem Changes. Chapter 4 of *The Impact of Climate Change on Regional Systems*, Smith JB and Mendelsohn R, eds. Edward Elgar Publishing Inc., Northampton MA.

Lenihan M, Conklin DR, Neilson RP, Bachelet D (2006b). MCFire Model Description. Unpublished, 93 pages.

Lenihan JM, Bachelet D, Neilson RP, Drapek R (2008a). Response of vegetation distribution, ecosystem productivity, and fire to climate change scenarios for California. *Climatic Change* 87 (Suppl 1), S215-S230.

Lenihan JM, Bachelet D, Neilson RP, Drapek R (2008b). Simulated response of conterminous United States ecosystems to climate change at different levels of fire suppression, CO2 emission rate, and growth response to CO2. *Global and Planetary Change* 64, 16-25.

Levy PE, Cannell MGR, Friend AD (2004). Modelling the impact of future changes in climate, CO_2 concentration and land use on natural ecosystems and the terrestrial carbon sink. *Global Environmental Change* 14, 21-30.

Lowe JA, Hewitt CD, van Vuuren DP, Johns TC, Stehfest E, Royer J, van der Linden PJ (2009). New study for climate modeling, analyses, and scenarios. *Eos* 90(21), 181-182.

Lucht W, Schaphoff S, Erbrecht T, Heyder U, Cramer W (2006). Terrestrial vegetation redistribution and carbon balance under climate change. *Carbon Balance and Management* 1:6. www.cbmjournal.com/content/1/1/6

Lundquist JD, Cayan DR (2007). Surface temperature patterns in complex terrain: Daily variations and long-term change in the central Sierra Nevada, California. *Journal of Geophysical Research* 112, D11124, doi:10.1029/2006JD007561.

Lutz JA (2008). Climate, fire, and vegetation change in Yosemite National Park. *PhD dissertation.* University of Washington, Seattle, 158 pages.

Lutz JA, van Wagtendonk JW, Franklin JF (2009). Twentieth-century decline of large-diameter trees in Yosemite National Park, California, USA. *Forest Ecology and Management* In press.

Manabe S, Wetherald RT, Mitchell JFB, Meleshko V, Tokioka T (1990). Equilibrium Climate Change—and its Implications for the Future. In *Climate Change: The IPCC Scientific Assessment*, Houghton JT, Jenkins GJ, Ephraums JJ, eds.. Cambridge University Press, New York. pp. 131-172.

McGuire AD, Sitch S, Clein JS, Dargaville R, Esser G, Foley J, Heimann M, Joos F, Kaplan J, Kicklighter DW, Meier RA, Melillo JM, Moore B III, Prentice IC, Ramankutty R, Reichenau T, Schloss A, Tian H, Williams LJ, Wittenberg U (2001). Carbon balance of the terrestrial biosphere in the twentieth century: Analyses of CO_2, climate and land use effects with four process-based ecosystem models. *Global Biogeochemical Cycles* 15(1), 183-206.

Mearns LO, Gutowski W, Jones R, Leung R, McGinnis S, Nunes A, Qian Y (2009). A Regional Climate Change Assessment Program for North America. *Eos* 90(36), 311 (8 Sep 2009).

Meissner KJ, Weaver AJ, Matthews HD, Cox PM (2003). The role of land surface dynamics in glacial inception: a study with the UVic Earth System Model. *Climate Dynamics* 21, 515-537.

Millar CI, Woolfenden WB (1999). Sierra Nevada Forests: Where Did They Come From? Where Are They Going? What Does It Mean? *Transactions of the Sixty-fourth North American Wildlife and Natural Resource Conference*, pages 206-236. Wildlife Management Institute, Washington DC.

Millar CI, Westfall RD, Delany DL, King JC, Graumlich LJ (2004). Response of Subalpine Conifers in the Sierra Nevada, California, U.S.A., to 20th-Century Warming and Decadal Climate Variability. *Arctic, Antarctic, and Alpine Research* 36(2), 181-200.

Miller DA, White RA (1998). A Conterminous United States Multi-Layer Soil Characteristics Data Set for Regional Climate and Hydrology Modeling. *Earth Interactions,* **2.** [Available on-line at http://EarthInteractions.org]

Mitchell JFB, Johns TC (1997). On Modification of Global Warming by Sulfate Aerosols. *Journal of Climate*, 10, 245-267.

Morales P, Hickler T, Rowell DP, Smith B, Sykes MT (2007). Changes in European ecosystem productivity and carbon balance driven by regional climate model output. *Global Change Biology* 13, 108-122.

Moritz C, Patton JL, Conroy CJ, Parra JL, White GC, Beissinger SR (2008). Impact of a Century of Climate Change on Small-Mammal Communities in Yosemite National Park, USA. *Science* 322, 261-264.

Mueller-Dombois D, Ellenberg H (1974). *Aims and Methods of Vegetation Ecology.* John Wiley & Sons, New York. 547 pages.

Muir J (1911). *My First Summer in the Sierra.* Houghton Mifflin Co., Boston MA. Republished in 1992 in *John Muir: The Eight Wilderness Discovery Books.* The Mountaineers, Seattle WA.

National Park Service (2009). Yosemite Vegetation Map. http://www.nps.gov/yose/naturescience/vegetation-map.htm

NatureServe (2007). *Classification of the Vegetation of Yosemite National Park and Surrounding Environs in Tuolumne, Mariposa, Madera and Mono Counties, California.* Unpublished final report submitted to the National Park Service. 409 p.

Neilson RP (1995). A model for predicting continental-scale vegetation distribution and water balance. *Ecological Applications* 5, 362-385.

Nemani R, Hashimoto H, Votava P, Melton F, Wang W, Michaelis A, Mutch L, Milesi C, Hiatt S, White M (2009). Monitoring and forecasting ecosystem dynamics using the Terrestrial Observation and Prediction System (TOPS), *Remote Sensing of Environment* doi:10.1016/j.rse.2008.06.017

Norby RJ, DeLucia EH, Gielen B, Calfapietra C, Giardina CP, King JS, Ledford J, McCarthy HR, Moore DJP, Ceulemans R (2005). Forest response to elevated CO2 is conserved across a broad range of productivity. *Proceedings of the National Academy of Sciences* 102(50), 18052-18056.

Panek J, Conklin D, Kuhn B, Bachelet D, van Wagtendonk J (2009). *Projected Vegetation Changes Over the 21st Century in Yosemite National Park Under Three Climate Change and CO_2 Emission Scenarios.* Report to the National Park Service under task agreement #J8R07070021.

Parton WJ, Schimel DS, Cole CV, Ojima D (1987). Analysis of factors controlling soil organic levels of grasslands in the Great Plains. *Soil Science Society of America* 51, 1173–1179.

Parton WJ, Scurlock JMO, Ojima DS, Gilmanov TG, Scholes RJ, Schimel DS, Kirchner T, Menaut JC, Seastedt T, Garcia Moya E, Kamnalrut A, Kinyamario JI (1993). Observations and modeling of biomass and soil organic matter dynamics for the grassland biome worldwide. *Global Biogeochemical Cycles* 7 (4), 785–809.

Petoukhov V, Ganopolski A, Brovkin V, Claussen M, Eliseev A, Kubatzki C, Rahmstorf S (2000). CLIMBER-2: a climate system model of intermediate complexity. Part 1: model description and performance for present climate. *Climate Dynamics* 16, 1-17.

Prentice IC, Cramer W, Harrison SP, Leemans R, Monserud RA, Solomon AM (1992). A Global Biome Model Based on Plant Physiology and Dominance, Soil Properties and Climate. *Journal of Biogeography* 19(2), 117-134.

Prentice IC, Sykes MT, Lautenschlager M, Harrison SP, Denissenko O, Bartlein PJ (1993). Modelling global vegetation patterns and terrestrial carbon storage at the last glacial maximum. *Global Ecology and Biogeography Letters* 3, 67-76.

Prentice IC, Heimann M, Sitch S (2000). The carbon balance of the terrestrial biosphere: Ecosystem models and atmospheric observations. *Ecological Applications* 10, 1553-1573.

Raupach MR, Marland G, Ciais P, Le Quéré C, Canadell JG, Klepper G, Field CB (2007). Global and regional drivers of accelerating CO_2 emissions. *Proceedings of the National Academy of Sciences* 104(24, June 12), 10288-10293.

Roeckner E, Bengtsson L, Feitcher J et al. (1999) Transient climate change simulations with a coupled atmosphere-ocean GCM including the tropospheric sulfur cycle. *Journal of Climate* 12, 3004–3032.

Roeckner E, Bauml G, Bonaventura L, Brokopf R, et al. (2003). *The general circulation model ECHAM5. Part I: Model description.* Max-Planck-Institute for Meteorology, Hamburg, Report 349.

Rogers BM (2009). Potential Impacts of Climate Change on Vegetation Distributions, Carbon Stocks, and Fire Regimes in the U.S. Pacific Northwest. *Masters thesis*. Oregon State University.

Sawyer JO, Keeler-Wolf T (1995). *A Manual of California Vegetation*. California Native Plant Society, Sacramento CA. 471 pages.

Schlesinger ME, Zhao ZC (1989). Seasonal climate changes induced by doubled CO_2 as simulated by the OSU atmospheric GCM – mixed layer ocean model. *Journal of Climate*, 2, 459-495.

Schwind B, Gordon H (2001). *CALVEG geobook: a comprehensive information package describing California's wildland vegetation, version 2.* USDA Forest Service, Pacific Southwest Region, Remote Sensing Lab, Sacramento CA.

Shaw R, Pendleton L, Cameron D, Morris B, Bratman G, Bachelet D, Klausmeyer K, MacKenzie J, Conklin DR, Lenihan J, Haunreiter E, Daly C (2008). The impact of climate change on Californrnia's ecosystem services. *Report to California Energy Commission and California Environmental Protection Agency*.

Shinneman DJ, Baker WL (2009). Historical fire and multidecadal drought as context for piñon-juniper woodland restoration in western Colorado. *Ecological Applications* 19(5), 1231-1245.

Sitch S (2000). The role of vegetation dynamics in the control of atmospheric CO_2 content. *PhD dissertation.* Lund University, Lund, Sweden.

Sitch S, Smith B, Prentice IC, Arneth A, Bondeau A, Cramer W, Kaplan JO, Levis S, Lucht W, Sykes MT, Thonicke K, Venevsky S (2003). Evaluation of ecosystem dynamics, plant geography and terrestrial carbon cycling in the LPJ Dynamic Global Vegetation Model. *Global Change Biology* 9, 161-185.

Smith B, Prentice IC, Sykes MT (2001). Representation of vegetation dynamics in the modelling of terrestrial ecosystems: comparing two contrasting approaches in European climate space. *Global Ecology and Biogeography* 10, 621–638.

SNEP (1996). *Sierra Nevada Ecosystem Project: Final Report to Congress. Vol. I. Assessment Summaries and Management Strategies.* University of California, Centers for Water and Wildland Resources, Report No. 36. Davis CA. 209 pages.

Sørenson T (1948). A method of establishing groups of equal amplitude in plant sociology based on similarity of species content. *Det Kongelige Danske Videnskabernes Selskab Biologiske Skrifter* 5(4), 1-34.

Steppeler J, Doms G, Schättler U et al. (2003) Meso-gamma scale forecasts using the nonhydrostatic model LM. *Meteorological and Atmospheric Physics* 82, 75–96.

Thompson SL, Govindasamy B, Mirin A, Caldeira K, Delire C, Milovich J, Wickett M, Erickson D (2004). Quantifying the effects of CO_2-fertilized vegetation on future global climate. *Geophysical Research Letters* 31, L23211.

Thorne JH, Kelsey R, Honig J, Morgan B (2006). *The Development of 70-Year-Old Wieslander Vegetation Type Maps and an Assessment of Landscape Change in the Central Sierra Nevada.* California Energy Commission, PIER Energy-Related Environmental Program. CEC-500-2006-107.

Thorne JH, Morgan BJ, Kennedy JA (2008). Vegetation change over sixty years in central Sierra Nevada, California, USA. *Madroño* 55 (3), 223-237.

Thornton PE (1998). Regional ecosystem simulation: combining surface- and satellite-based observations to study linkages between terrestrial energy and mass budgets. *PhD dissertation.* University of Montana, Missoula, 208 pages.

Tian H, Melillo JM, Kicklighter DW, McGuire AD, Helfrich J (1999). The sensitivity of terrestrial carbon storage to historical climate variability and atmospheric CO_2 in the United States. *Tellus, Series B* 51, 414-452.

van Mantgem PJ, Stephenson NL, Byrne JC, Daniels LD, Franklin JF, Fulé PZ, Harmon ME, Larson AJ, Smith JM, Taylor AH, Veblen TT (2009). Widespread Increase of Tree Mortality Rates in the Western United States. *Science* 323, 521-524.

VEMAP Members (1995). Vegetation/ecosystem modeling and analysis project: Comparing biogeography and biogeochemistry models in a continental-scale study of terrestrial ecosystem responses to climate change and CO_2 doubling. *Global Biogeochemical Cycles* 9, 407-437.

Walker RE (2000). Investigations in vegetation map rectification, and the remotely sensed detection and measurement of natural vegetation changes. *PhD dissertation*. University of California, Santa Barbara CA.

Washington WM, Weatherly JW, Meehl GA, Semtner AJ Jr., Bettge TW, Craig AP, Strand WG Jr, Arblaster J, Wayland VB, James R, Zhang Y (2000). Parallel climate model (PCM) control and transient simulations. *Climate Dynamics* 16, 755-774.

Wetherald RT, Manabe S, Cubasch U, Cess RD (1990). Processes and Modelling. In *Climate Change: The IPCC Scientific Assessment*, Houghton JT, Jenkins GJ, Ephraums JJ, eds.. Cambridge University Press, New York. pp. 69-91.

Wieslander AE (1935). First steps of the forest survey in California. *Journal of Forestry* 33, 877-884.

Wilson CA, Mitchell JFB (1987). A doubled CO_2 climate sensitivity experiment with a global climate model including a simple ocean. *Journal of Geophysical Research*, 92(D11), 13315-13343.

Woodward FI (1987). *Climate and Plant Distribution.* Cambridge University Press, Cambridge. 174 pages.

Woodward FI, Smith TM, Emanuel WR (1995). A global land primary productivity and phytogeography model. *Global Biogeochemical Cycles* 9, 471-490.

Woodward FI, Lomas MR, Betts RA (1998). Vegetation-climate feedbacks in a greenhouse world. *Philosophical Transactions of the Royal Society of London Series B* 353, 29-38.

Woodward FI, Lomas MR, Lee SE (2001). Predicting the Future Productivity and Distribution of Global Terrestrial Vegetation. Chapter 22 in *Terrestrial Global Productivity*, Roy J, Saugier B, Mooney HA, eds. Academic Press, London. 573 pp.

Woolfenden WB (1996). Quaternary Vegetation History. Chapter 4 in *Sierra Nevada Ecosystem Project: Final report to Congress*, vol. II, *Assessments and scientific basis for management options.* University of California, Davis, Centers for Water and Wildland Resources.

Zeng N, Qian H, Munoz E (2004). How strong is carbon cycle-climate feedback under global warming? *Geophysical Research Letters* 31, L20203, 5 pp.

APPENDIX

APPENDIX: Map Series Difference Index - Derivation and Properties

How much has the vegetation in Yosemite changed in the past? How much do we expect it to change in the future? How much more (or less) change do we expect in the future than in the past? Questions posed with phrases such as “how much” and “how much more” invite quantitative answers. But giving quantitative answers to these questions about change in vegetation across space and time is not straightforward. I begin by substituting more precise questions.

Given two gridded map series with an associated categorical attribute (such as vegetation type), how similar are they? How different are they?

Given one location, represented by a gridcell chosen at random, and two points in time, represented by single years chosen at random, one from each of the time intervals of interest, what is the probability that the vegetation type associated with the gridcell at the second time is different from the vegetation type associated with the gridcell at the first time? The answer to that question, if we could determine it, is formally a number on the closed interval [0,1], often expressed a percentage ranging from 0% to 100%. Designate that quantity *d*, for the single cell probability of difference.

Assuming that we could calculate *d*, what then is the most likely fraction of all the gridcells which would have different values at the later time than at the earlier time (i.e. on what percentage of the landscape is the vegetation different now than it was before)? The intuitive answer is the correct one: the most likely fraction of different gridcells is the same as the single cell probability of difference, so long as the “single cell” represents one chosen at random. For the question, how different is the vegetation at time B from the vegetation at time A, I substitute the equivalent question, what is the probability that for a gridcell chosen at random, and two years *a* and *b* chosen at random, the vegetation type is different in year *b* from what it was in year *a*?

But there is a complication. The original question was not phrased in terms of likelihood of difference, but rather in terms of the magnitude of “change”. Implicit in the question is the understanding that some change is normal and not significant. Different locations are in different seral stages spatially, and the same location may transition through different seral stages over time, but none of those differences would be considered significant, so long as the relative proportions of the landscape in the various seral stages stay stable.

To deal with this complication, it is useful to pose another question: in the absence of significant change, what would the value of *d* be? That is, assuming that there are no trends

in the vegetation patterns over time, then what is the probability that a gridcell chosen at random will have a different vegetation type in year *b* than it had in year *a*? There is no single answer to this question. For example, the no-trend value of *d* for an ecosystem with a shorter fire return interval will likely be larger than the no-trend value for one with a longer fire return interval.

Nevertheless, supposing that we could calculate the no-trend value for *d*, call it *d0,* then consider what we would get by subtracting *d0* from *d*. Wouldn't that give us the probability of difference attributable to any trend, separate from the probability of difference arising from "normal" change? If there is in fact no trend, then *d* and *d0* are the same, their difference is 0, and *voila!* we have gotten the right answer: the probability of difference arising from a trend is zero.

But again there is a complication. Suppose there really is a trend. For the sake of argument, suppose precipitation has increased and the fire return interval is also increasing as a result. Think about the "no-trend" *d0* value appropriate to the new, wetter ecosystem; quite possibly it will be smaller: less fire, more of the landscape is relatively stable or in old-growth seral stage.

We may attempt to deal with this additional complication as we did the first one: assume that we could calculate the different no-trend values of *d* appropriate to year *a* and year *b*, and then subtract both values, call them $d0_a$ and $d0_b$, from the original *d:*

$$\textit{probability of difference due to trend} \stackrel{?}{=} di = d - d0_a - d0_b \qquad \text{eq. A1}$$

where

d = probability of difference

$d0_a$, $d0_b$ = probability of difference due to interannual variability for map series A and B

But wait... now in the case where there really isn't a trend, *d,* $d0_a$, and $d0_b$ are all the same, and $d - d0_a - d0_b$ turns out to be simply $-d$, a negative number, which doesn't make any sense as a probability of difference.

Even so, the quantity produced by the expression $d - d0_a - d0_b$ (hereafter denoted *di* for difference index) has some interesting properties. First, imagine a completely stable ecosystem represented by an unchanging map: no interannual variability and no trend. All the maps in both series are copies of a single map. *d,* $d0_a$ and $d0_b$ are all 0, and *di* itself is 0. Now imagine an ecosystem with some interannual variability but no trend, the case from the previous paragraph. In this case, *di* is negative, but its magnitude is twice the probability of difference arising from interannual variability. Next consider the complementary case, where there is a trend but no interannual variability at either time A or time B: two series of maps, in which the maps within a series are identical to each other, but different from those of the other

series. This time $d0_a$ and $d0_b$ are 0, but d is not, and di is just the same as d, and measures the difference arising from the trend. Finally, return to the case where there is both interannual variability and a trend. di can be either positive or negative, and its sign is an indication of whether the trend is more significant (positive di) or the interannual variability is more significant (negative di). Furthermore, the range of possible values for di is from about -1 to +1. di gets the value +1 when the maps within a given series are identical to each other, but the pattern in the first series has no cells which match the pattern in the second series. di gets the value $-(1 + 1/n)$, where n is the length of the series, when the two series are identical to each other, but every map in each series is completely different from every other map in the same series. Think of the degree of difference due to a trend as the residue from the total difference after the degree of difference due to interannual variability has been taken out. $d0_a$ and $d0_b$ are one way to measure the degrees of difference due to interannual variability; d is a similar measure of the total difference; so $d - d0_a - d0_b$ (a.k.a. di) is a measure - not a probability, exactly, but nevertheless a measure - of the difference due to the trend.

Having concluded that di's properties are interesting, perhaps useful, motivates us to return to the question of whether it can be calculated, that is, can we calculate d, $d0_a$, and $d0_b$? Sometimes it is useful in working with probabilities to invert the sense of the question. We start again by asking the original question in terms of similarity rather than difference: Given one location, represented by a gridcell chosen at random, and two points in time, represented by single years chosen at random, one from each of the time intervals of interest, what is the probability that the vegetation type associated with the gridcell at the second time is *the same as* the vegetation type associated with the gridcell at the first time? We'll call this quantity s, and clearly s and d are related by the necessity that they must add up to 1: the only two possibilities are that the vegetation types are different or they are the same. Let $s0_a$ and $s0_b$ be the no-trend versions of s, analogous to the way $d0_a$ and $d0_b$ were defined previously. Express $d - d0_a - d0_b$ in terms of similarity probabilities instead of difference probabilities:

$$di = d - d0_a - d0_b = (1 - s) - (1 - s0_a) - (1 - s0_b) = s0_a + s0_b - s - 1 \qquad \text{eq. A2}$$

where

di = difference index
d = probability of difference
$d0_a$, $d0_b$ = probability of difference due to interannual variability for map series A and B
s = probability of similarity
$s0_a$, $s0_b$ = probability of similarity despite interannual variability within map series A and B

Now suppose that one of the two series of maps consists of just a single map. Then for a single gridcell *s* is just the number of times the value of that grid cell in the single map recurs in the corresponding gridcells of the maps in the series, divided by the length of the series:

$$s = \frac{\sum_{tb=1}^{nb}\left(A[i,j] \equiv B_{tb}[i,j]\right)}{nb} \qquad \text{eq. A3}$$

where

s = probability that grid cell[i,j] has the same attribute value in a map chosen at random from map series B as it does in map A
nb = the number of maps in map series B
tb = index to map series B
A[i,j] = the attribute value of grid cell i,j in map A
$B_{tb}[i,j]$ = the attribute value of grid cell i,j in the tbth map in map series B
and
$\left(A[i,j] \equiv B_{tb}[i,j]\right)$ is 1 when the attribute values are the same, otherwise 0

To obtain the value of *s* appropriate when the gridcell is chosen at random, we average over all the gridcells

$$s = \frac{\sum_{i=1}^{nrows}\sum_{j=1}^{ncols}\left(\frac{\sum_{tb=1}^{nb}\left(A[i,j] \equiv B_{tb}[i,j]\right)}{nb}\right)}{nrows \cdot ncols} \qquad \text{eq. A4}$$

where

s, nb, tb, A[i,j], $B_{tb}[i,j]$ and are as in eq. A3
nrows, ncols = the numbers of rows and columns in the grid

The double summation over the rows and columns of the grid can be moved inside the summation over the map series:

$$s = \frac{\sum_{tb=1}^{nb}\left(\frac{\sum_{i=1}^{nrows}\sum_{j=1}^{ncols}\left(A[i,j] \equiv B_{tb}[i,j]\right)}{nrows \cdot ncols}\right)}{nb} \qquad \text{eq. A5}$$

where

all variables are as in eq. A4

Equation A5 is a gridded version of Keane's 2009 formulation of Sorenson's index (eq. 4.3).

We are trying to work out a way to calculate *di,* approaching the problem through the probabilities of similarity rather than difference. So far, we've gotten an expression for *s* for the special case of one map series consisting of just a single map. What about $s0_a$ and $s0_b$? Note that the *s0*s are probabilities of a cell in one map of a series having the same value as the corresponding cell in another map in the same series. When the series consists of just a single map, then it is a certainty that the cell will have the same value as the same cell *in every map of its series*, so for our special case, $s0_a$ must be 1. Recall that $s0_b$ is the probability of similarity for corresponding cells in time series B, exclusive of the effects of differences between A and B. The map series similarity index MSSI (eqs. 4.6 and 4.7), a generalization of the expression for *s* given just above, when applied between a map series and itself, gives *s0:*

$$s0_b = MSSI(B, B) \qquad \text{eq. A6}$$

where

B = a time series of maps
$s0_b$ = probability of similarity due to interannual variability for B
MSSI(B, B) = map series similarity index applied between B and itself

We have now what we need to calculate the difference index for the special case:

$$di = s0_a + s0_b - s - 1 = 1 + MSSI(B, B) - SI(A,B) - 1 = MSSI(B,B) - SI(A, B) \qquad \text{eq. A7}$$

where

di = difference index
A = a reference map (i.e. a "series" of length 1)
B = a time series of maps
$s0_a$, $s0_b$ = probabilities of similarity despite interannual variability within A and B
MSSI(B, B) = map series similarity index applied between B and itself
SI(A, B) = Sorenson's index (*sensu* Keane et al. 2009) applied to A and B

We have determined how to calculate *di* for the special case of comparing a single reference map to a time series of maps. How can we do it for the general case of comparing two map series to each other? When A is a series rather than a single map, $s0_a$ becomes MSSI(A, A), and SI(A, B) generalizes to MSSI(A, B). Finally, *di* becomes

$$di = s0_a + s0_b - s - 1 = MSSI(A, A) + MSSI(B, B) - MSSI(A, B) - 1 \qquad \text{eq. A8}$$

where

di = difference index
A, B = two time series of maps
$s0_a$, $s0_b$ = probabilities of similarity despite interannual variability for A and B
MSSI(A, A) = map series similarity index applied between A and itself
MSSI(B, B) = map series similarity index applied between B and itself
MSSI(A, B) = map series similarity index applied to A and B

which is exactly how the map series difference index MSDI was defined in eq. 4.8.

MSDI therefore has the properties previously identifed for *di:*

- its range is the interval [-(1 + 1/*n*), +1], where *n* is the length of the series
- when there is no trend, its value is negative and its magnitude represents the probability of difference due to interannual variability
- when there is no interannual variability, its value is positive and represents the probability of the difference due to a trend
- its sign represents the relative significance of interannual variability versus the trend